UNIVERSIDADE FEDERAL DE SANTA CATARINA
CAMPUS FLORIANÓPOLIS
PROGRAMA DE PÓS-GRADUAÇÃO EM ENGENHARIA MECÂNICA

PABLO ANTUNES DA ROSA

NON-RIGID PARTS INSPECTION BY VIRTUAL CLAMPING METHOD WITH SIMULATED DISPLACEMENTS

FLORIANÓPOLIS
2019

Pablo Antunes da Rosa

NON-RIGID PARTS INSPECTION BY VIRTUAL CLAMPING METHOD WITH SIMULATED DISPLACEMENTS

Dissertação submetida ao Programa de Pós-Graduação em Engenharia Mecânica da Universidade Federal de Santa Catarina para a obtenção do título de Mestre em Engenharia Mecânica.
Orientador: Prof. Dr. Gustavo Daniel Donatelli

Florianópolis
2019

Ficha de identificação da obra elaborada pelo autor,
através do Programa de Geração Automática da Biblioteca Universitária da UFSC.

Antunes da Rosa, Pablo
Non-Rigid Parts Inspection by Virtual Clamping Method with Simulated Displacements / Pablo Antunes da Rosa ; orientador, Gustavo Daniel Donatelli, 2019.
114 p.

Dissertação (mestrado) - Universidade Federal de Santa Catarina, Centro Tecnológico, Programa de Pós-Graduação em Engenharia Mecânica, Florianópolis, 2019.

Inclui referências.

1. Engenharia Mecânica. 2. inspeção geométrica. 3. peças não rígidas. 4. fotogrametria ativa. 5. método de elementos finitos. I. Daniel Donatelli, Gustavo. II. Universidade Federal de Santa Catarina. Programa de Pós-Graduação em Engenharia Mecânica. III. Título.

Pablo Antunes da Rosa

Non-Rigid Parts Inspection by Virtual Clamping Method with Simulated Displacements

O presente trabalho em nível de mestrado foi avaliado e aprovado por banca examinadora composta pelos seguintes membros:

Prof. Gustavo Daniel Donatelli, Dr. Eng.
Universidade Federal de Santa Catarina

Prof. Armando Albertazzi Gonçalves Jr., Dr. Eng.
Universidade Federal de Santa Catarina

Prof. Christian Raffaelo Baldo, Dr. Eng.
Universidade Federal do ABC

Certificamos que esta é a **versão original e final** do trabalho de conclusão que foi julgado adequado para obtenção do título de mestre em Engenharia Mecânica.

Assinado de forma digital por Jonny Carlos da Silva:51451506449
Dados: 2019.08.15 14:19:31 -03'00'

Prof. Dr. Jonny Carlos da Silva
Coordenador do Programa

Assinado de forma digital por Gustavo Daniel Donatelli:00469452960
Dados: 2019.08.14 08:46:25 -03'00'

Prof. Dr. Gustavo Daniel Donatelli
Orientador

Florianópolis, 19 de junho de 2019.

Dedico este trabalho aos meus pais: Nelsi e Ivandete;
e ao meu esposo Wellington.

ACKNOWLEDGMENTS

This work would not have been possible without the financial support of the CAPES (Coordenação de Aperfeiçoamento de Pessoal de Nível Superior – Brazil – Financial Code 001) and CERTI Foundation.

I am especially grateful to Prof. Gustavo Donatelli, my research supervisor, who guided me patiently, encouraged me enthusiastically and contributed strongly to the development of this research work. As my teacher and mentor, he taught me more than I could ever give him credit for here.

I would also like to thank the collaboration of Professor Armando Albertazzi Jr. and Professor Eduardo Fancello during the development of this work and the strong support of Tiago M. Zilio. The trainings on using equipment and software were valuable to my professional growth.

My gratitude is also extended to Mateus D. de Oliveira, Thiago L. Fernandes, Talles de Oliveira, Neudimar M. do Nascimento, Leonardo C. Miguel and Dionatan O. Fernandes for their valuable technical support in this project;

I am grateful also to all those with whom I have had the pleasure to work during this and other projects. That is why I must also thank all the staff of the CMI (Center of Metrology and Instrumentation) for the friendship and support.

To LABMETRO colleagues, my thanks for all the help and good times, especially Débora R. Simioni, Helton F. Medeiros, Lívia R. Lothhammer, Thiago Wilvert and Rosana Vieira.

Thanks also to my friends Leticia Reinheimer and Jalline Freire for being always with me, even at a distance.

And finally, nobody has been more important to me in the pursuit of this project than the members of my family. I would like to thank my parents, whose love and guidance are with me in everything I seek. And most importantly, I would like to thank my loving and supportive husband Wellington, who provides me unending inspiration.

RESUMO

Devido à ação da gravidade e a tensões residuais, peças não rígidas podem apresentar variações geométricas significativas em condições de estado livre. Dessa forma, dispositivos de fixação são utilizados para manter essas peças estáveis durante o processo de inspeção 3D. Geralmente eles são projetados e fabricados com a finalidade de simular as condições de montagem e/ou as restrições definidas na etapa de especificação geométrica do produto. Entretanto, eles podem ser complexos e caros, além de exigirem manutenção e qualificação periódicas para permanecerem em condições de uso. Somando-se a isso, dispositivos também são altamente sensíveis a desvios geométricos que afetam as superfícies das peças que estão em contato com as esferas de referência e elementos fixadores, resultando em consideráveis efeitos na repetibilidade, reprodutibilidade e erros de tendência que diminuem significativamente a capabilidade do processo de medição. Este trabalho explora a aplicação de sistemas ópticos de medição associados à utilização de dispositivos virtuais de fixação na inspeção de peças não rígidas, avaliando o desempenho metrológico e identificando vantagens e dificuldades operacionais do método. Com a utilização de um sistema de fotogrametria ativa, uma densa nuvem de pontos é gerada e posteriormente transformada em arquivo CAD, representando virtualmente a geometria da peça na condição de estado livre. Após isso, em ambiente de simulação computacional, condições de contorno de deslocamentos específicos são aplicadas para reproduzir o processo de montagem. E, finalmente, a comparação da geometria da peça simulada com a geometria nominal fornece informações sobre os desvios locais que a peça pode apresentar após a montagem. Experimentos utilizando peças aeronáuticas com diferentes índices de flexibilidade e com tamanho médio característico de aproximadamente um metro mostraram que a distância máxima entre o modelo virtual simulado e a superfície real medida sobre um dispositivo físico apresenta uma variação de até 6% do deslocamento requerido para a montagem. Desse modo, a análise dos resultados mostrou que o método de fixação virtual associado a sistemas ópticos de medição pode ser usado com sucesso no controle de qualidade auxiliado por computador e inspeção automatizada de peças não rígidas.

Palavras-chave: inspeção geométrica. peças não rígidas. sem fixação. fotogrametria ativa. método de elementos finitos.

RESUMO EXPANDIDO

Introdução

Atualmente, uma das principais tendências da indústria aeronáutica e automotiva é o uso de componentes mais leves para reduzir o consumo de combustível e as emissões de CO_2. A redução de massa é geralmente realizada otimizando o projeto de acordo com a distribuição de tensões ou através do uso de ligas leves. Com essas técnicas, as peças podem se tornar não rígidas e apresentar variações geométricas significativas na condição de estado livre devido a fatores como a carga gravitacional e a tensão residual resultante da fabricação, que não podem ser completamente e exatamente quantificados. A inspeção geométrica de peças não rígidas requer uma abordagem e especificação especiais, sendo necessário considerar se a condição de estado livre se aplica ou se é necessário simular suas relações com os outros componentes, considerando tanto as superfícies de contato quanto as forças de restrição. Recentemente, alguns autores investigaram novos métodos e sistemas para a automação do processo de inspeção tentando eliminar a necessidade do uso de sistemas especiais de fixação. Há uma tendência de os métodos de inspeção desses componentes terem uma abordagem sem fixação associado ao uso de técnicas numéricas para comparar virtualmente a forma da peça medida em condições de estado livre com seu modelo CAD nominal.

Objetivos

O objetivo geral deste trabalho é testar a viabilidade e o desempenho metrológico do processo de inspeção de peças não rígidas por meio de sistemas ópticos de medição combinado com um método de fixação virtual (simulação numérica). O objetivo descrito ainda pode ser dividido em quatro principais objetivos específicos: a) identificar os métodos de inspeção de peças não rígidas; b) propor uma metodologia para análise das simulações de deformações; c) avaliar o desempenho metrológico do método proposto através da comparação com o método convencional; d) analisar as vantagens operacionais e dificuldades do método proposto.

Metodologia

Para a avaliação do desempenho metrológico foram realizadas comparações do método proposto com o método convencional (utilizando dispositivos físicos de fixação) já amplamente utilizado e aceito no ambiente industrial. O método proposto consiste na captura da geometria da peça em apoiada em um dispositivo simplificado de fixação, utilizando digitalizador óptico GOM ATOS Compact Scan®. A partir dessa etapa todo o processo de inspeção torna-se virtual. A densa malha gerada no processo de digitalização é transformada em um sólido CAD aplicável à simulação de elementos finitos no software Siemens NX®. Já em ambiente de simulação, no mesmo software, deslocamentos específicos são aplicados na malha, de forma a deformá-la simulando a montagem em dispositivo de fixação. Após a etapa de simulação, a malha deformada é comparada com o modelo CAD nominal no *software* GOM Inspect®, onde é possível identificar os erros de forma que a peça pode apresentar após a montagem. Para a avaliação do método, o mesmo foi aplicado em dois painéis de revestimento aeronáutico, com cinco replicações em cada um. Após a inspeção geométrica das peças realizada através do método convencional os dois resultados foram comparados através de testes estatísticos de análise de variâncias permitindo identificar semelhanças, benefícios e malefícios dos métodos. Além disso, para uma avaliação completa do método foram realizados alguns ensaios intermediários a fim de identificar as etapas do processo que apresentam significativo acréscimo de erros aos resultados parciais. Nessas avaliações intermediárias, adotou-se o método apresentado por Donald J Wheeler em suas publicações, através de análise gráfica de médias e amplitudes do processo.

Resultados e discussões

Os resultados experimentais mostraram que, quando o método de fixação virtual (VCM – *Virtual Clamping Method*) é comparado com o método convencional (PCM – *Physical Clamping Method*), ambos apresentam desempenhos metrológicos similares e consistentes, desde que as condições de contorno apropriadas sejam bem definidas e observadas. No entanto, o VCM resulta em uma melhor repetibilidade, visto que elimina as interações entre as peças e o sistema de fixação. Os resultados também permitiram uma análise das etapas do processo com maiores chances de interferir nos resultados e os principais fatores que levaram a esse desempenho. É evidenciado que a maior contribuição para erros e/ou incertezas provém do processo de digitalização. No entanto, se o sistema de fixação simplificado for bem representado no processo simulação da neutralização da gravidade com condições de contorno, tais erros podem ser absorvidos. Outro fator identificado que pode causar grande impacto nos resultados é o processo de definição das especificações do sistema de coordenadas (*Reference Datum System*), utilizado para o referenciamento da malha digitalizada com o modelo nominal CAD.

Conclusões

O método de fixação virtual segue a tendência atual de transferir a complexidade do mundo físico para o mundo cibernético, apresentando grande potencial de: remover limitações à realização física de restrições de GD&T; fornecer acesso fácil a todas as superfícies de peças relevantes; reduzir a configuração de medição e os tempos de aquisição de imagem; reduzir o capital envolvido com sistemas de fixação caros e complexos; e diminuir os custos operacionais com armazenamento, manutenção e verificação dimensional dos sistemas de fixação. Adicionalmente, foi possível identificar algumas limitações de uso desse método, como: sistemas de fixação físicos, ainda que simplificados, continuam sendo necessários para manter a peça estável durante a digitalização e possibilitar a correção precisa dos efeitos de gravidade; os processos de modelagem (engenharia reversa) e de simulação de elementos finitos devem ser simplificados para promover a aceitação industrial do método; a comprovação metrológica de processos de medição que fazem uso intensivo de simulação por computador ainda é um tema pendente.

Palavras-chave: inspeção geométrica. peças não rígidas. sem fixação. fotogrametria ativa. método de elementos finitos.

ABSTRACT

Due to gravity forces and residual stress, non-rigid parts may show significant geometric variations in free-state condition. Clamping systems are intended to stabilize non-rigid parts during 3D inspection and are usually designed and built to emulate assembly conditions and/or the constraints defined in geometric product specification step. However, clamping systems can be complex and expensive, requiring periodic maintenance and qualification to remain useful and reliable. They are highly sensitive to geometric deviations, affecting the part surfaces that are in contact with the tooling balls and clamping devices, resulting in relevant repeatability, reproducibility and bias effects that knock down the measurement capability. This work explores the application of optical measurement systems associated with virtual clamping method to inspect non-rigid parts in free-state condition, without employing specialized clamping systems, comprising the metrological performance evaluation and the identification of operational advantages and difficulties of the method. Using a fringe projection system, a dense mesh is generated and later transformed into a CAD file, which is the virtual representation of the part geometry in free-state condition. In a computer simulation environment, specific displacement boundary conditions are applied to reproduce the assembly process. Finally, the comparison of the simulated part geometry with the nominal CAD provides information on the local deviations that the part could show after being assembled. Experiments using aeronautical covering panels with different flexibility ratios, different curvature levels and with an average characteristic size of approximately one meter showed that the maximum distance between the simulated virtual model and the actual surface measured on a physical clamping system varies of up to 6 % of displacement required for assembly. The analysis results showed that the virtual clamping method associated with optical measurement systems can be used successfully in computer-aided quality control and automated inspection of manufactured parts.

Keywords: geometric inspection. non-rigid parts. fixtureless. active photogrammetry. finite element method.

LIST OF FIGURES

Figure 2.1 - Logarithmic scale representation for flexibility classification. 25
Figure 2.2 - Categorization of restriction methods used for non-rigid parts. 26
Figure 2.3 - (a) 3-2-1 positioning scheme; (b) N-2-1 positioning scheme. 28
Figure 2.4 - Definition of surface profile tolerance zone. 29
Figure 2.5 - Conventional approach flow for non-rigid parts inspection. 30
Figure 2.6 - Clamping system assembled on the baseplate of the coordinate measuring machines. 31
Figure 2.7 - Surface comparison principle. 33
Figure 2.8 - Main methods for the virtualization of the part inspection process. 34
Figure 2.9 - Technical approach presented by Blaedel et al. 35
Figure 2.10 - Contour plot of radial displacements for the experimental data and initial finite element discretization. 36
Figure 2.11 - Triangle mesh (right) created from point cloud (left). 37
Figure 2.12 - Generalized Numerical Inspection Fixture method. 38
Figure 2.13 - Simulation results of assembled geometry. 39
Figure 2.14 - Schematic flowchart of VMASI method. 40
Figure 2.15 - Schematic diagram of (a) a part without a zone with profile deviations and (b) a part with a zone with profile deviations. 41
Figure 2.16 - Results of the proposed method by Aidibe and Tahan. 42
Figure 2.17 - General route identified in the virtual clamping methods. 43
Figure 2.18 - Typical range of measuring uncertainty vs. part dimension for different categories of measuring systems. 45
Figure 2.19 - Ishikawa diagram of the main sources of errors in optical measurements. 46
Figure 2.20 - General flowchart of CAD reconstruction. 49
Figure 2.21 - Reconstruction results of industrial parts by Wang et al. 50
Figure 2.22 - Typical flowchart for Finite Element Analysis (FEA). 51
Figure 2.23 - Different types of Finite Elements. 52
Figure 3.1 - Virtual clamping approach flow 54
Figure 3.2 - Modular components used for the CS assembly. 55
Figure 3.3 - 3D optical scanner ATOS Compact Scan (a and b); virtual representation of the measuring volume (c). 56

Figure 3.4 - Examples of discretized surfaces with triangular elements. 60
Figure 3.5 - Forced displacement representation. 60
Figure 3.6 - Flowchart of the methods steps. 63
Figure 3.7 - Example of control chart. 66
Figure 3.8 - Artifact constructed to evaluate the metrological performance of ATOS. 67
Figure 3.9 - Evaluated trajectories and the reference points positions. 69
Figure 3.10 - Micrometer with control of the applied force. 70
Figure 3.11 - Representation of the amount increase of mesh elements. 70
Figure 3.12 - Example of a passenger aircraft winglet. 73
Figure 3.13 - Part A: design and geometric specifications. 73
Figure 3.14 - Part B: design and geometric specifications. 74
Figure 3.15 - Part A: Control points. 75
Figure 3.16 - Part B: Control points. 75
Figure 3.17 - Part A: Points for process evaluation. 75
Figure 3.18 - Part B: Points for process evaluation. 76
Figure 4.1 - Process evaluation: 3D scanning - used artifact. 78
Figure 4.2 - Process evaluation (A): 3D scanning - graphical results. 78
Figure 4.3 - Process evaluation (A): 3D scanning - graphical results. 79
Figure 4.4 - Part A: Simplified clamping system. 80
Figure 4.5 - Part A: Intermediate evaluation (B) - clamping system VCM. 80
Figure 4.6 - Part A: Intermediate evaluation (C) - 3D data capture. 81
Figure 4.7 - Part A: Intermediate evaluation (C) - 3D data capture. 82
Figure 4.8 - Part A: Mesh segmentation for modeling process. 82
Figure 4.9 - Part A: Modeling method using a grid of splines. 83
Figure 4.10 - Part A: Visual evaluation (D) - modeling. 83
Figure 4.11 - Part A: Intermediate evaluation (E) - modeling 84
Figure 4.12 - Part A: Representation of mesh and the boundary conditions. 85
Figure 4.13 - Part A: Process Evaluation (F) - meshing size analysis 85
Figure 4.14 - Part A: Intermediate evaluation (G) - VCM 86
Figure 4.15 - Part A: Visual evaluation (H) - VCM 87
Figure 4.16 - Part A: Physical clamping system. 87
Figure 4.17 - Part A: Intermediate evaluation (I) - PCM. 88
Figure 4.18 - Part A: Intermediate evaluation (J) - PCM. 89
Figure 4.19 - Part A: Visual evaluation (K) - PCM 89

Figure 4.20 - Part A: Comparison between VCM and PCM (L).....90
Figure 4.21 - Part A: Statistical evaluation.....91
Figure 4.22 - Part B: Simplified clamping system. 91
Figure 4.23 - Part B: Intermediate evaluation (B) - clamping system VCM.....92
Figure 4.24 - Part B: Intermediate evaluation (C) - 3D data capture. 93
Figure 4.25 - Part B: Mesh segmentation for modeling process. 94
Figure 4.26 - Part B: Modeling method using a grid of splines. 94
Figure 4.27 - Part B: Visual evaluation (D) – modeling. 95
Figure 4.28 - Part B: Intermediate evaluation (E) – modeling. 95
Figure 4.29 - Part B: Representation of mesh and the boundary conditions. 96
Figure 4.30 - Part B: Process evaluation (F) - meshing size analysis. 96
Figure 4.31 - Part B: Intermediate evaluation (G) - VCM. 97
Figure 4.32 - Part B: Visual evaluation (H) - VCM. 97
Figure 4.33 - Part B: Physical clamping system.....98
Figure 4.34 - Part B: Intermediate evaluation (I) clamping system PCM. 99
Figure 4.35 - Part B: Intermediate evaluation (J) - PCM. 99
Figure 4.36 - Part B: Visual evaluation (K) - PCM. 100
Figure 4.37 - Part B: Comparison between VCM and PCM (L) 100
Figure 4.38 - Part B: Representation of the force required for fixation. 101
Figure 4.39 - Part B: Statistical evaluation. 102
Figure 4.40 - Numerical comparison between VCM and PCM. 103

LIST OF TABLES

Table 2.1 - Virtual clamping methods classification based on the displacement direction.....43
Table 3.1 - Technical characteristics of the articulated measuring arm. 55
Table 3.2 - Technical characteristics of ATOS Compact Scan. 57
Table 3.3 - ATOS Compact Scan measurement parameters. 57
Table 3.4 - CMM Mitutoyo parameters. 62
Table 3.5 - Organization of measurement results. 64
Table 3.6 - Average and Range charts factors for using the Average Range. 65
Table 3.7 - Bias correction factors for using Average Ranges to estimate Variances. 66
Table 3.8 - CMM Zeiss parameters. 68
Table 3.9 - General data and artifact dimensions. 68
Table 3.10 - Mechanical properties of Aluminum 2024-O. 74
Table 4.1 - ATOS Compact Scan calibration parameters and results. 77
Table 4.2 - Process evaluation: 3D scanning. 78
Table 4.3 - Part A: Intermediate evaluation (C) - 3D data capture. 81
Table 4.4 - Part A: Process evaluation (F) - meshing size analysis. 85
Table 4.5 - Part A: Physical clamping system deviations. 88
Table 4.6 - Part A: Statistical evaluation - profile of the surface error. 90
Table 4.7 - Part B: Intermediate evaluation (C) - 3D data capture. 92
Table 4.8 - Part B: Process evaluation (F) - meshing size analysis. 96
Table 4.9 - Part B: Physical clamping system deviations. 98
Table 4.10 - Part B: Statistical evaluation - profile of the surface error. 101
Table 4.11 - Performed evaluations. 102

LIST OF ACRONYMS

AM	Additive Manufacturing
ANOVA	Analysis of Variance
CAD	Computer-Aided Design
CAE	Computer-Aided Engineering
CAM	Computer-Aided Manufacturing
CAPEX	Capital Expenditure
CERTI	Centers of Reference in Innovative Technologies
CI	Confidence Interval
CMI	Center of Metrology and Instrumentation
CMM	Coordinate Measuring Machine
COE	Conventional Evaluation
CPD	Coherent Point Drift
CS	Clamping System
DOF	Degrees of Freedom
DRF	Datum Reference Frame
EMP	Evaluating the Measurement Process
FEA	Finite Element Analysis
FEM	Finite Element Method
GD&T	Geometric Dimensional and Tolerance
GNIF	Generalized Numerical Inspection Fixture
GPS	Geometrical Product Specification
HDF	Hyperstatic Datum Frame
ICP	Iterative Closest Point
IDI	Iterative Displacement Inspection
JT	Jupiter Tessellation
LABMETRO	Laboratory of Metrology and Automatization
LCL	Lower Control Limit
MOD	Modeling
OPEX	Operational Expenditure
PCM	Physical Clamping Method
PCS	Physical Clamping System

RE	Reverse Engineering
RPS	Reference Point System
SCS	Simplified Clamping System
SIM	Simulation
UCL	Upper Control Limit
UFSC	Federal University of Santa Catarina
VCM	Virtual Clamping Method
VMASI	Virtual Mounting Assembly-State Inspection

LIST OF SYMBOLS

Capital Letters:

A_2	Factor used in control limit calculation for average chart [-]
D_4	Factor used in control limit calculation for range chart [-]
F_0	F-test value [-]
F_α	Critical F-test value [-]
LCL_R	Lower control limit for range chart [mm]
$LCL_{\bar{\bar{X}}}$	Lower control limit for average chart [mm]
R	Flexibility ratio [-]
$\bar{R}$	Average range [mm]
SQ_{trat}	Quadratic sum of treatments [mm²]
SQ_E	Quadratic sum of the error [mm²]
Tol	Profile tolerance [mm]
UCL_R	Upper control limit for range chart [mm]
$UCL_{\bar{\bar{X}}}$	Upper control limit for average chart [mm]
$\bar{X}$	Average [mm]
$\bar{\bar{X}}$	Grand average [mm]
X_{pj}	Individual value [mm]
X_{ij}	Individual value for ANOVA study [mm]
Y_{ij}	Random variable [mm]

Lowercase Letters:

a	Total number of treatments [-]
d_2	Bias correction factor [-]
d_2^*	Bias correction factor to estimate variance [-]
i	Index to identify the treatment [-]
j	Index for repetition [-]
k	Coefficient of t-student [-]
m	Total number of control points [-]
n	Total number of repetition [-]
p	Index for control point [-]
t	Tolerance [mm]

Greek Letters:

δ_{max}	Maximum displacement [mm]
ϵ_{ij}	Component of random error [mm]
μ	Global average [mm]
ν	Degree of freedom
$\hat{\sigma}_e$	Estimated standard deviation [µm, mm]
$\widehat{\sigma^2}_e$	Estimated variance [µm²]
τ_i	Effect of i-th treatment [mm]

CONTENTS

1 INTRODUCTION 21
1.1 OBJECTIVES 22
1.2 DESCRIPTION OF THE RESEARCH FIELD 22
1.3 THESIS STRUCTURE 23
2 LITERATURE REVIEW 24
2.1 DEFINITION AND SPECIFICATION OF NON-RIGID / FLEXIBLE PARTS 24
2.1.1 Definition 24
2.1.2 Specification 26
2.1.3 Influences on the inspection process 29
2.2 INSPECTION USING PHYSICAL CLAMPING SYSTEMS 30
2.2.1 Clamping 30
2.2.2 Tactile measurement 32
2.2.3 Conformity assessment 33
2.3 INSPECTION USING VIRTUAL CLAMPING SYSTEMS 33
2.3.1 Methods based on FEM to evaluate part deformation 35
2.3.2 Methods not based on FEM to evaluate part deformation 40
2.3.3 Overview 42
2.4 OPERATIONAL ISSUES 44
2.4.1 Acquisition 44
2.4.2 Point cloud treatment 46
2.4.3 CAD reconstruction 48
2.4.4 FEM simulation 50
2.5 CHAPTER SUMMARY 52
3 EXPERIMENTAL PLANNING 54
3.1 METHOD DEFINITION 54
3.1.1 CAD and geometric specifications 54
3.1.2 Simplified fixturing 54
3.1.3 Optical scanning 56
3.1.4 Modeling 59
3.1.5 Virtual clamping 59
3.1.6 Part evaluation 61

3.2 METROLOGICAL EVALUATION 62
3.2.1 Intermediate evaluation 62
3.2.2 Process evaluation 67
3.2.3 Statistical evaluation 70
3.2.4 Visual evaluation through color maps 72
3.2.5 General evaluation 72
3.3 CASE STUDIES 72
4 RESULTS AND DISCUSSIONS 77
4.1 PROCESS EVALUATION: 3D SCANNING 77
4.2 CASE STUDY: PART A 79
4.2.1 Simplified clamping system and 3D data capture 79
4.2.2 Modeling 82
4.2.3 FEM Simulation 84
4.2.4 Evaluation 86
4.2.5 Conventional Method 87
4.2.6 Comparison of VCM and PCM 89
4.3 CASE STUDY: PART B 91
4.3.1 Simplified clamping system and 3D data capture 91
4.3.2 Modeling 93
4.3.3 Simulation 95
4.3.4 Evaluation 97
4.3.5 Conventional Method 98
4.3.6 Comparison of VCS and PCS 100
4.4 GENERAL EVALUATION 102
5 CONCLUSION 105
REFERENCES 107

1 INTRODUCTION

Nowadays, one of the main characteristics of the manufacturing processes is the increased demand for small series of products, allowing a great level of customization. At the same time, there is a great demand for productivity [1]. Another characteristic is a trend towards the use of lighter components, such as in the aeronautical and automotive industry, to reduce fuel consumption and CO_2 emissions.

The weight reduction is usually accomplished by optimizing the design according to the stress distribution or through the use of light alloys. With these techniques, the parts can become non-rigid and present significant geometric variations in the free-state condition due to factors such as gravitational load and residual stress resulting from fabrication, which cannot be completely and accurately quantified [2, 3].

The increased quality requirements of the production components reflect the need for better dimensional control techniques and non-contact methods for shape inspection. In order to inspect the non-rigid components, it is necessary to consider whether the free-state condition applies or whether it is necessary to simulate its relations with the other components, considering both the contact surfaces and the restraining forces.

If applicable, clamping systems (CS) can be used to stabilize non-rigid parts during the 3D inspection. They are usually designed and built to emulate the assembly conditions. However, such systems can be complex and expensive, requiring periodic maintenance and qualification to remain useful [3]. They are also highly sensitive to geometric deviations that affect the parts surfaces resulting in significant repeatability, reproducibility and bias effects that knock down the measurement capability.

Thus, the geometric inspection of non-rigid parts requires a special approach and specification. Recently, some authors have investigated new methods and systems for the automation of the inspection process, attempting to eliminate the need for special clamping systems. In fact, there is a trend for non-rigid part inspection methods to have a fixtureless approach and use numerical techniques to compare virtually the shape of the measured part under free-state conditions with its nominal CAD model.

Considering the current scenario just described, this work focuses on developing a methodology for the virtualization of the geometric inspection of non-rigid parts, which aimed

to eliminate the need of physical clamping systems by compensating the deformation by FEM (Finite Element Method). This work is a result of cooperation between the Laboratory of Metrology and Automatization (Laboratório de Metrologia e Automatização – LABMETRO/UFSC) and the CERTI (Centers of Reference in Innovative Technologies) Foundation.

1.1 OBJECTIVES

The main objective of this research is to test the feasibility and metrological performance of inspecting non-rigid / flexible parts by means of optical scanning systems and the virtual clamping method.

In order to achieve the main objective, the following specific objectives can be specified:

a) to identify the inspection methods for non-rigid / flexible parts;
b) to propose a methodology for analysis, using optical scanning systems and finite element method;
c) to test the metrological performance of the proposed method by comparing with the results obtained with the conventional method;
d) to analyze the operational advantages and difficulties of the proposed method.

1.2 DESCRIPTION OF THE RESEARCH FIELD

The method presented in this work was developed and experimentally tested in parts of the aeronautical industry. In this field, the main geometric characteristics of the components are as follows:

a) they are relatively large (several meters for some components), and often of slender shape;
b) their thicknesses are relatively small in view of the dimensions of the components (a few millimeters or centimeters);
c) they can be considered flexible;
d) they are subject to geometric defects typical of the materials used in forming processes.

These characteristics are true regardless of the material used. However, with the advancements of the modeling process, the geometries tend to be even more complex. In addition, with the appearance of new materials, the thicknesses of the components tend to be reduced, which can result in an increase in the number of non-rigid parts.

1.3 THESIS STRUCTURE

The introductory chapter of the thesis contextualizes the subject and the definition of the problem and presents the objectives and hypothesis of this work.

Chapter 2 presents a literature review of the processes involved in a non-rigid parts inspection methodology, both with the conventional method and with the developing method, along with previously developed researches.

Chapter 3 explores a new proposal for the geometric inspection process, describes the phases of the proposed procedure and the means of evaluation used to obtain the results.

Chapter 4 presents the experimental results of the proposed method application in two parts, exposing some facts about the advantages and limitations identified during experimental development.

Finally, in Chapter 5 the main conclusions drawn from this work are summarized and suggestions for future works are presented.

2 LITERATURE REVIEW

The reliability of data related to component geometry affects the performance of assembly operations. However, the flexible nature of some components results in a variable geometry depending on the clamping and measuring processes, that still causes difficulties in the assembly stations.

In order to identify the main steps and characteristics of the conventional approach to non-rigid parts inspection, the state of the art is presented in this chapter. In addition, a review of the inspection methods that do not use special clamping systems is also presented. This analysis aims to figure out their main strengths and to describe the steps of the methods under development.

2.1 DEFINITION AND SPECIFICATION OF NON-RIGID / FLEXIBLE PARTS

2.1.1 Definition

For the specification of part requirements, it is necessary to consider whether the component is rigid or flexible. The boundary between the two definitions depends mainly on the point of view and the assumptions made. The standard ISO 10579 [4] defines a non-rigid part as a "part which deforms to an extent that in the free state is beyond the dimensional and/or geometrical tolerances on the drawing", and the free state is defined as the "condition of a part subjected only to the force of gravity".

More specifically, Aidibe and Tahan [5] propose a classification of flexible components into three categories, which correspond to zones that will not be treated in the same way, especially during the inspection process. The classification depends on the flexibility ratio:

$$R = 2 \cdot \delta_{max}/Tol \tag{1.1}$$

where δ_max is the maximum displacement induced by a certain force and Tol is the profile tolerance of the compliant part. In this way, the parts can be classified into different zones, as presented in the logarithmic graph in Figure 2.1.

Figure 2.1 - Logarithmic scale representation for flexibility classification.

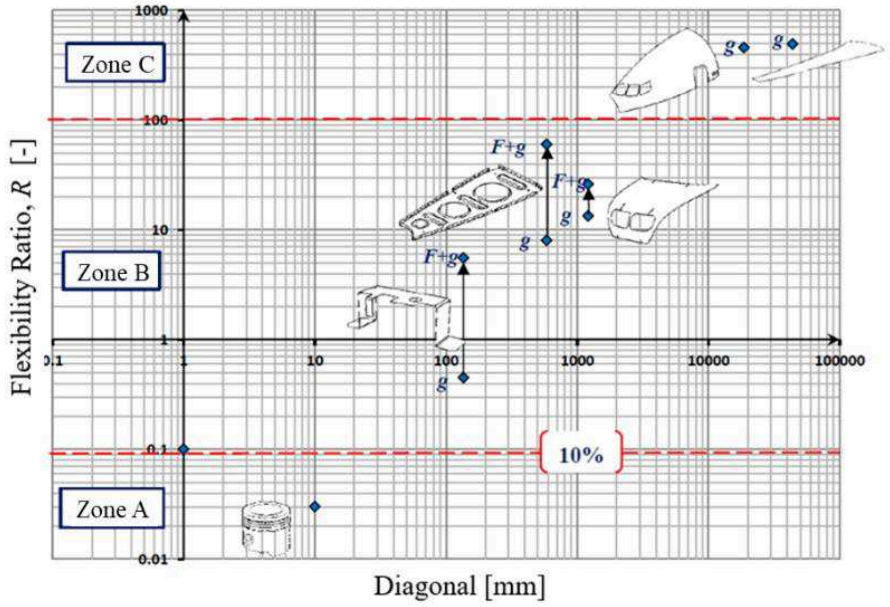

Source: [5].

Three different zones are proposed in the logarithmic graph as follows:

a) **Zone A** for parts considered rigid ($R < 0.1$). Deformations caused by inspection efforts (clamping, probe contact, etc.) have no significant influence on the tolerances assigned to the part (less than 10%). This applies to classic mechanical parts such as boxes, connecting rods, crankshafts.

b) **Zone B** for relatively flexible, or also named non-rigid parts ($0.1 < R < 100$). The deformations that the part may undergo during the assembly process may exceed 10% of the tolerance value. This is the case, for example, of automotive bodies and aeronautical parts.

c) **Zone C** for flexible parts ($R > 100$). The deformations they may undergo are of a magnitude much greater than the value of the specified tolerances. This is the case to elastomeric components and very flexible aircraft parts.

Parts of zones B and C require a particular process of defining their specifications, which is the subject of the next section.

2.1.2 Specification

The geometric state of a flexible component is highly dependent on its environment. The orientation of the component in relation to gravity as well as the geometry of the support that holds the component affects its geometry. For this reason, some techniques are used to determine the component condition during the inspection process (free-state condition, with the help of movable datum targets, under predefined stress, etc.). The different manners to restrain non-rigid part inspection are shown in Figure 2.2.

Figure 2.2 - Categorization of restriction methods used for non-rigid parts.

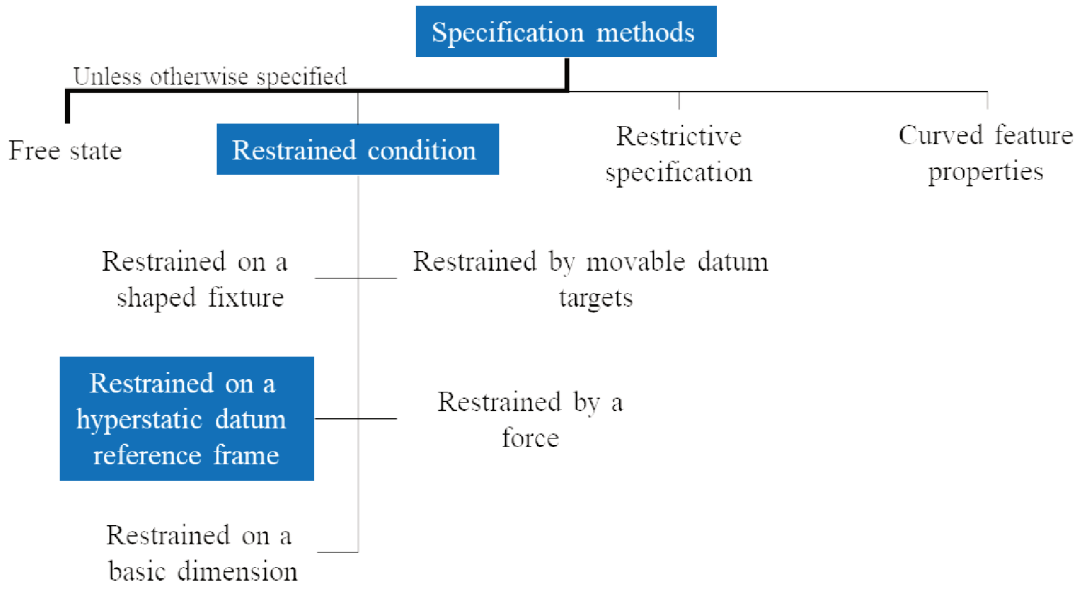

Source: [6].

Unless otherwise specified, the standard ISO 10579 states that non-rigid parts shall be inspected in free-state condition [4]. On the other hand, parts that require a specific condition for inspection require the use of clamping systems (CS). The use of clamping systems makes it possible to place the component under stable conditions. However, due to the size of the structural components in various fields, such as in aeronautics, these CS can be very expensive, heavy and with great need of space for storage. Generally, the CS are constructed according to the part GPS (Geometrical Product Specifications).

The GPS is a group of standards that allow the mutual interpretation of the part requirements from the point of view the design, the manufacturing and the inspection. In the ISO 14638 technical report, the objective of GPS system is described as: “to define the

geometrical requirements in engineering specifications, and the requirements for their verification" [7].

The group of standards ISO GPS is formed by fundamental standards that can be divided into three categories:

- Global GPS Standards: influence the general and complementary standards;
- General GPS Standards: present the requirements for:
  - Codification of Geometric Dimensional and Tolerance;
  - Theoretical definition of tolerances and values;
  - Characteristics or parameters for actual features;
  - Assessment of the deviations;
  - Measurement equipment;
  - Calibration.
- Complementary GPS Standards: present requirements for specific geometries or manufacturing process.

In the standards ISO 10579 [4] and ASME Y14.5 [8] it is recommended to define, in addition to the conventional GPS specification, the conditions under which the component must be located during its measurement or control, as already presented in Figure 2.2. Thus, the measurement process of non-rigid / flexible components must take into account, in addition to the measurement system and the required inspection procedure, the configuration in which the component is subjected.

In the specification process, the main step is the delimitation of a datum reference frame (DRF) in order to constrain the six degrees of freedom (DOF). Parts are mated to the DRF in the clamping systems so measurements, processing, and calculations can be performed [9]. Theoretical geometries, consisting of basic geometric elements (such as points, lines and planes) are used to define the DRF. These theoretical geometries might be derived from a single datum feature or are composed of two, three datum features [10].

Specifying the DRF for large and non-rigid parts, such as aircraft covering panels, requires a combination of datum geometries. However, the positioning is rarely isostatic due to their large dimensions and the large deformations to which they may be subjected. In this case,

it is often necessary to add supporting points to make the parts more stable or to minimize the component deformations.

Under these circumstances, the 3-2-1 conventional positioning, represented in Figure 2.3a (using a plane for the primary datum feature, one straight line for the secondary and a point for the tertiary) is then replaced by N-2-1 schemes, with N greater than 3 (Figure 2.3b) producing a hyperstatic datum frame (HDF) [11, 12]. Related to the DRF/HDF, all surfaces can be specified with geometric tolerances, which ensure product conformity and prevent unwanted interference with adjacent parts [13].

Figure 2.3 - (a) 3-2-1 positioning scheme; (b) N-2-1 positioning scheme.

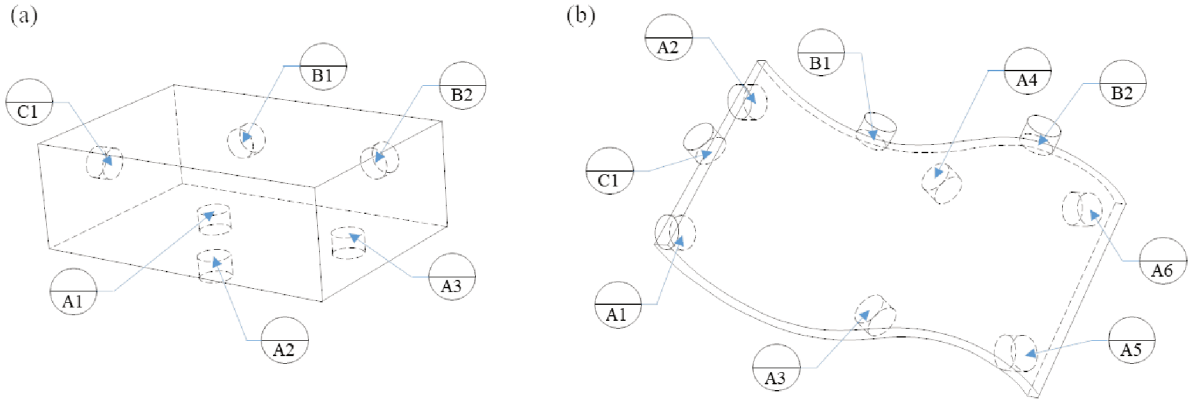

Source: the author.

The appropriate callout to control for surface location, orientation and form, except in the case of flat surfaces, is the profile of a surface, as specified in ISO 1101 [14]. To be considered approved, the actual surface shall be contained between two equidistant surfaces enveloping spheres of diameter *t* (tolerance), the centers of which are situated on a surface having the theoretically exact geometrical form. An example is shown in Figure 2.4. The surface profile error is defined as the distance between the equidistant surfaces that involves the real surface geometry. The use of geometric tolerances shall be applied according to the functional requirements of the part, even though the manufacturing and inspection requirements can also influence the geometric tolerances specification [14].

Figure 2.4 - Definition of surface profile tolerance zone.

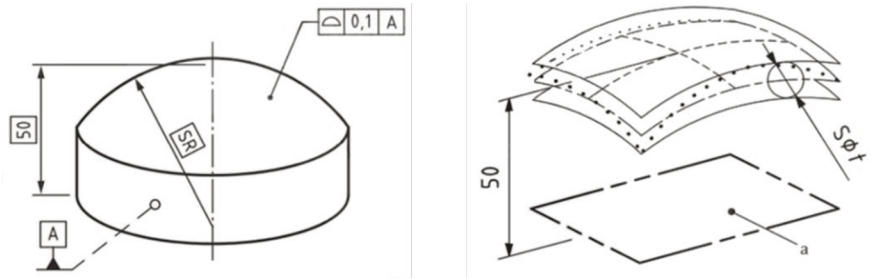

Source: [14].

2.1.3 Influences on the inspection process

Measuring non-rigid parts is a difficult task if insufficient constraints, as the datum reference frame, are specified to maintain the part stable during the measurement process. Even if a large number of datum features are specified to the part, and after used as constraints in the inspection process, there is no guarantee of effectiveness. It is not always possible to accurately represent the assembly conditions using few datum features.

The distribution of the datum points on the part surface can add significant errors to the results if it is not performed correctly. An overabundance of datum features tends to conform the part to its clamping system, but this can be also a problem. Several studies have analyzed the influence of the number of datum in the repeatability of inspection process. For example, the work presented in [6] highlights the influence of these additional fixtures on the component geometry they support. Depending on the number and position of the clamping systems and supporting components, the actual restricted shape of the component is changed. The repeatability of the positioning has been studied and tends to decrease as the number of contact points grows.

Another important issue to be considered during the geometric product specification is the inspection method, which can be through physical or virtual clamping systems. An analysis of both methods is presented in the following sections.

2.2 INSPECTION USING PHYSICAL CLAMPING SYSTEMS

The conventional method of non-rigid parts measurement, widely diffused in industry, uses physical clamping systems in order to hold the part during the measurement. The general flow of this methodology (PCM – Physical Clamping Method) follows the steps as shown in Figure 2.5, in which the specifications are defined in accordance with the GPS standards described in Section 2.1.2. The measurement process, according Figure 2.5, is detailed in the following sections.

Figure 2.5 - Conventional approach flow for non-rigid parts inspection.

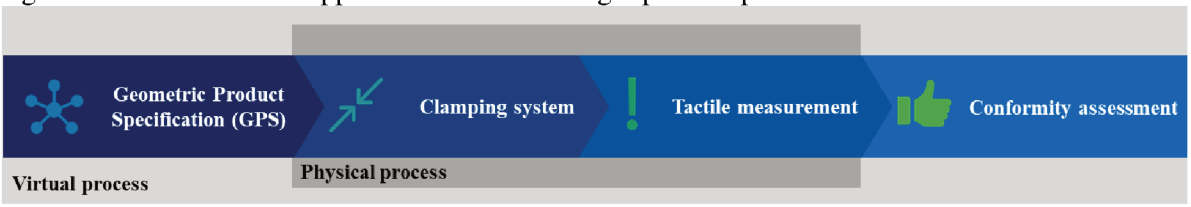

Source: the author.

2.2.1 Clamping

To measure non-rigid components, the clamping system is built on the premise of minimizing the number of constraints. In fact, it is more economically advantageous to use relatively simplified or universal clamping systems. The difficulty is then to evaluate the result of the measurement carried out in a given (measurement) setup relative to the specifications that are valid in a different setup (usually, the final configuration).

For the metrology of rigid components, as mentioned earlier, clamping systems (for machining or measuring) are designed to make positioning of the component isostatic and to ensure good repeatability. In the case of flexible components, this isostatic positioning is sometimes more complicated to define. In fact, Zirmi et al. [15] detailed the design of a machining fixture, which can be compared to a metrological CS in certain aspects. Besides the technological choice of the elements in contact with the part, the work details the criteria to be considered in order to optimize the placement of those elements. Three criteria are directly related to the context of flexible components metrology:

a) **stability:** the elements that constitute the main support must be placed in such a way as to obtain the largest supporting triangle. Efforts should also be taken into

account. In the case of metrological CS, the efforts refer to the clamping and probing forces, as well as to the weight of the component itself;

b) **deformation:** the contact points in the clamping system are arranged in such a way as to minimize deformation of the component;

c) **rigidity (assembly):** it is only referred to limit vibrations within the machining structure.

In the context of metrology of flexible components, it is necessary to control the rigidity of the assembly, which ensures that the positioning setup does not change during measurement and, thus, modifies the geometry in the actual shape of the component. Cai et al. [16] proposed a method for optimizing the number and position of these N datum targets in order to minimize the component deformation. The positioning is performed as part of the assembly and not of the measurement, but the problem remains the same. Camelio et al. [17] also showed that the positioning setup of a flexible component influences its geometry and, therefore, the result of the assembly with another component. In this case, the positioning optimization of the datum target point aims to minimize the deformations when the components are subjected to welding forces during assembly.

Figure 2.6 - Clamping system assembled on the baseplate of the coordinate measuring machines.

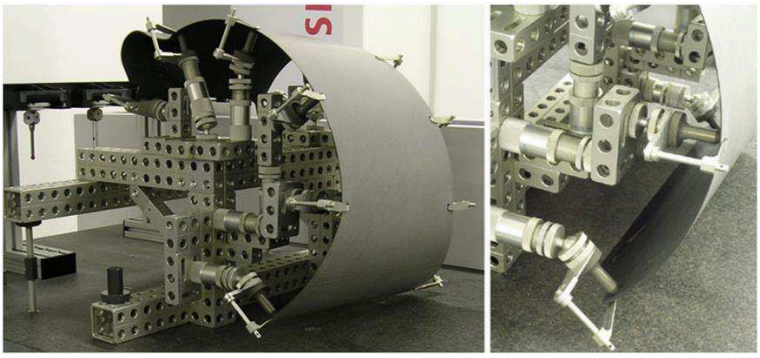

Source: [3].

On the other hand, the studies [3, 18] aimed to use specific systems to conform the components before the measurement. Under assembly constraints, the component presents consistent geometry when compared to its nominal geometry. Figure 2.6 shows an example of these CS. However, it is necessary to build a clamping system adapted to each component and

faithfully reproducing the mounting constraints. In addition, each geometric deviation in this clamping system will be reflected in the geometry of the component, resulting in additional geometric deviations in the measured geometry. Normally, after the CS design, manufacturing and calibration, the 3D position of points on tolerated surfaces are captured using tactile measurement systems, subject of the following section.

2.2.2 Tactile measurement

The measurement step is generally performed by coordinate measuring machines (CMM). Tactile CMMs operate by positioning the tip of a probing system in contact with the part surface to obtain the spatial location of a point on the surface. By using either point-to-point or scanning mode to sample the par surface, a measurement point cloud can be used to dimensionally characterize the part. For freeform surfaces, the use of computer-aided design (CAD)-based software is particularly important for the preparation of the measuring program, where the CAD model may be used as nominal element [3].

Arámbula et al. [19] highlighted some advantages of using CMMs in the inspection process as: relative low maintenance cost and frequency, possibility of measuring points in space with high accuracy and traceability towards the unit of length. Kupriyanov [20] also pointed out some advantages of CMMs such as their accuracy and the ability to measure reflective surfaces. However, he also highlighted some disadvantages:

- CMMs are not portable devices;
- CMMs cannot take more than one point per touch;
- CMMs are relatively expensive;
- CMMs generally require a special measurement room, due to their size and in order to meet the accuracy specifications.

It is still worth mentioning that CMMs present difficulties in the measurement of complex geometries, mainly because they may require special styli (tip) and accessories. Similar to CMMs, articulated measuring arms can also be used for the same measurement purpose.

2.2.3 Conformity assessment

The conformity assessment step determines if the detected deviations on tolerated surfaces are acceptable [3, 19, 21]. The conformity assessment can be performed through linear or geometric tolerances; the latter may also include the direct comparison with nominal geometry, allowing a better visual understanding of the actual shape of the part. For the surface comparison, the deviation for each point of the used mesh in relation to the nominal surface is calculated. Figure 2.7 illustrates this process. The blue line and points represent the CAD triangles. The green lines and points show the triangles of the actual mesh. The red lines show the calculated deviations of the surface comparison. In the software the vector deviations are displayed through a color scale. Usually warm colors represent positive deviations and cold colors, negative deviations [22].

Figure 2.7 - Surface comparison principle.

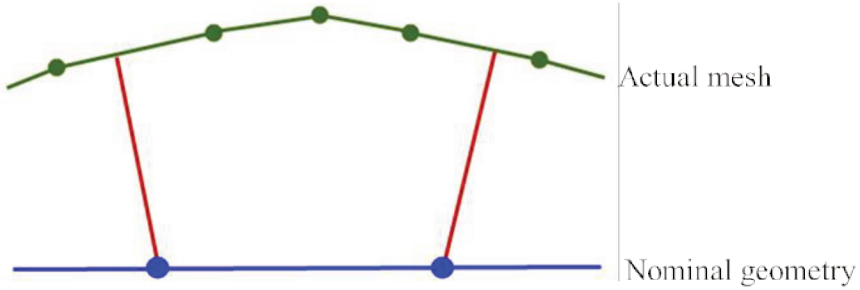

Source: [22].

2.3 INSPECTION USING VIRTUAL CLAMPING SYSTEMS

The main methods, under study, for the virtualization of the part inspection process are shown in Figure 2.8. They can be classified into two groups: those based on the Finite Element Method (FEM) or those that are not based on FEM. Both groups are described in the next sections.

Figure 2.8 - Main methods for the virtualization of the part inspection process.

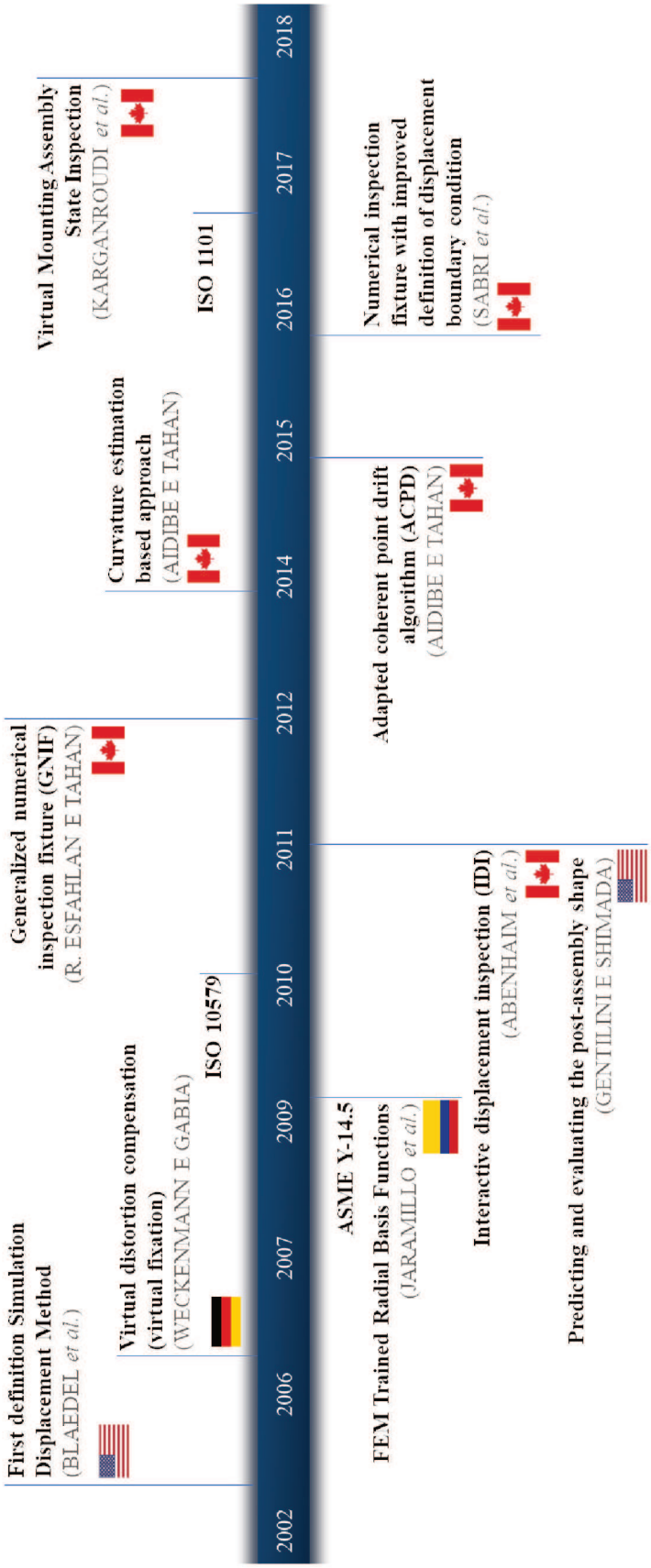

Source: the author.

2.3.1 Methods based on FEM to evaluate part deformation

The first approach with this theme was presented by Blaedel et al. [23]. They set out the principle of the method that allows one to evaluate the geometry of a flexible component. The first step is, after measuring the component in its measurement configuration, remove the effects of the environment by simulation to obtain a representation of its free geometry. The second step is then to impose virtually the effects of a different environment, corresponding to that specified for the verification of the specifications, in order to verify compliance with them (Figure 2.9).

Figure 2.9 - Technical approach presented by Blaedel et al.

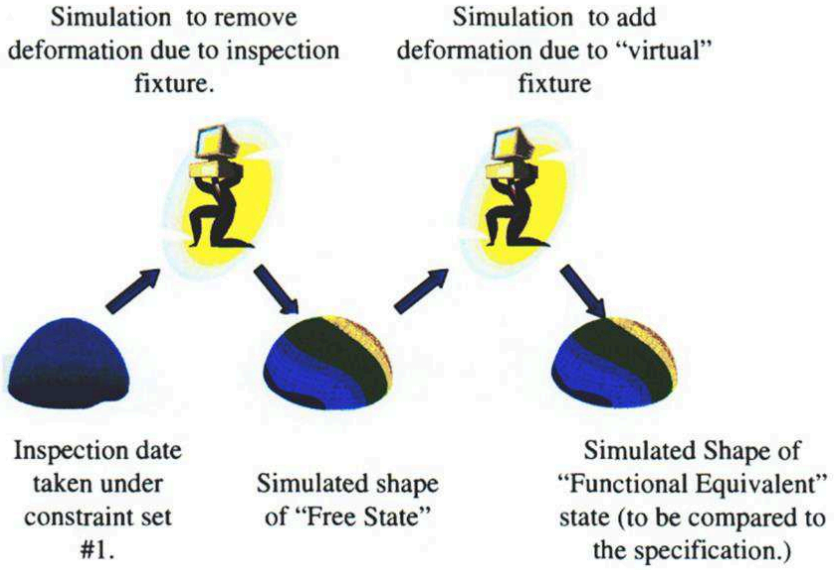

Source: [23].

The experimental approach was comprehensively detailed. It was applied to the case of a thin hollow cylinder where a load is applied physically to the component while its geometry is measured before and after the load application. On the other hand, the finite element simulation support mesh is defined from a nominal mesh and measurements performed on the component before loading (the measurement grid corresponds directly to the reference mesh). The geometry under load is simulated. The results obtained are shown in Figure 2.10. Some relevant remarks on the implementation were also included: (a) the modeling of the boundary conditions is difficult, so it is advisable to define experimental support that limits friction, for

example; (b) the uncertainties related to acquisition and treatment are not insignificant. A non-exhaustive list of sources of uncertainty and precautions to be taken to limit them is proposed: measurement, geometric idealization, Finite Element type and properties, contour conditions identification, etc. Finally, the knowledge of the material parameters is of great importance in the simulations result. They were evaluated experimentally by standard tests on test bodies (Young's modulus and Poisson's coefficient).

Figure 2.10 - Contour plot of radial displacements for the experimental data and initial finite element discretization.

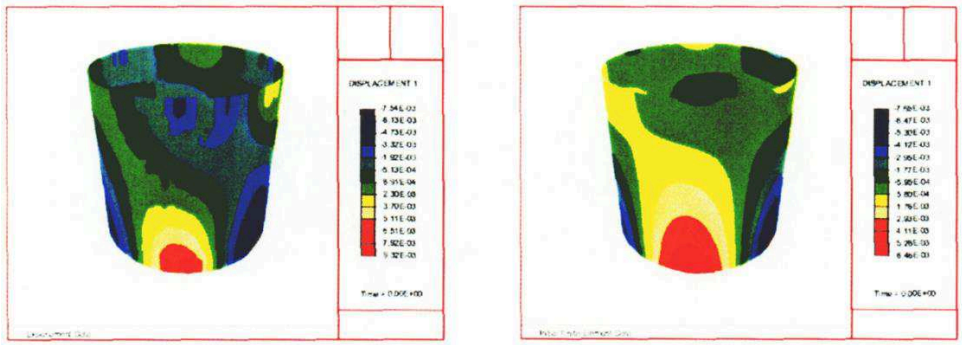

Source: [23].

Many studies are based on the same reasoning to evaluate, by measurement and simulation, the free-form geometry of flexible components. Lartigue et al. [24] considered that it is theoretically possible to consider the actual shape geometry in a given configuration as the sum of the geometry of its shape in the free state and its deformation due to its measurement environment (measurement and gravity support) under the hypothesis of small displacements. Some ways are given to evaluate the geometry of the actual shape by the non-contact measurement and the deformation generated by the finite element simulation measurement environment. It is then possible to determine the geometry in the free state by the difference between the two terms.

Similar to the Blaedel method, Hirata et al. [25] proposed the patented method applied to the measurement of a windshield of motor vehicles. In this case, the measurement is performed when the component is placed in three support points., The purpose is to determine the geometry of the same component installed in a different geometry support (different position and number of supports).

Weckenmann and Gabbia [26] and Weckenmann and Weickmann [27] chose to construct a finite element mesh directly at the measurement points. In both works, the measurements of the components were carried out by means of a fringe projection system,

which makes it possible to obtain a large number of measurement points. The construction of a finite element mesh is therefore performed directly at these points. It can be seen in Figure 2.11 that the mesh is very dense and not optimized for the finite element calculation. This may require a heavy computational effort.

Figure 2.11 - Triangle mesh (right) created from point cloud (left).

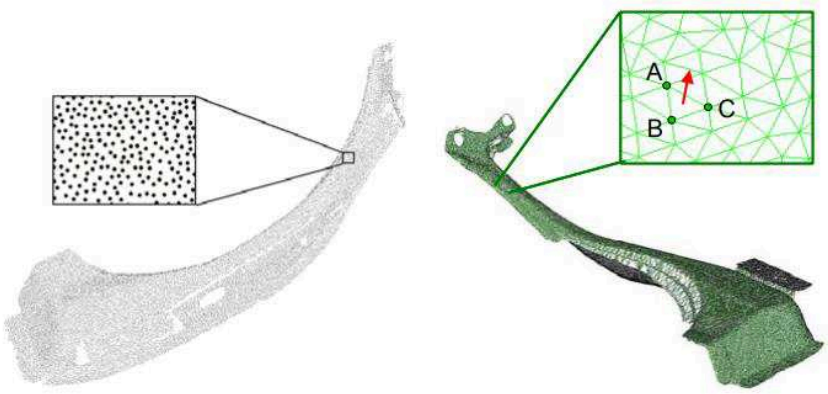

Source: [27].

The strategy followed by Jaramillo et al. [28] is different because it depends on a previous deformation of the nominal to stick to the measurement points. The use of the basic radial functions approximates the measurement and simplifies the representation of the finite element. The paper [29] also shows that this method allows one to take into account any failures in the scanning process. In the same way Radvar-Esfahlan and Tahan [30] performed a non-rigid registration by deforming the mesh at the measurement points. The presented method is then based on the notion of geodesic distance (shortest path between two points, drawn on a surface) to determine correspondences between two geometries of the same part in two different configurations. The principle is detailed in Figure 2.12.

The Generalized Numerical Inspection Fixture (GNIF) algorithm generates sets of corresponding sample points between CAD and meshes considering them as geodesic distance metric spaces (assuming that the deformation of a non-rigid part in the free state is isometric) and finding distributions of the sample points that minimize the distortion. It is thus possible to compare certain characteristics of the components measured in different configurations. However, the sample points (which are used as boundary conditions in the simulations) were

considered free of error, i.e., they were assumed to be measured on an ideal measurement system, which is not the case in practice.

Figure 2.12 - Generalized Numerical Inspection Fixture method.

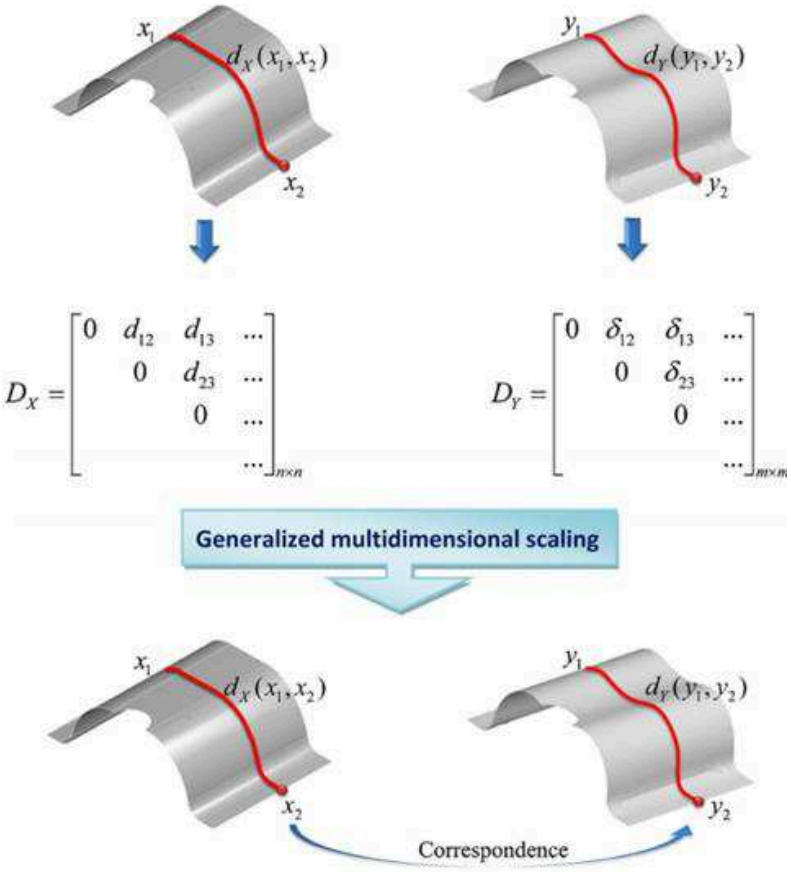

Source: [30].

Gentilini and Shimada [31] implemented a similar method. First a mesh in the cloud of measurement points is built in the manner of Weckenmann and Weickmann [27]. However, they introduced in the process an operation to convert the mesh in order to adapt it to the simulation of finite elements. The mechanical support model of the simulation is first recalculated by comparing a theoretical geometry under load with an actual geometry under identical load. In this case, the method of calibrating the parameters of the material depends strongly on the assumption of a low-defect shape of the component in relation to the magnitude of the deformations. The theoretical geometry assembled is then simulated. The results were compared to the geometry of the actual mounted shape, an application case is shown in Figure 2.13. The author focused on characterizing the performance of the implemented method, analyzing the reflection lines. These are visually very close to the examples presented. Finally,

the author hardly addressed the notion of the gap between the two geometries, stating that the results were acceptable to him. The average difference between the assembled geometry measured and the simulated mounted geometry was of the order of one millimeter for 550 mm and 150 mm plates.

Figure 2.13 - Simulation results of assembled geometry.

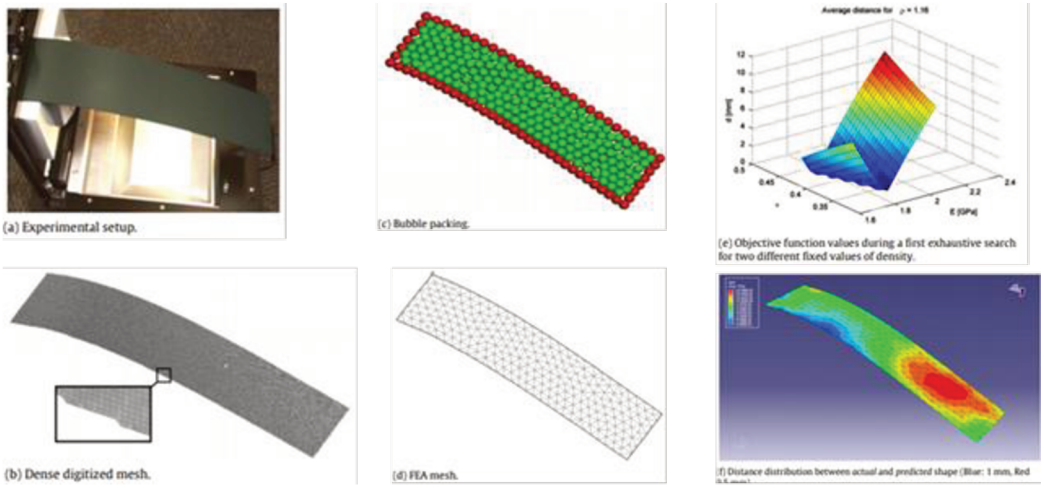

Source: [31].

In another work, Abenhaim et al. [32] detailed the implementation of a similar method, with the purpose to deform the restricted theoretical geometry to correspond to the measures. This deformation is a function of the component measurement configuration and the measurement point cloud. An important contribution was the implementation of a method to exclude measurement data corresponding to local defects due to its environment. It is then possible to verify compliance with the formal requirements. In [33] Abenhaim also provided a state of the art of measurement techniques for flexible components without dedicated support, presenting the methods already mentioned.

Inspired by industrial inspection techniques, Karganroudi et al. [34] presented a method, named "Virtual Mounting Assembly-State Inspection (VMASI)". This method consists of applying virtually weights as restraining loads on non-rigid parts predicting the functional shape of a deviated part. Also defects such as plastic deformation can be detected, as shown in the schematic flowchart (Figure 2.14). The authors concluded that the amplitude of defects seriously affects the possibility of recovering the shape of a deviated manufactured part in assembly-state.

Figure 2.14 - Schematic flowchart of VMASI method.

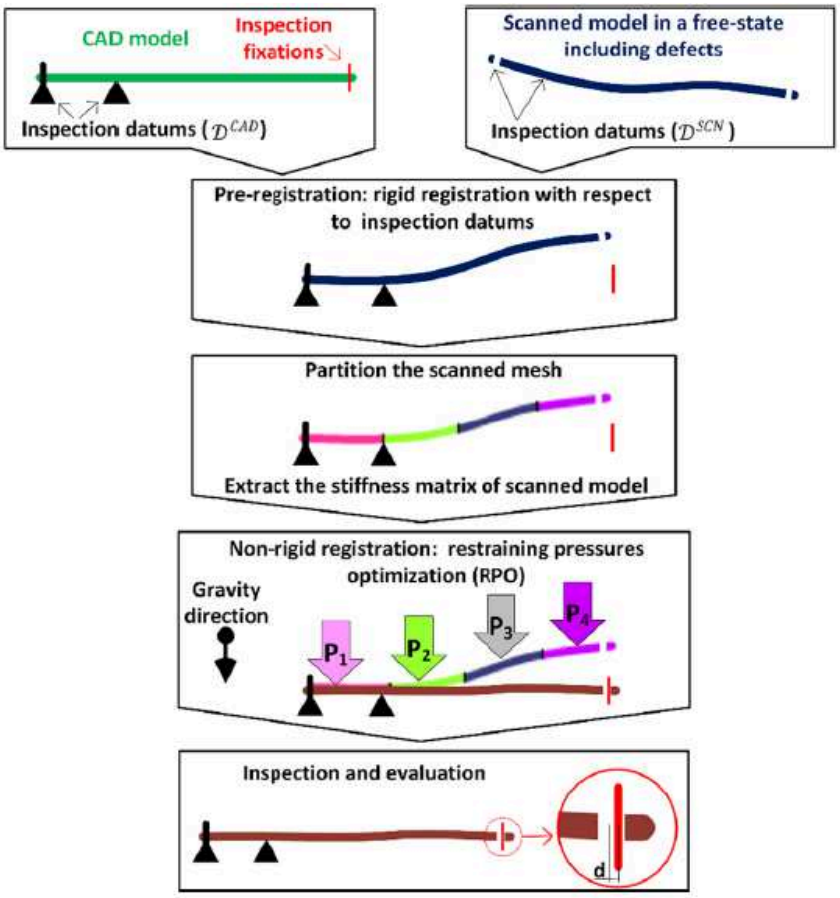

Source: [34].

2.3.2 Methods not based on FEM to evaluate part deformation

As it is a matter of identifying geometric characteristics in the measurement data Aidibe et al. [35] and Abenhaim et al. [36] proceeded in the same way to recalibrate the discrete measurement data and limited theoretical geometry, calculating the projected distances between the actual points and the corresponding reference points, as shown in Figure 2.15. However, the Abenhaim's work was not based on finite element analysis. The method, called Iterative Displacement Inspection (IDI), iteratively deforms the CAD until it resembles the scanned mesh of the manufactured part. This deformation occurs in such a way as to ensure smoothness of the surface by combining rigid and non-rigid registration. The algorithm can still distinguish surface deviations from the part's distortion.

Figure 2.15 - Schematic diagram of (a) a part without a zone with profile deviations and (b) a part with a zone with profile deviations.

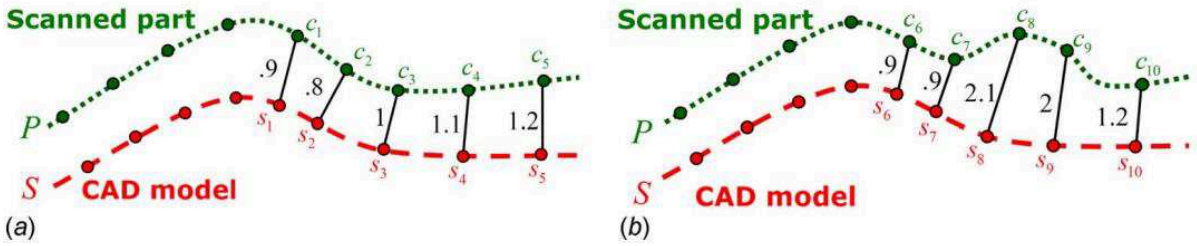

Source: [36].

The IDI method becomes inefficient for parts with large defects (global) because it is limited to localized defects. Other drawback is the lack of FEA, the method depends on the identification of some flexibility parameters that depend on the thickness. By means of a statistical analysis of the calculated distances values, it is possible to locate the geometric deviations. This method seems to be well suited for identifying local defects, typical of composite materials. Aidibe [37] addressed the matter of detecting local geometric defects by performing a Thompson-Biweight test, based on the variation of the curvature.

However, the related works deal with the point cloud registration of rigid components relative to their nominal geometry. In flexible components, combining the two geometries can be a complicated process. In fact, the deformation the component undergoes may be of an order of magnitude greater than the geometric deviations. The results of measuring flexible parts depend on the configuration of the component, as this affects its geometry. However, it is often necessary to explore the measurement result, obtained in a given configuration, and a non-rigid registration of the measurement data is required.

Another approach presented by Aidibe and Tahan [5] uses the identification method to compare two data sets and to recognize the profile deviation by combining the curvature properties and the extreme value of statistic tests. Satisfactory results in terms of error percentage in defect areas and the estimated peak profile deviation were found when using a typical industrial sheet metal for tests and simulations. But the method is limited to relatively-flexible parts where small displacements are predictable because the core of the algorithm is based on the Gaussian curvature comparison. The same authors (Aidibe and Tahan) proposed a method for optimization of the Coherent Point Drift algorithm (CPD) in order to adapt it to the relatively-flexible parts problem [38]. They realized it by introducing two criteria: the

stretch criterion between the nominal model and the aligned one, and the Euclidian distance criterion between the aligned nominal model and the scanned part. The results using this method are shown in Figure 2.16.

Figure 2.16 - Results of the proposed method by Aidibe and Tahan.

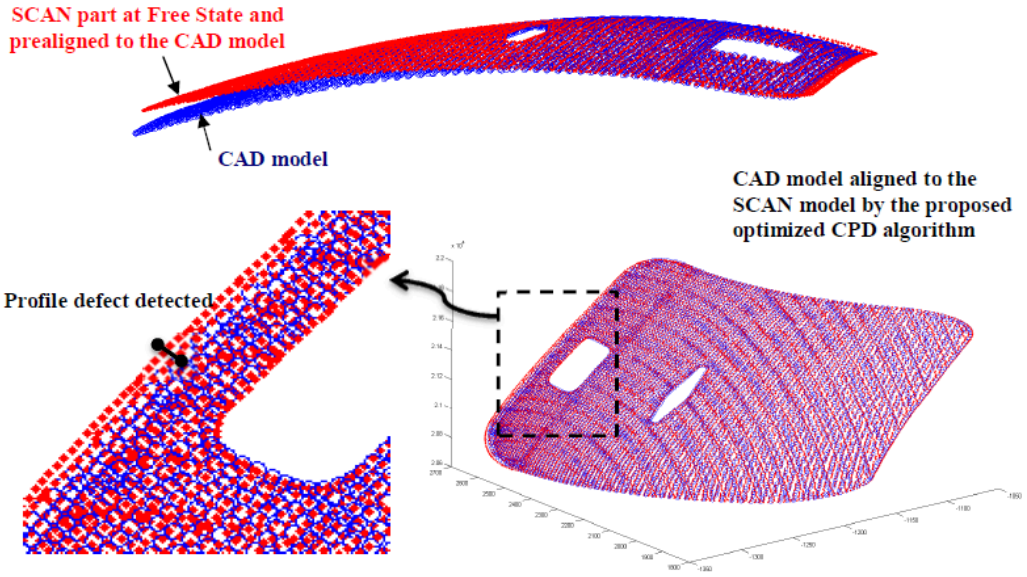

Source: [38].

An approach to compensate the spring-back that occurs during the inspection of parts in the stamping forming process was developed by Wang et al. [39] using an optical measurement system. In this process, after the scanning, the point cloud is converted into a polygonal object (mesh), repaired and filled the holes, and compared with the deformed CAD model. This method proved to be more accurate and complete than the traditional method and the spring-back compensation can effectively reduce die tryout time.

2.3.3 Overview

With the literature review, it was possible to identify the main methods for inspection of non-rigid parts without the need of specialized devices. In addition to the classification presented in the previous sections, it is possible to classify the inspection methods according to the direction of the applied displacement: some of them deform the scanned mesh, targeting the nominal geometry, while others deform the nominal geometry (CAD) to approximate the actual digitalized surfaces. This classification is shown in Table 2.1.

Table 2.1 - Virtual clamping methods classification based on the displacement direction.

Scanned mesh to CAD	Blaedel [23] - First definition Simulated Displacement Method
	Wecknmann et al. [26] - Virtual Distortion Compensation
	Gentilli and Shimada [31] - Predicting and evaluation the post-assembly shape
	Karganroudi [34] - Virtual Mounting Assembly-State Inspection
CAD to Scanned mesh	Jaramillo et al. [28] - FEM trained radial basis functions
	Abenhein et al. [36] - Iterative Displacement Inspection
	Radvar-Esfahlan and Tahan [30] - Generalized Numerical Inspection Fixture
	Aidibe and Tahan [5] - Curvature estimation-based approach
	Aidibe and Tahan [38] - Coherent Point Drift

Source: the author.

From the different approaches outlined, however, it is possible to recognize a common route to the process. This route is shown in Figure 2.17. For the measurement step, several authors proposed the acquisition of the part surface using optical measurement systems, highlighting the ability of these systems to capture a dense amount of information for subsequent studies of deformation. The data processing step may include point cloud treatment, meshing, CAD reconstruction, or simply the mesh preparation for further virtual deformation (through FEM or not). And finally, the conformity assessment of the part by comparing it with its reference geometry (CAD or the scanned mesh).

Figure 2.17 - General route identified in the virtual clamping methods.

Source: the author.

The operational issues of the steps identified are detailed in the following section in order to identify major difficulties and opportunities for improvement, as well as to define the study methodology.

2.4 OPERATIONAL ISSUES

2.4.1 Acquisition

In this section, the 3D data acquisition of flexible components geometry of complex form is considered. Many aeronautical and automotive components are flexible because of their thin shape and small thickness. It is also possible to consider them complex because, besides presenting more than one curvature, the geometric deformations resulting from their flexibility may be important.

Li and Gu reviewed the state of the art in the inspection of free-form surfaces [21]. A wide range of measurement technologies, with contact or not, was detailed. Non-contact measurement systems are considered much faster than contact measurement systems, because they can acquire a large number of points relatively quickly. However, the quality of the measurement is worse and the measurement conditions are restrictive (surface appearance or material quality). Li and Gu also discussed the data analysis methods associated with these technologies.

Savio et al. carried out a state of the art study of the measurement technologies for these free-form components [40] and classified the main methods as shown in Figure 2.18. A comparison of the measurement systems (contact and non-contact) was also performed by Martinez et al. [41]. The authors pointed out that the large number of points obtained by non-contact measurements makes it possible to have a detailed representation of the digitized object. However, the dispersion of the points can affect the measurement accuracy, usually resulting in a measurement uncertainty greater to that of contact measurement. Vagovský et al. evaluated the performance using optical measuring system with fringe projection technology [42]. The authors concluded that the 3D scanner is incapable of providing acceptable results when measuring small and high accuracy parts. However, the 3D scanner is really sufficient and provides acceptable results when digitizing medium and large sized objects.

Figure 2.18 - Typical range of measuring uncertainty vs. part dimension for different categories of measuring systems.

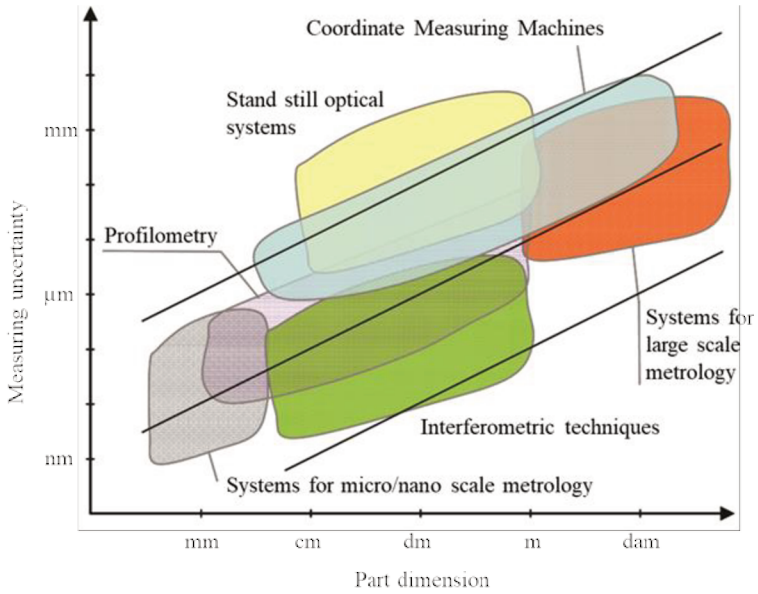

Source: [40].

Li et al. evaluated the influence of brightness in the scanning process using the optical measurement system (with fringe projection technology) [43]. The experimental results indicated that the ambient light does not contribute obvious systematic errors in terms of accuracy. However, notable random errors were observed when the artifact was scanned in different capture sequences under the same lighting condition. Besides that, the experiments revealed that the measurement repeatability is still a significant issue for the optical triangulation and techniques based on active scanning.

The laser line scanning on a CMM was investigated by Van Gestel et al. [44]. They concluded that the scan depth has an important influence on systematic and random errors of the tested scanner. In-plane and out-of-plane angles have an important effect on the measured standard deviations, because the measurement noise is mainly concentrated in the depth direction of the scanner. The stability test showed that warming-up effects have a major influence on the accuracy of the laser line scanner. Satyanarayana et al. [45] evaluated the scanning process parameters for the dimensional inspection of standard spheres and defined the optimal parameters for these measurements: scanning intensity 2.0 ms and scanning speed 5 mm/s.

Lima [46] performed a comparative study of measurement systems (contact and non-contact) applicable to the dimensional control of freeform surfaces in medium and large parts. The work addressed the measurement uncertainty associated with the photogrammetry scanning process. However, the analysis can be extended to other optical measurement systems. In this way it is possible to map the main sources of uncertainty associated with each point of the cloud, as shown in Figure 2.19.

Figure 2.19 - Ishikawa diagram of the main sources of errors in optical measurements.

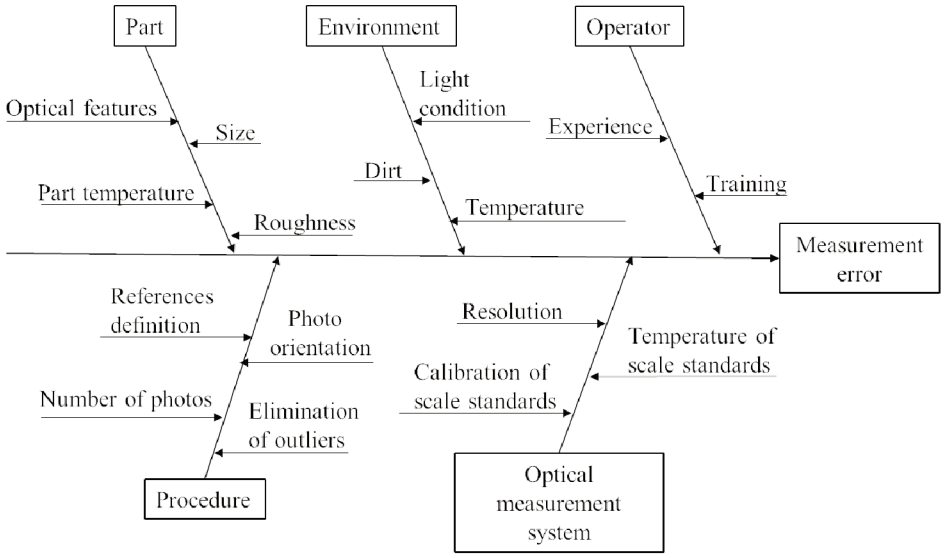

Source: adapted from [46].

2.4.2 Point cloud treatment

Whatever the acquisition system used, it is necessary to process the raw data to extract the requested information. This section outlines methods adapted for the treatment of point clouds resulting from non-contact optical measurement. The first step is to combine the measurement data with the reference geometry. This is usually the nominal geometry when an inspection is executed. In the context of flexible component metrology, it can be a distorted nominal geometry.

The classical method presented by Besl and McKay [47] uses an ICP (Iterative Closest Point) algorithm, which allows one to combine two representations of the same geometry. It is based on a preliminary survey of the so-called neighboring points, that is, the points of the cloud closest to the points of reference. A minimization of the distances between the measuring points and the corresponding reference points, in the least-squares direction, allows a recalibration of

the measuring points in relation to the nominal, applying a rigid movement of the body to all these points. It is necessary that the measuring points are in a configuration relatively close to the reference, making a preliminary registration, to speed up the convergence and improve the quality of the final result.

The measurement point clouds can be very dense, so it is interesting to use methods to quickly navigate through the data, mainly based on a preliminary partitioning space. For this reason, another method was introduced by Bentley in [48]. In the present case, the most efficient partitioning methods in terms of computational time are those of the k-d-tree type. It is a matter of dividing the space of the measuring points by successive divisions. Then, a closer neighbor search algorithm, described by Friedman et al. [49], creates a link between the two discrete geometries. Alternatives to researching the nearest k neighbors or searching for the nearest neighbor in a specific area also exist. When working with raw measurement data with noise, it is interesting to select a set of points instead of an isolated point.

Another method, the work of Bispo and Fisher [50], was based on the Besl ICP algorithm, as it involves the matching of a measurement point cloud with a nominal geometry. After this, it is necessary to determine the defect in a measured way by analyzing the residual distances between the incompatible measuring points and the reference geometry. The validation of specification compliance was performed by verifying whether the reconstructed image using the residual distances is within the specified tolerance zone. By presenting some variations, but also based on this principle, Huang et al. [51] and Gu and Huang [52] analyzed the use of a partial point cloud to perform the registration based on the less noisy data.

Additionally, Pahk and Ahn [53] proposed the use of six specific points to perform a preliminary registration. If the points are selected correctly, the preliminary register allows the dense point cloud to be positioned in a sufficiently close configuration to ensure fast convergence and a quality result. Li and Gu [54, 55] performed the preliminary registration using feature-based alignment measurements (curvature and geometric elements). However, the related works deal with the point cloud registration of rigid components relative to their nominal geometry. In flexible components, combining the two geometries can be a complicated process, if the point clouds represent different conditions of the part. In fact, the deformation the component undergoes may be of an order of magnitude greater than the geometric deviations.

With the point clouds consistent and aligned, the next step is to analyze them. Lartigue et al. [56] proposed some quality indicators to characterize a point cloud, as follows:

a) **noisy**: linked to data sampling errors, considering the deviations between the points and the surface model;
b) **density**: linked to the sampling density, dependent on the user's scan planning and the digitizing technology;
c) **completeness**: figures out the importance of the gaps existing in the point cloud;
d) **accuracy**: is close to the common notion of measurement uncertainty.

These indicators allow one to qualify a point cloud and judge the quality of a scan data. It may also be interesting to observe the influence of these parameters on the quality of the final result of a measurement, i.e. the value of the characteristic identified from the scanned points. As an example, these concepts were used by Mahmud et al. [57] in the optimization of the scanning path of a laser sensor in order to maximize the quality of all digitized data. The requirement for accuracy was defined as 1/8 of the tolerance range of the specification in question. The density is dependent on the density of the laser line and the scanning speed. Accuracy is determined by the choice of scanning angles and distances; and noise is limited by the choice of scanning angles and the application of a matte layer on the component. With a good quality mesh, it may be necessary to reconstruct the 3D part to use in the next steps. Some of the developed methods perform the deformation only with the points of the cloud, however, there are still difficulties to represent mechanically possible movements.

2.4.3 CAD reconstruction

After the acquisition phase, some steps are required to prepare the 3D data obtained until the final CAD model is reached. The process named "Reverse Engineering" (RE) or "CAD Reconstruction" aims at the generation of 3D mathematical surfaces and geometrical features representing the real geometry of a physical part [58]. Modeling a physical object geometry from scanned data still presents some issues in providing a consistent representation, mainly considering the mechanical engineering perspective. In this respect, the process calls for methods capable of producing virtual parts:

a) accurate and close to the original design of the part;
b) obtained in a limited time span;

c) easily spendable for the designer's final need, which usually involves a step in a CAD/CAM/CAE software [59].

Breaking the CAD Reconstruction process into the five steps illustrated in Figure 2.20, the vast majority of techniques available in literature are considered [60, 61, 62, 63, 64].

Figure 2.20 - General flowchart of CAD reconstruction.

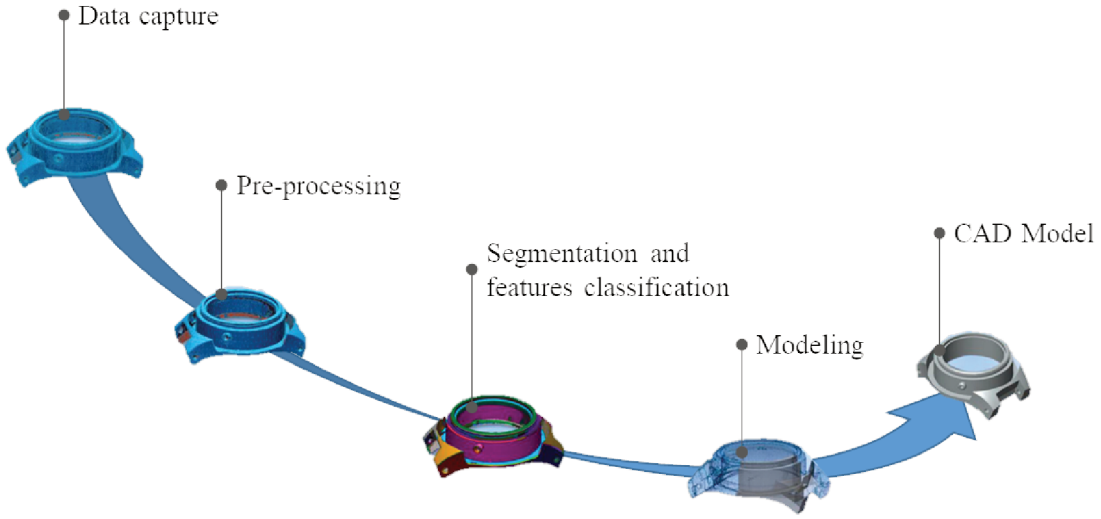

Source: adapted from [58].

With the point cloud, a polygonal mesh can be automatically and efficiently created. The fundamental concept of triangulation is Delaunay triangulation, even though many other mathematical algorithms have been proposed, including marching cubes [65], alpha shapes [66], ball pivoting algorithm (BPA) [67], Poisson surface reconstruction [68], moving least squares [69], etc. Using some geometrical criteria (e.g. curvature analysis) it is possible to segment the acquired tessellated model or point cloud into separated regions. The goal of this step is to separate the structure of regions that are as close as possible to a mathematically perfect geometric elements that compose the model to be reconstructed [70].

Theologou et al., in [71], presented a classification of segmentation techniques by subdividing them into ten principal categories (clustering, region growing, surface fitting, topology, spatial subdivision, spectral analysis, boundary detection, motion characteristics, probabilistic models and co-segmentation). The results obtained in the modeling step may differ

significantly depending on the strategy chosen to perform the task. Therefore, the modeling phase is the most important step of the whole process presented in Figure 2.20. For example, the compliance of geometric constraints, time required to build the model and readiness of the obtained digital representation for downstream applications are relevant aspects that can provide different results [58].

In the case of freeform surfaces, adjusting a single surface to a point cloud has been extensively investigated and reconstruction algorithms have been proposed [72]. However, freeform surfaces methods generally generate an aesthetically pleasing result and potentially very little deviation errors, but they do not allow one to retrieve any additional level of information in the reconstructed model beyond the mere 3D geometry. In other words, no geometrical feature is generally identified by using these approaches, thus limiting the subsequent use of the generated model (at least for engineering purposes) [58].

An approach where the reconstruction process can handle various types of conventional CAD features (i.e. extrusion, revolution, sweep, loft) as well as B-Spline surface features is presented by Wang et al. using an appositely devised segmentation system [60]. Some applications examples are shown in Figure 2.21. The final step of the whole process flow (generation and finishing of the CAD model) depends the kind of the desired result obtainable by using a given RE strategy. For example, for Additive Manufacturing (AM), the final CAD can be optimized for this purpose.

Figure 2.21 - Reconstruction results of industrial parts by Wang et al.

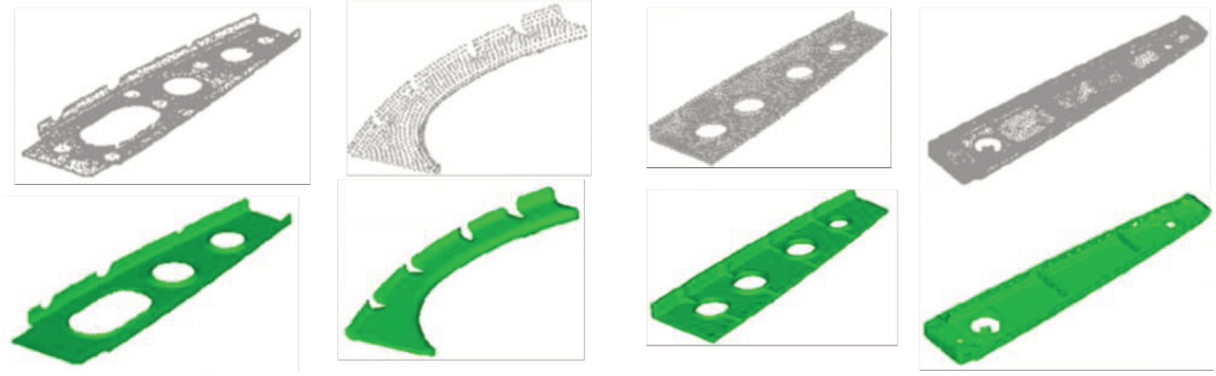

Source: [60].

2.4.4 FEM simulation

Wilvert [73] defines the FEM as a numerical method to solve differential equations, which is widely employed in many fields of study for finding approximate solutions to real

continuous problems. Typically, a finite element analysis has some principal steps, as shown in Figure 2.22. After creating the 3D CAD model, it is necessary to assign the properties of the material to the elements that will be simulated. Typically, the materials are assumed homogeneous and isotropic. In most cases, these assumptions are not completely accurate. These variations result in uncertainties in the simulation results [23].

Figure 2.22 - Typical flowchart for Finite Element Analysis (FEA).

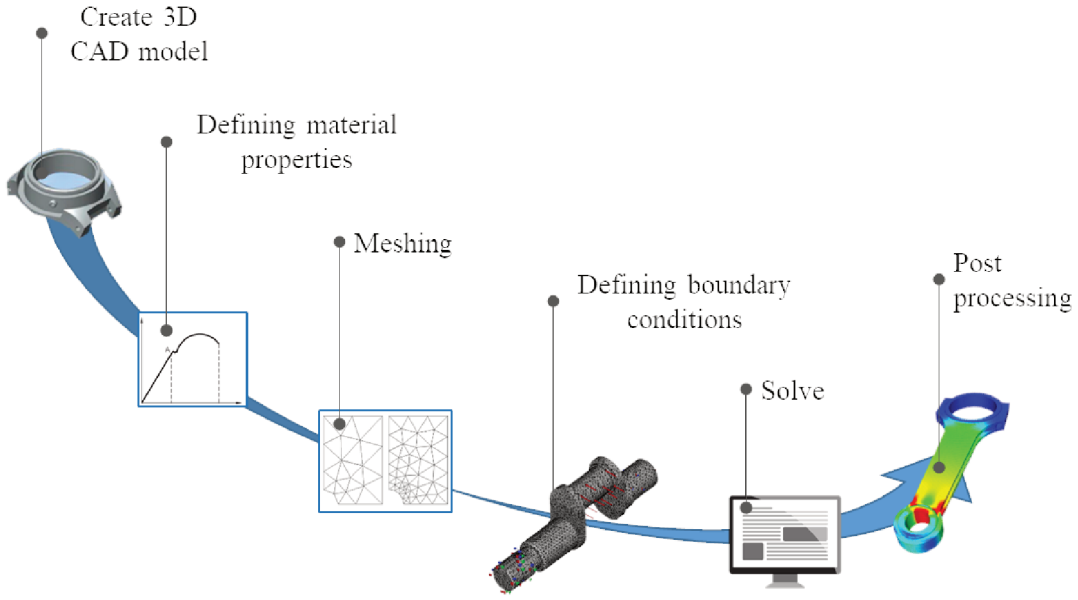

Source: the author.

When using FEA, different types of one-, two- or three-dimensional elements can represent the model's geometry, as shown in Figure 2.23.This step is named as meshing or discretization. The size of the element, at least in the test period, should be large, in order to avoid unnecessary waste of computing resources and time [74]. However, the element size significantly affects the accuracy of the simulation results and, consequently, finer meshes certainly lead to better results. To speed up the solution, it is common practice to implement different mesh densities according to local gradients [76]. The influence of element size can be identified with a refinement study of the mesh, keeping the other parameters constant [77].

Figure 2.23 - Different types of Finite Elements.

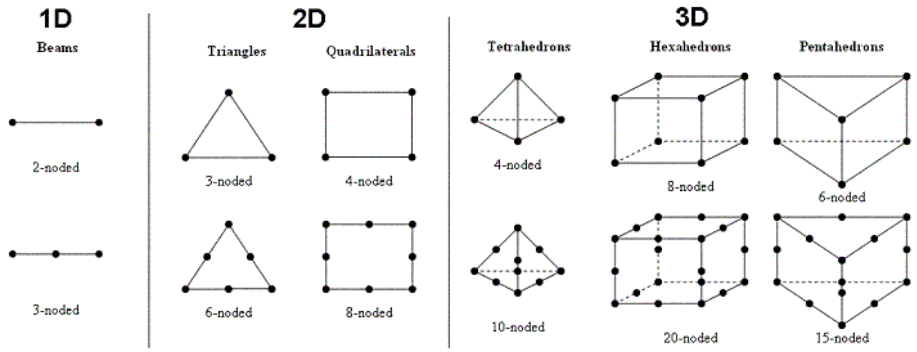

Source: [75].

The complexity of the physical interactions of the modeled geometry results in boundary conditions that are difficult to model. The boundary conditions have an essential influence on the results, since they form the stiffness matrix, along with material properties [1]. For experimental purposes, it is possible to design geometries and accessories to create the desired boundary conditions. Exact constrain fixture also reduces unknown forces acting on the model [23].

For solving, the linear static solutions are more common. The popularity of this solution often obscures the fact that it represents a significant assumption of linear events. Linear events are typically idealized in most problems and usually does not really exist [78]. Finally, the post-processing step involves performing the evaluation of output data.

2.5 CHAPTER SUMMARY

Through the literature review, it was possible to identify the main methods used for inspection of non-rigid / flexible parts using physical clamping systems and also the methods in development, which simulate the deformations to evaluate the geometric deviations of the parts, without the use of specialized clamping systems.

Considering the virtual clamping method, a more in-depth investigation of the key steps of the process used by several authors in their studies was carried out. Nevertheless, no studies using enforced displacements as boundary conditions, having as reference the datum system specified in the GPS step were identified, as well as an evaluation of the metrological performance in comparison to the methodology currently used. For this reason, a methodology

was developed and tested on parts of a real application. The method, materials and equipment used are described in the next chapter.

3 EXPERIMENTAL PLANNING

The previous chapter presented conceptual descriptions that were essential for the definition of a methodological proposal for the virtual inspection of non-rigid parts. This methodology is presented in detail in this chapter, together with definitions of equipment and parts used in the experimental tests.

3.1 METHOD DEFINITION

Considering the processes studied in Chapter 2 and evaluating the advantages and disadvantages highlighted by the authors, a new methodology for virtualization of the process for non-rigid parts inspection was proposed. The aim of this research is to assess the metrological performance of this process, which uses optical scanning systems in combination with virtual clamping (numerical simulation) for the geometric inspection of non-rigid parts. The virtual clamping proposed method (VCM – Virtual Clamping Method) is represented in a simplified manner in Figure 3.1.

Figure 3.1 - Virtual clamping approach flow

Source: the author.

3.1.1 CAD and geometric specifications

As already mentioned (Section 2.1.2), the CAD and the geometric specifications define the requirements that the part must comply with to be considered functionally proper and they are defined by the part designer.

3.1.2 Simplified fixturing

Even though we are working with virtual inspection, it is still necessary to use simplified clamping systems in order to hold the part stable while capturing the data. In

addition, correction of direction or neutralization of the gravity may be necessary in the simulation steps. In this way, knowing the supporting points is essential.

Simplified fixture systems do not necessarily have to be accurate and do not need to follow the specified geometric conditions as they will only be used as part support. However, their repeatability should be evaluated if it is used for more than one measurement. For its manufacture many materials can be used. In this work, the simplified CS have been developed and fitted with modular components made from high tensile aluminum (EN AW 7075) from Witte® Company, as showed in Figure 3.2, featuring a coefficient of thermal expansion of $23.2 \cdot 10^{-6}$ K^{-1}, ensuring dimensional stability during the measurements [79]. They can be easily coupled smoothly by means of special elements.

Figure 3.2 - Modular components used for the CS assembly.

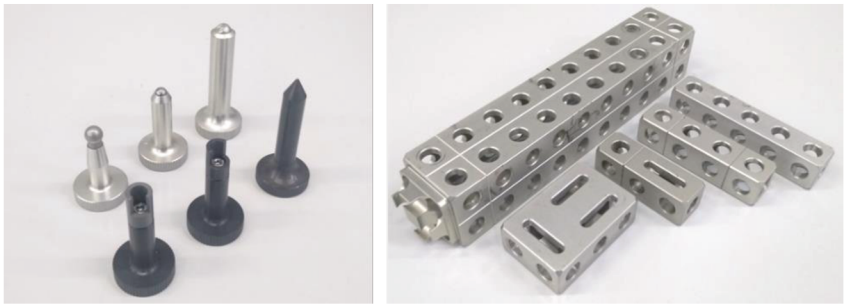

Source: the author.

These fixturing systems were designed for easy part mounting and minimum interference with the optical scanning. Pins, tooling balls and clamps can also be used. To know the contact points between the part and the fixturing system, after the assembly, it is necessary to measure them. These data are used in the simulation of gravity neutralization.

Since the elements to be digitized are geometric and can be measured with a low density of points, it is possible to perform this process with tactile measurements. The technical characteristics of the used articulated measuring arm for data capture are presented in Table 3.1.

Table 3.1 - Technical characteristics of the articulated measuring arm.

Continue

Model	Platinum FARO®
Software	CAM 10

Conclusion

Measuring radius	1200 mm
Digital increase	0.001 mm
Probe diameter	3.00 mm
Calibration date	20/11/2016
Calibration certificate	3618/16
Max. Error (2.RMS)	0.070 mm

Source: the author.

3.1.3 Optical scanning

In order to capture the surface data of the parts with a high density of points, the optical systems are indicated. In this work, the measurements were carried out by the ATOS Compact Scan 3D optical scanner, manufactured by GOM GmbH Germany (Figure 3.3a) configured to "camera position 300" (Figure 3.3b) configuration with one projector and two cameras. This optical 3D scanner is based on the principle of triangulation. Fringe patterns are projected with the central projector and observed with two cameras. The 3D coordinates of each pixel are calculated and the surface is represented by a point cloud in the software.

Figure 3.3 - 3D optical scanner ATOS Compact Scan (a and b); virtual representation of the measuring volume (c).

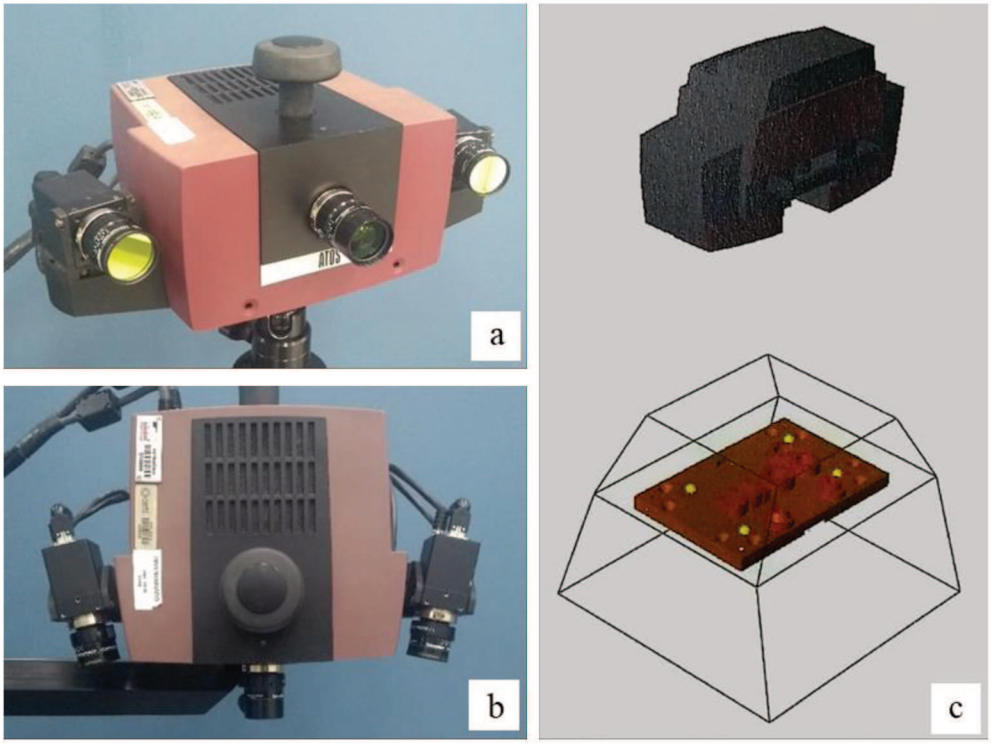

Source: the author.

The whole optical system had to be warmed up to be in operating condition. Warming up took approximately 30 min. The technical characteristics of ATOS Compact Scan are listed in Table 3.2. After the acquisition step, a polygon mesh of the part surface is generated. All the scans were performed in laboratory environment at CMI (Center of Metrology and Instrumentation – CERTI Foundation).

Table 3.2 - Technical characteristics of ATOS Compact Scan.

	Measuring volume	
	MV250	MV500
Camera resolution	2 megapixels (1624 x 1236 pixels)	
Measuring volume (L x W x H)	(250 x 190 x 190) mm	(500 x 380 x 380) mm
Measuring point distance	0.153 mm	0.309 mm
Angle between cameras	25°	25°
Measuring distance	570 mm	570 mm
Software	GOM ATOS Professional	

Source: [80].

The dimensional consistency of a measuring system is ensured by the calibration procedure recommended by the manufacturer – GOM GmbH, as in [80]. The calibration process consists of multiple image records of a standard panel at various distances and orientations. Based on the characteristics of the camera lenses and the projector, the software calculates the 3D coordinates of the points from the calibration object in the 2D image. At the end of calibration process are shown the calibration results for camera and projector.

For the used measuring volumes the manufacturer recommends the use of reference points markers with diameter of 3.0 mm for MV250 and 5.0 mm for MV500, which are attached on the clamping system or on the scanned object, allowing the tracking of the scanned part or the ATOS in the measuring space. The measurement standard parameters for the calibration process, proposed by the manufacturer, are shown in Table 3.3.

Table 3.3 - ATOS Compact Scan measurement parameters.

Continue

Number of exposure times	1
Min. fringe contrast	15 grays values
Max. residual	0.20 pixel
Depth limitation mode	Automatic limitation mode

Conclusion

Corner mask size	0
Measurement resolution	Full resolution
Settings of Checks	
Check: Sensor movement?	Enabled
Max. sensor movement	0.10 pixel
Check: Lighting change?	Enabled

Source: the author.

Another point to note is that the scanned parts should be able to return the fringes back to the camera system. For this reason, shiny parts, which reflect the most of the incident light, it is necessary the use of a surface coating. For this coating, Nonaqueous Developer (Type 2 - Visible Dye according AMS-2644) SKD-S2 from Magnaflux Spotcheck® was used, which allows correct reflection of light and contrast of the part surface.

After the part is ready for scanning, it is important to define a scanning procedure, because the non-standardization introduces deviations which would propagate to the final measurement results. Lemes, in [1], defined the main steps of the scanning process:

a) scanned part preparation (application of reference points markers and anti-reflection spraying if necessary);
b) set of scans taken at different positions (number of scans depends on part complexity);
c) the partial views are joined together using the reference points (automatic step performed by software);
d) surface extraction with trimming of unnecessary parts and background objects;
e) automatic and manual error corrections (filling holes, smooth mesh, bridges, etc.);
f) and finally, export the scanned surface into appropriate format for further processing.

In this case, the chosen file format was the STL (Surface Tessellation Language), which is a simple file format to specify triangle meshes. Lemes cites in his work [1] some problems related to the use of STL files: the main problem with STL file is that file size is dependent upon the number of vertices. The STL files have many redundant features which make the file larger unnecessarily. Higher resolution parts with smooth curves require extremely large file sizes. Even so, this is the most common file format for 3D scanners.

However, it is very inadequate for finite element analysis. Therefore, a modeling step is required.

3.1.4 Modeling

The transformation of the file from scanning to a 3D solid for finite element simulation (mesh pre-processing, segmentation and modeling), as mentioned in the previous sections, is necessary. For the pre-processing and segmentation steps the use of the software GOM® Inspect V2017, Hotfix 7 was adopted.

In the segmentation step, the 3D mesh is divided into regions which represent distinct surfaces of the part and can be approximated by various primitive geometries like planes, cylinders, spheres, polynomials, etc., and then exported separately for the modeling process. This step followed the segmentation process based on a topology method [71].

The modeling step was performed within a well-established CAD environment (Siemens NX® Version 9.0) allowing a known and familiar environment for the designer and provided with state-of-the art CAD modelling tools to be used in the template design. The surfaces obtained by 3D scanning are represented as meshes of triangles and are converted to 3D parametrized surfaces which are mathematical representations of 3D geometry that can accurately describe any shape from a simple 2D-line, circle, arc or curve to the most complex 3D organic free-form surface or solid [1].

3.1.5 Virtual clamping

In the proposed method the virtualization of the assembly process occurs simulating the clamping operation by means of finite element method. If the part has been scanned in a position other than the assembly position, it is necessary to neutralize the gravity force of the first position for subsequent application in the correct direction (when simulating the assembly conditions). The simulation software used for this analysis was Siemens NX® Version 9.0. This software was chosen due to its capabilities of exporting analysis results and its efficient user environment for mesh definition and boundary conditions tasks.

Figure 3.4 - Examples of discretized surfaces with triangular elements.

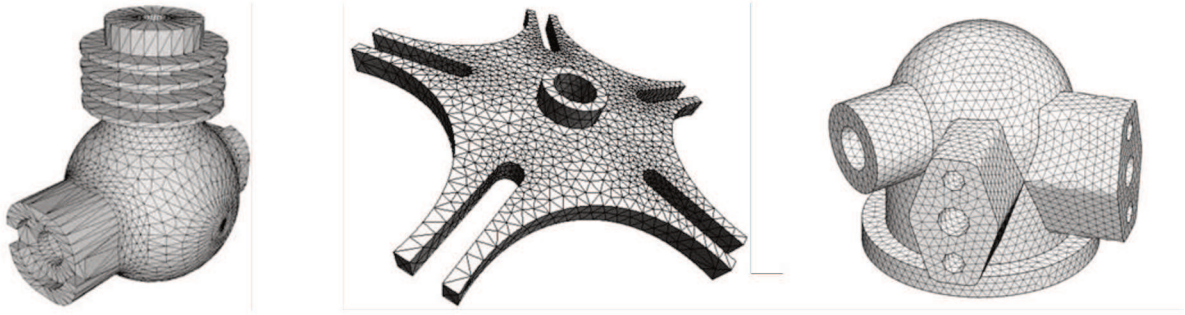

Source: the author.

The first step in finite element analysis (FEA) is to discretize the surface with finite elements (Figure 2.23). The FEA software is capable of meshing the regular CAD surfaces automatically or manually. In this work, parabolic tetrahedral elements were used, which better represent the deformation field within the element (when compared to the linear tetrahedral element) and due to its versatility, can represent any solid body. According to Alves Filho [81], these elements are widely used in applications where the calculation of tensions and deformations requires accurate results. Some examples of these surfaces discretized with tetrahedral elements are shown in Figure 3.4.

The second step is to choose the appropriate boundary conditions. To define boundary conditions that correspond 100% to the actual model is impossible, because the contact between the model and the reference points was realized through curved surfaces. The parts are virtually clamped setting forced displacements determined from measurement between the modeled CAD and the reference points (datum from part specification) as shown in Figure 3.5.

Figure 3.5 - Forced displacement representation.

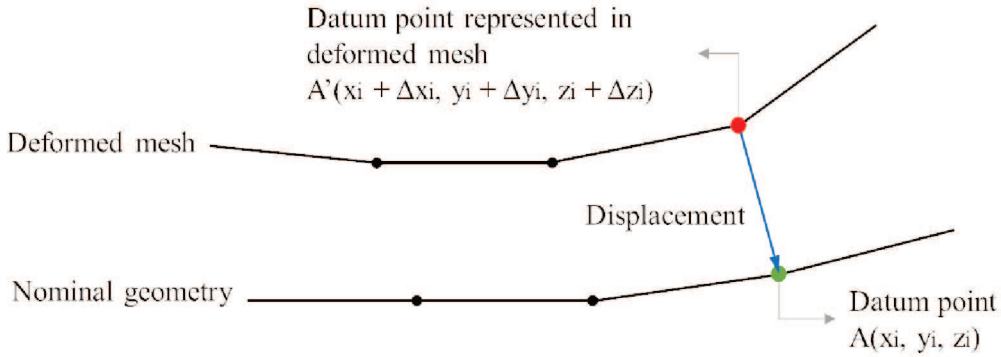

Source: the author.

However, since the FE analysis has to have node to node connections, these boundary conditions are also node-based and they have to be defined for each node separately. In these circumstances, it is unjustifiable to set the displacements for each node of the mesh, because it would require too much manual operations. For these reasons, in this work, the displacements were applied only in the datum points, specified for the study. After the simulation, the deformed mesh is exported in a JT (Jupiter Tessellation) file for the comparison with the nominal geometry and tolerances evaluation.

3.1.6 Part evaluation

The final step is the evaluation, comparing the FEA results and the specifications, resulting in a color map with the vectorial deviations and GD&T values. With this information, it is possible to classify if the part is compliant or not with its specifications. This step was performed using also GOM Inspect software.

Now, since the CAD model and the final meshes generated after the simulations are spatially in different positions, it is necessary to consider the different alignment methods. Following the parts specifications and evaluating the possibilities presented by the software, the most adequate alignment concept is RPS (Reference Point System). The RPS alignment is based on given reference points with coordinates (X, Y and Z). Based on these coordinates, the meshes are aligned to the coordinate system of the nominal CAD by means of linked measuring elements. For the RPS alignment it is necessary to adjust the effective direction for each linked RPS point.

The link between the nominal and the actual elements (measured surface) is related to the measuring principle. In this case, the RPS points require an intersection with the actual mesh. Therefore, considering the normal axis to the surface of the RPS point, an intersection point is created on the mesh. With the points created in both geometries (CAD and mesh), the software moves the mesh by rotating and translating it iteratively until it reaches the lowest combined points deviations. After the alignment, the surface deviations and geometric tolerances could be checked. The surface profile evaluation occurs through the method described in Section 2.1.2.

3.2 METROLOGICAL EVALUATION

For the metrological performance evaluation, the main objective of this work, two aeronautical parts were evaluated, allowing an evaluation of real industrial applications. Both parts are in the zone B of the plot presented in

Figure 2.1. The comparisons were performed between the proposed method (using virtual clamping system) and by the conventional method (using physical clamping system). The results obtained through the two methods were also subjected to a statistical analysis. To evaluate the general performance of the process, some intermediary checks were defined, in order to identify the contribution of each step in the overall process repeatability.

For an overview of the both methods, a detailed flowchart is presented in Figure 3.6 (next page), along with the checks and evaluations performed. To evaluate the conventional method, the clamping systems were also constructed with high tensile aluminum (EN AW 7075) from Witte® Company, and calibrated on a CMM. The technical specifications of the CMM used in this step are shown in Table 3.4.

Table 3.4 - CMM Mitutoyo parameters.

Model	Beyond A916 Mitutoyo
Software	MCOSMOS
Calibration date	18/04/2018
Calibration certificate	1521/17
Maximum permissible error	(3.3 + 6.3·L/1000) µm; L in millimeters
Probe tip	3.00 mm
Probing method	Single points

Source: the author.

Using the physical clamping systems, it is impossible to capture the underside of the parts. Therefore, only the specifications of the upper surfaces were evaluated. All method evaluation forms, as identified in Figure 3.6, will be detailed in the following sections.

3.2.1 Intermediate evaluation

Through intermediate numerical evaluations, it is still possible to identify which steps can negatively influence the process and add errors to the results. For this, as identified in Figure 3.6, intermediate tests were carried out to evaluate the preliminary results. The process of

identifying, evaluating and prioritizing the risks associated with the process and how they affect the results is defined as “risk management” [82].

Figure 3.6 - Flowchart of the methods steps.

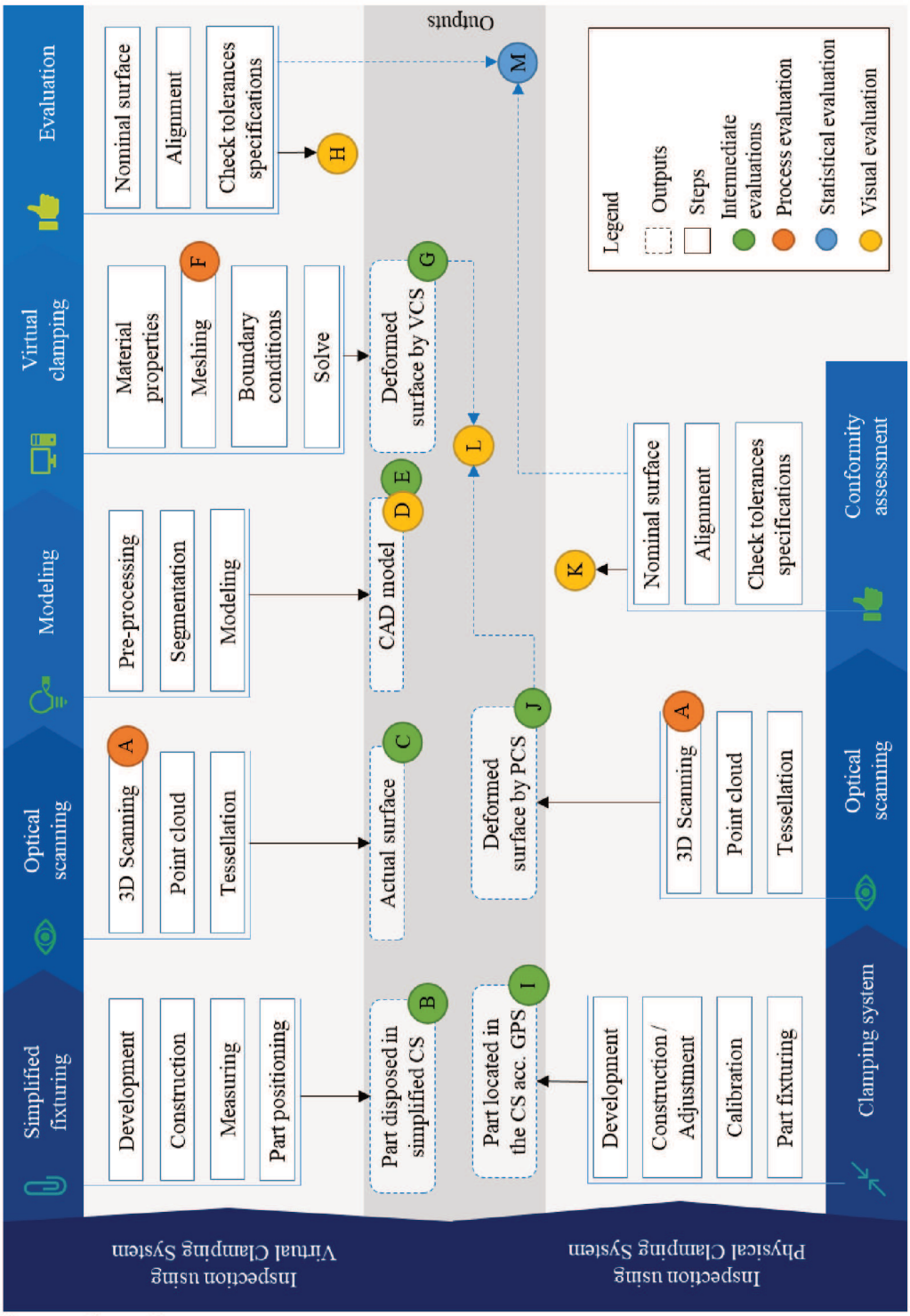

Source: the author.

For each step associated with green circles shown in Figure 3.6, the intermediate evaluations were done following the method 'Short Version of Evaluating the Measurement Process (EMP)' presented by Wheeler and Lyday in [83]. The method uses range and average charts, and estimates a standard deviation of the irreducible core of measurement error due to the measurement process. In the case of this work, since the processes were performed by the same operator and using the same measuring instruments, this standard deviation estimates just how good the measurement could be. For this analysis were used control points randomly distributed on the upper part surface.

The measurement results were organized, as shown in Table 3.5, by adopting two indexes, and each value being represented by 'X_{pi}', where:

- (p) represents the control points adopted to evaluate the part surface. The number of control points is represented by the letter (m) and;
- (j) represents the repetition. The number of repetitions is represented by the letter (n).

Table 3.5 - Organization of measurement results.

j		1	2	3	… n
P	1	X_{11}	X_{12}	X_{13}	X_{1n}
	2	X_{21}	X_{22}	X_{23}	X_{2n}
	3	X_{31}	X_{32}	X_{33}	X_{3n}
	… m	X_{m1}	X_{m2}	X_{m3}	X_{mn}

Source: the author.

The basic computations for this analysis are shown below:

I. Control limits for Range Chart:

The average range can be calculated using the equation

$$\bar{R} = \frac{1}{m}\sum_{p=1}^{m}[(max\, X_{pj} - min\, X_{pj}) \;\forall\; j] \tag{3.1}$$

where $max\ X_{pj}$ and $min\ X_{pj}$ represent, respectively, the maximum and the minimum value for each line (p value). And the Upper Control Limit (UCL) can be calculated through the equation:

$$UCL_R = \bar{R} \cdot D_4 \tag{3.2}$$

where the D_4 value is a constant based on the subgroup size (n). The D_4 values for a subgroup size of 2 to 5 are shown in Table 3.6. Other constants that will be used later are also presented.

Table 3.6 - Average and Range charts factors for using the Average Range.

I	D_4	A_2	d_2
2	3.268	1.880	1.128
3	2.574	1.023	1.693
4	2.282	0.729	2.059
5	2.114	0.577	2.326

Source: [83].

The Lower Control Limit (LCL) for Range Chart is null for subgroup size up to 6.

II. Control limits for Average Chart:

The Grand Average can be calculated using the equation

$$\bar{\bar{X}} = \frac{1}{m}\sum_{p=1}^{m}\frac{1}{n}\sum_{j=1}^{n}X_{pj} \tag{3.3}$$

and it is possible to estimate the three Standard Deviations values for $\bar{X}$ through the equation

$$3\sigma_e = A_2 \cdot \bar{R} \tag{3.4}$$

where the A_2 value can be found in Table 3.6. The Upper and the Lower Control Limits for Average Chart can be calculated through the equations (3.5) and (3.6).

$$UCL_{\bar{X}} = \bar{\bar{X}} + \bar{R} \cdot A_2 \tag{3.5}$$

$$LCL_{\bar{X}} = \bar{\bar{X}} - \bar{R} \cdot A_2 \tag{3.6}$$

III. Standard Deviation:

Considering that measurement processes are statistically under control, according to [83], an estimation of the Standard Deviation of the measurement errors can be calculated through the equation

$$\hat{\sigma}_e = \frac{\bar{R}}{d_2} \tag{3.7}$$

where the d_2 value can be found also in Table 3.6.

IV. Variance:

In the same way, the Variance can be calculated through the equation

$$\widehat{\sigma^2}_e = \left(\frac{\bar{R}}{d_2^*}\right)^2 \tag{3.8}$$

where the d_2^* value depends on the number of subgroups used for $\bar{R}$ and the number of observations per subgroup. The values for some combinations are shown in Table 3.7.

Table 3.7 - Bias correction factors for using Average Ranges to estimate Variances.

p	$j = 4$	$j = 5$
5	2.096	2.358
10	2.078	2.342
15	2.071	2.337
20	2.068	2.334

Source: [84].

The estimates of standard deviation and variance, as presented, are defined by Wheeler as unbiased estimators [84]. The author also defines them as best estimates using a small sampling. With the calculated values, it is possible to plot the data on control charts. An example is shown in Figure 3.7.

Figure 3.7 - Example of control chart.

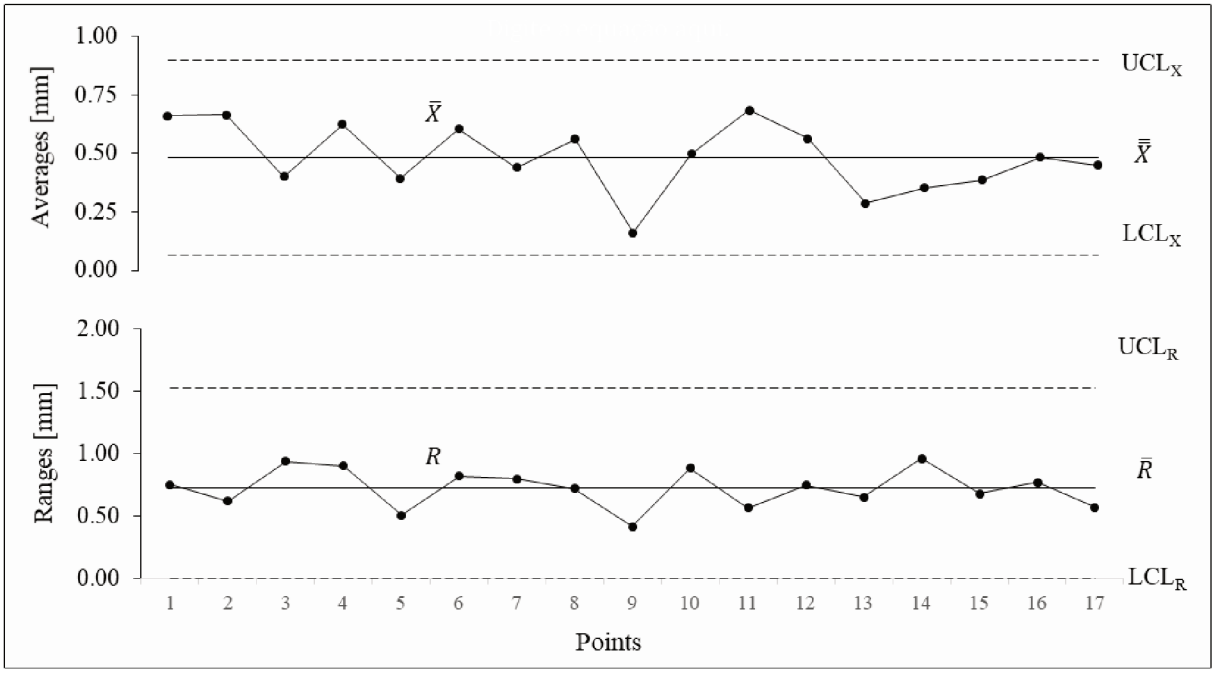

Source: the author.

3.2.2 Process evaluation

The parameters used in some steps were defined through convergence tests, knowing the reference values. These specific steps are identified in Figure 3.6, with orange circles. One of these specific steps refers to 3D scanning process. For scanning of parts larger than the measurement volume, it is necessary to move the scanner. The different images are processed in a way that concatenates the captured surfaces through the reference points markers, present in each capture. Under these circumstances, different trajectories during the process of image capture and concatenation of the acquired geometries were tested. For this test an artifact, (Table 3.9. The numbers represent the diameters of the spheres and the letters the spacing between them.

Figure 3.8) based in [85], was used, and a similar process to the acceptance test for 3D optical measurement systems was performed.

To know the nominal values of sphere spacing and the spheres diameter the artifact was calibrated on a CMM. The technical characteristics and the measurement parameters are shown in Table 3.8 and the reference results are presented in Table 3.9. The numbers represent the diameters of the spheres and the letters the spacing between them.

Figure 3.8 - Artifact constructed to evaluate the metrological performance of ATOS.

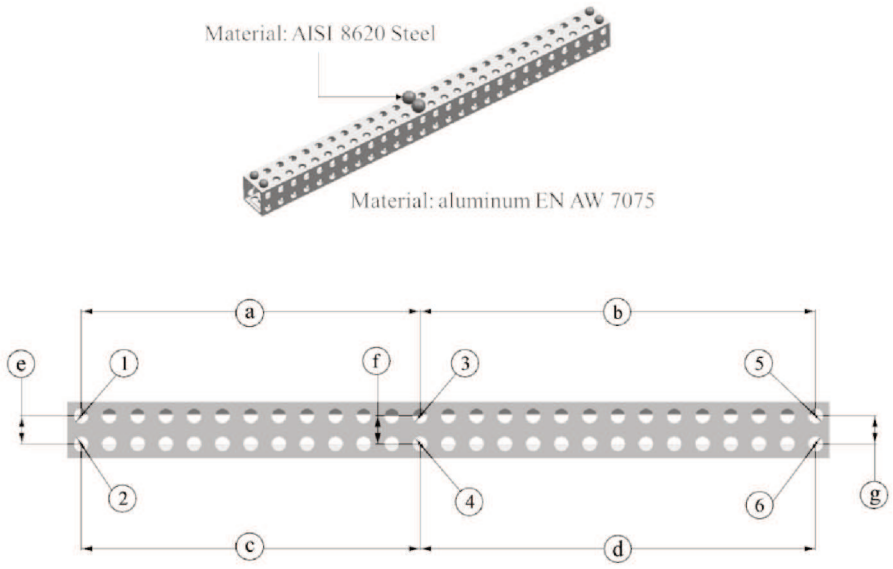

Source: the author.

Table 3.8 - CMM Zeiss parameters.

Model	PRISMO ZEISS
Software	CALYPSO
Calibration date	19/12/2017
Calibration certificate	4254/17
Maximum permissible error	(0.2 + L/1100) µm; L in millimeters
Probe tip	3.00 mm
Probing method	Single points

Source: the author.

Table 3.9 - General data and artifact dimensions.

General data		
Calibration temperature		293.25 K (20.1 °C)
Coefficient of thermal expansion for sphere spacing		23.2e-6 K^{-1}
Coefficient of thermal expansion for diameter		6.6e-6 K^{-1}
Basic dimensions		
Sphere spacing		325 mm / 25.5 mm
Diameter of the lateral spheres		14.5 mm
Diameter of the center spheres		22.2 mm
Calibrated dimensions		
Characteristic	Value*	Measurement Uncertainty**
Spacing a	324.708 mm	0.005 mm
Spacing b	324.945 mm	0.005 mm
Spacing c	325.017 mm	0.005 mm
Spacing d	324.972 mm	0.005 mm
Spacing e	25.409 mm	0.005 mm
Spacing f	25.728 mm	0.005 mm
Spacing g	24.875 mm	0.005 mm
ØSph.01	14.499 mm	0.002 mm
ØSph.02	14.499 mm	0.002 mm
ØSph.03	22.228 mm	0.002 mm
ØSph.04	22.228 mm	0.002 mm
ØSph.05	14.504 mm	0.002 mm
ØSph.06	14.502 mm	0.002 mm

Source: the author.

* As the other scans were taken in the same environmental conditions, equipment and operator, it is not necessary to correct the values for the reference temperature: 293.15 K (20 °C).

** The reported expanded uncertainty is stated as the standard uncertainty of measurement multiplied by k = 2, which for a t-distribution with ν_{eff} = infinite degrees of freedom corresponds to a coverage probability of approximately 95%.

To calculate the measurement uncertainties presented in Table 3.9, the following sources were considered: type A (five replications) and type B (CMM calibration uncertainty, temperature variation, thermal expansion coefficient and thermometer uncertainty). The evaluated movements and the reference points markers positions are shown in Figure 3.9. The scanning process for this evaluation was performed five times for each test. The best way to conduct the scanning process was chosen using the method presented in [83], Section 3.2.1, selecting the process with the lowest repeatability index and evaluating the bias of the measured data according [86].

Figure 3.9 - Evaluated trajectories and the reference points positions.

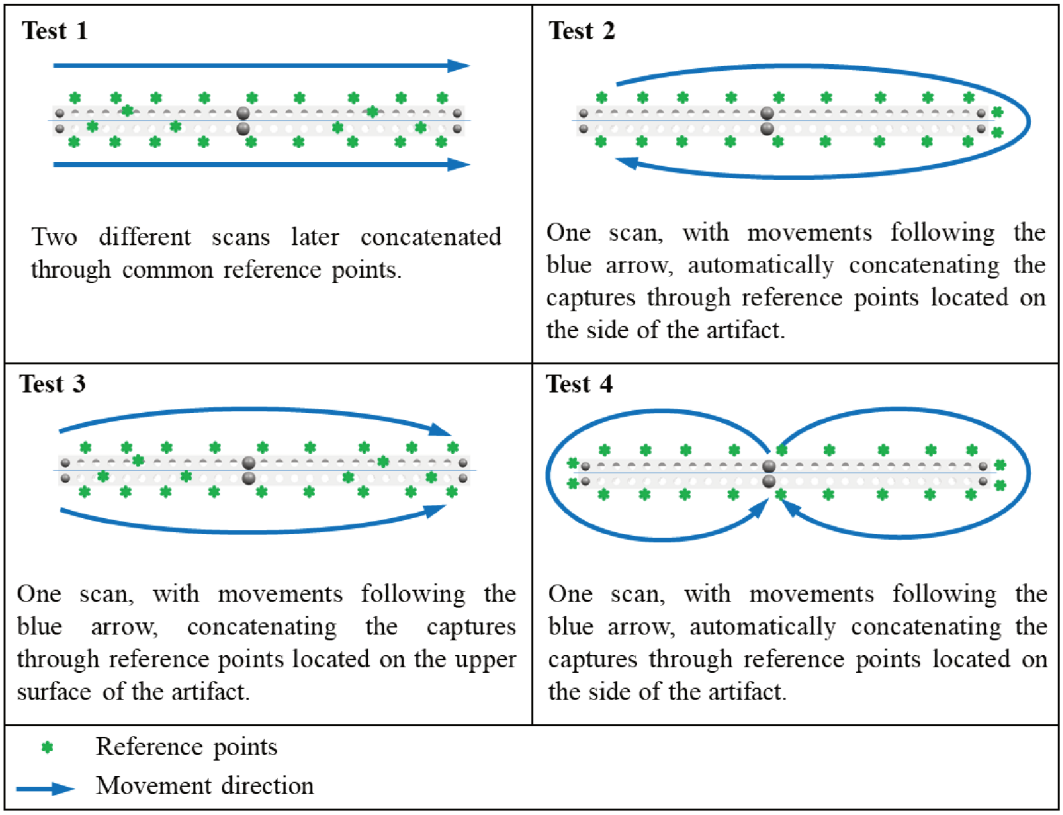

Source: the author.

As the thickness of the part is directly linked to the stiffness of the component, the actual vs. scanned thicknesses values were compared at specified points and located close to the edge regions of the parts. The reference measurements in the physical parts were done using a micrometer with control of applied force and adapted for measurement on curved surfaces

with the aid of standard spheres (Figure 3.10). The result of the average of 3 measurements of each point was considered. A deviation of up to 3% is acceptable.

Figure 3.10 - Micrometer with control of the applied force.

Source: the author.

Another specific step related to the meshing in the FEA step. The density of mesh elements was defined with a relation between accuracy and computational cost, performing the analyzes having as only variable the size of the mesh (same boundary conditions and same loads). The best combination was selected when, with a decrease in the amount of mesh element, an example is shown in Figure 3.11, there is no more significant gains in computational processing time. The analysis of the test results was performed by comparing the value of the maximum displacement in both parts. A deviation of up to 1% is acceptable.

Figure 3.11 - Representation of the amount increase of mesh elements.

Source: the author.

3.2.3 Statistical evaluation

For these tests, the used values were those identified as the profile of the surface error of the tolerated surface, considering all the points and following the methodology presented in Section 2.1.2. The hypotheses used for this evaluation were:

- H0: The virtualization of the geometric inspection process of non-rigid parts, using FEM has the same metrological performance as the inspection of physically

clamped parts. Considering that, the clamping process is simulated with boundary conditions that represents accurately the physical clamping process.

- H1: The virtualization of the geometric inspection process of non-rigid parts, using FEM has significantly smaller metrological performance as the inspection of physically clamped parts.

When the distribution of the process is unknown, the use of F-test for this inference becomes invalid, since it is extremely sensitive to non-normalities [87, 88]. A relatively robust alternative that allows one to consider that populations are normally distributed (or approximately normally distributed) is the one-way ANOVA (analysis of variance). The ANOVA produces an F-statistic, the ratio of the variance calculated among the means to the variance within the samples. If the group means are drawn from populations with the same mean values, the variance between the group means should be lower than the variance of the samples, following the central limit theorem. A higher ratio therefore implies that the samples were drawn from populations with different mean values [89].

The statistical model for a one-factor experiment is defined by the equation

$$Y_{ij} = \mu + \tau_i + \epsilon_{ij} \qquad \begin{cases} i = 1,2,\dots,a \\ j = 1,2,\dots,n \end{cases} \tag{3.9}$$

where Y_{ij} represents the random variable that represents the *ij*-th observation, μ is the global average, τ_i is the effect of *i*-th treatment, ϵ_{ij} is a component of random error, a is the number of treatment and n is the number of repetitions.

Considering the method (i) being able to assume values of 1 (for proposed method) or 2 (for the conventional method), the calculation of ANOVA test is performed using the following equations:

$$F_0 = \frac{2(n-1) \cdot SQ_{trat}}{SQ_E} \tag{3.10}$$

where

$$SQ_{trat} = \sum_{i=1}^{2} \frac{\left(\sum_{j=1}^{n} X_{ij}\right)^2}{n} - \frac{\left(\sum_{i=1}^{2}\sum_{j=1}^{n} X_{ij}\right)^2}{2n} \tag{3.11}$$

$$SQ_E = \sum_{i=1}^{2}\sum_{j=1}^{n} {X_{ij}}^2 - \frac{\left(\sum_{i=1}^{2}\sum_{j=1}^{n} X_{ij}\right)^2}{2n} - SQ_{trat} \quad (3.12)$$

This F-statistic follows the F-distribution with degrees of freedom 1 for and $2(n-1)$ under the null hypothesis. Considering the presented hypotheses, comparing the F_0 value with F_α (found in [90]), if the $F_0 > F_\alpha$ the null hypothesis is rejected and the alternative hypothesis is accepted as true.

3.2.4 Visual evaluation through color maps

According Figure 3.6, the intermediate evaluation of modeling step was evaluated visually comparing each modeled CAD with its respective scanned mesh. The final results were also visually evaluated in three comparisons:

a) comparison between the ideal CAD and the scanned surface, processed by virtual clamping method;
b) comparison between the ideal CAD and the scanned surface physically clamped;
c) comparison between the scanned surface physically clamped and the scanned surface, processed by virtual clamping method.

3.2.5 General evaluation

A measurement result is complete only when accompanied by a quantitative statement of this uncertainty. For this reason, an analysis of the influence factors and sources of errors was performed. The goal of this step is to identify the process steps that need to be better developed, or that require more attention in their application.

3.3 CASE STUDIES

To evaluate the presented methods, two parts of an aircraft winglet (named as Part A and Part B) were used, allowing an evaluation in a real industrial application. An example of winglet is shown in Figure 3.12. Both parts are in the zone B of the plot presented in

Figure 2.1. The first case, the Part A presents one curvature, being able to be considered uniformly conical, and has the flexibility ratio expressed by the value of 4.13. In the second case, the part B presents three curvatures, and has the flexibility ratio expressed by the value of 20.83.

Figure 3.12 - Example of a passenger aircraft winglet.

Source: [91].

The sample parts are relatively large non-rigid covering panels, typically used in aerospace industry, made of Aluminum 2024-O, having a mean thickness of 2.0 mm with machined reductions (pockets) in order to reduce weight. The parts also have different degrees of curvatures. The parts and their design specifications are shown in Figure 3.13 and Figure 3.14. The used specifications are adopted only for study purposes, and were defined according the International Standard for Geometrical Product Specifications (GPS): ISO 1101-2017 [14].

Following the content described in Section 2.1.2, for these parts the DRF (Datum Reference Frame) is specified using a HDF (Hyperstatic Datum Frame). For each part, a N-value was adopted, enough to keep the part stable during the scanning process, and at the same time, allowing the curvature evaluation by the methods previously described.

Figure 3.13 - Part A: design and geometric specifications.

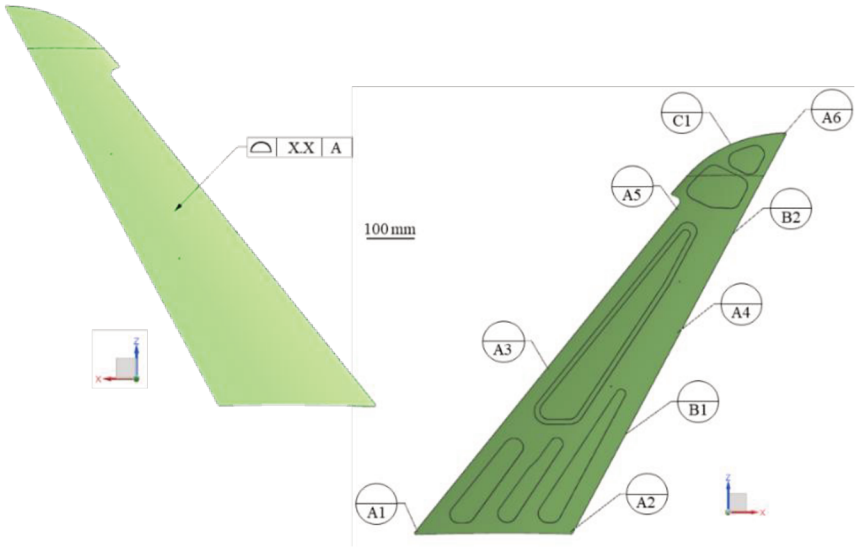

Source: the author.

Figure 3.14 - Part B: design and geometric specifications.

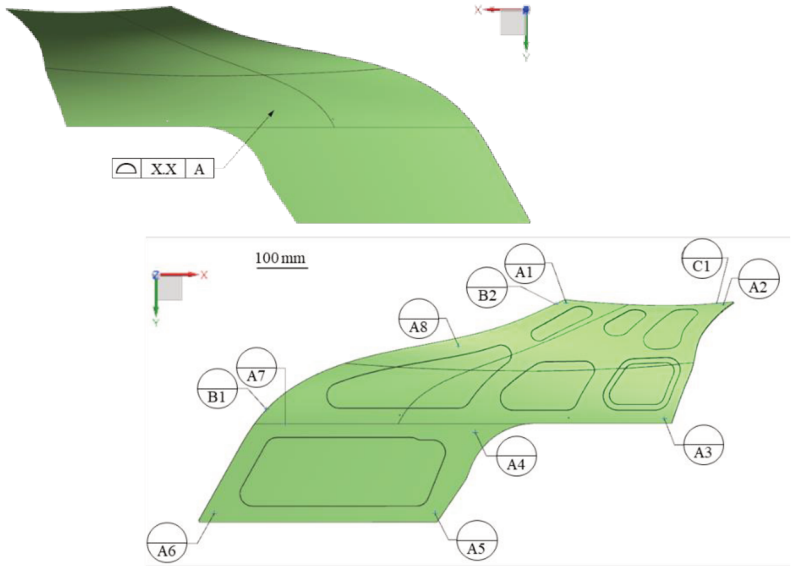

Source: the author.

In summary, the measured parts are large, thin and have non-uniform thickness. For this reason, it is necessary to scan both sides of the parts. It is well known that the anisotropy of the material is an important contributor to errors. However, due to the unavailability of material for material testing, the nominal values of the mechanical properties of the isotropic material were considered. These properties are shown in Table 3.10.

Table 3.10 - Mechanical properties of Aluminum 2024-O.

Characteristic	Value
Young Modulus	$73.1 \cdot 10^9$ N/m²
Poisson Ratio	0.33
Density	2780 kg/m³
Tensile Yield Strength	$9.5 \cdot 10^7$ N/m²
Ultimate Tensile Strength	$1.79 \cdot 10^8$ N/m²
Elongation at Break	12%

Source: [92].

The tests presented in Figure 3.6 were performed five times. The control points chosen for intermediate evaluations (Section 3.2.1) are presented in Figure 3.15 and Figure 3.16. The points chosen for the scanning process evaluation, according Section 3.2.2, are shown in Figure 3.17 and Figure 3.18.

Figure 3.15 - Part A: Control points.

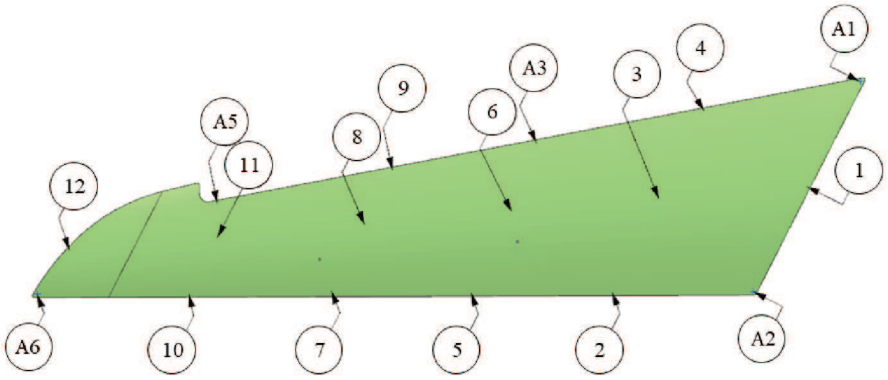

Source: the author.

Figure 3.16 - Part B: Control points.

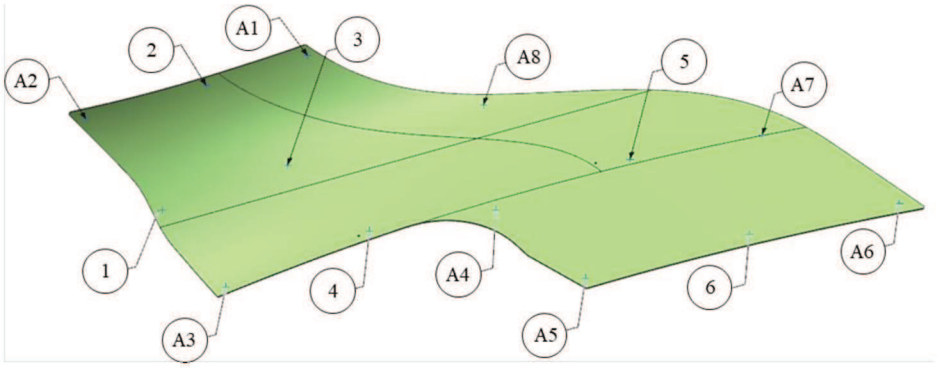

Source: the author.

Figure 3.17 - Part A: Points for process evaluation.

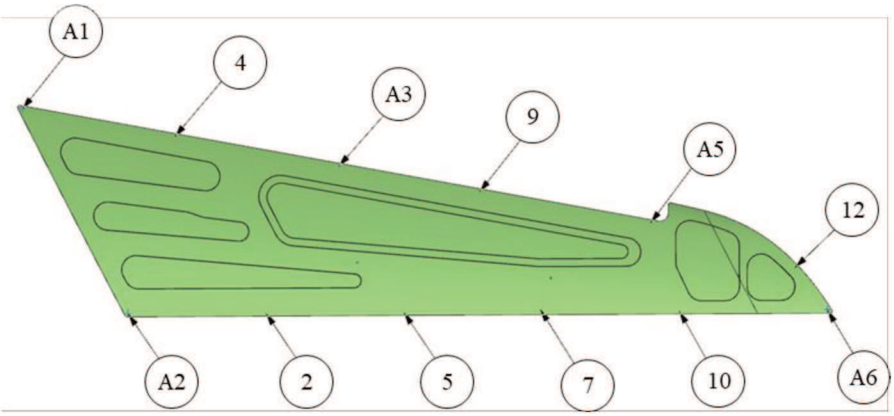

Source: the author.

Figure 3.18 - Part B: Points for process evaluation.

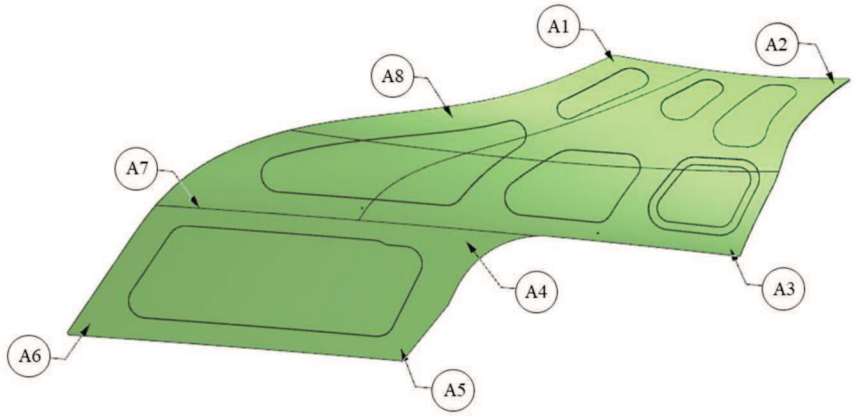

Source: the author.

4 RESULTS AND DISCUSSIONS

In this chapter, the experimental results are presented. First, the process evaluation for the 3D scanning process is analyzed. Then the results of virtual clamping method, followed by the comparison with the physical clamping are shown. The results follow the workflow presented in Figure 3.6. An analysis of the sources of measurement uncertainties identified in the process closes this chapter.

4.1 PROCESS EVALUATION: 3D SCANNING

As the 3D scanning process is common to all parts and used in both methods, the first step was to evaluate the performance of ATOS Compact Scan during the image capturing process and the concatenation of the acquired geometries, according the method described in Section 3.2.2. The ATOS Compact Scan was calibrated before the tests and the parameters and results are shown in Table 4.1.

Table 4.1 - ATOS Compact Scan calibration parameters and results.

Measurement temperature	(293.15 ± 1.00) K (20.1 ± 1.00) °C
Calibration object type	Calibrated panel
Test distances	574.33 mm / 574.34 mm
Coefficient of thermal expansion	$22.67 \cdot 10^{-6}$ K^{-1}
Light intensity	100 %
Calibration deviation	0.018 pixel (max. 30 pixel)
Calibration deviation (optimized)	0.011 pixel

Source: the author.

Due to the high reflectivity of the used spheres, it was necessary to use the surface coating, as shown in Figure 4.1. Under the same environmental conditions, the scans were performed three times each, in order to evaluate the repeatability of each test. The artifact was not moved during the scanning and the ATOS Compact Scan was freely moved around to capture all the geometries required for evaluations.

Figure 4.1 - Process evaluation: 3D scanning - used artifact.

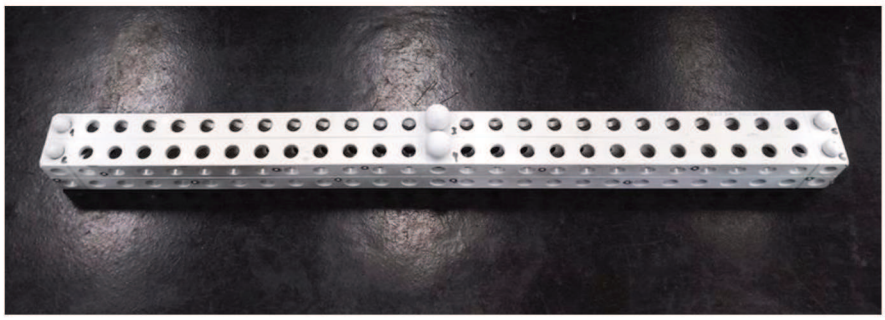

Source: the author.

The bias and the calculated process repeatability of each test, as shown in Figure 3.9, are presented in Table 4.2 and a graphical analysis is allowed through Figure 4.2 and Figure 4.3.

Table 4.2 - Process evaluation: 3D scanning.

		Test 1	Test 2	Test 3	Test 4
Sphere-spacing error	Bias Average [mm]	0.010	0.003	0.007	0.006
	Repeatability [mm]	0.012	0.007	0.018	0.018
Sphere-diameter error	Bias Average [mm]	0.032	0.028	0.031	0.030
	Repeatability [mm]	0.010	0.071	0.020	0.028

Source: the author.

Figure 4.2 - Process evaluation (A): 3D scanning - graphical results.

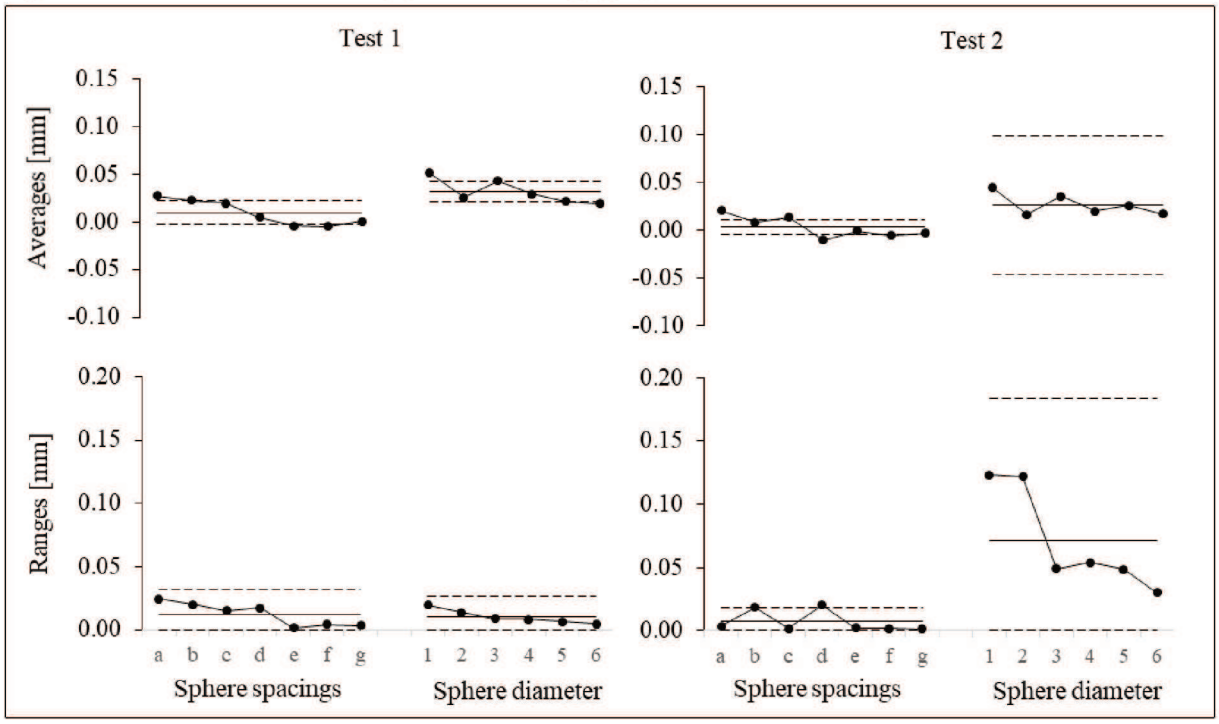

Source: the author.

Figure 4.3 - Process evaluation (A): 3D scanning - graphical results.

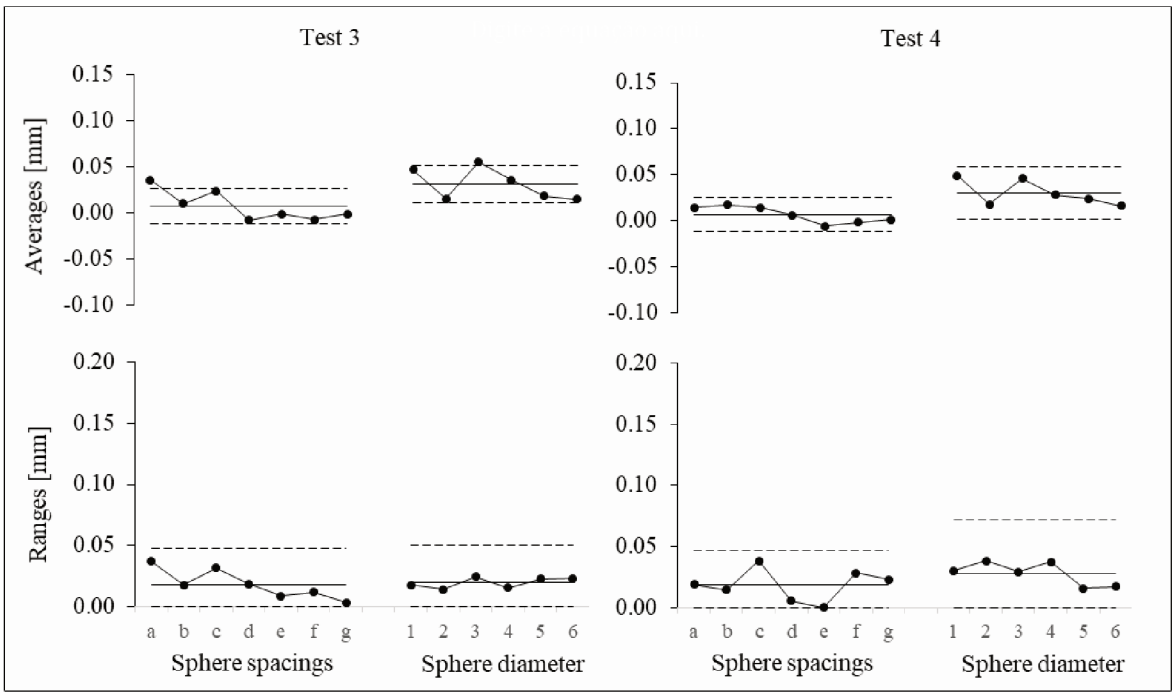

Source: the author.

By analyzing separately the results between sphere-spacing error (identified by letters) and sphere- diameter error (identified by numbers) it is possible to recognize a positive measurement bias present in all tests, that can be explained due to the application of the spray layer on the spheres. When the repeatability is evaluated, Test 1 presented better performance resulting in its adoption to measure the parts.

4.2 CASE STUDY: PART A

4.2.1 Simplified clamping system and 3D data capture

In order to keep the part stable during the 3D data capture, a simplified clamping system was needed. Following the guidelines of Ascione and Polini [3], the system should present the least possible interference with the optical measuring system. After the design and assembly, the part may be positioned and clamped, then scanning may begin. The final result of the simplified clamping system for this part is shown in Figure 4.4.

Figure 4.4 - Part A: Simplified clamping system.

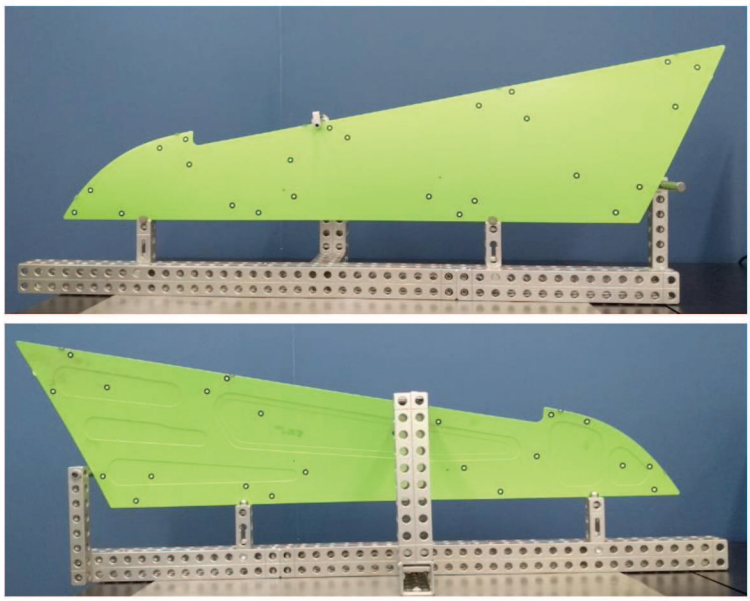

Source: the author.

The part was positioned on this device through the support on balls, pins and secured through a clamp-screw. As mentioned earlier, it is necessary to know the position of the part/CS support points for later use to neutralize the force of gravity. For the application of these points, measured with the articulated measuring arm only once, as boundary conditions in various measurements, it is necessary to evaluate the repeatability of the clamping system.

This evaluation was done by combining the five meshes resulting from the scans in an average mesh, and thus, in comparison with the scanned meshes, it is possible to verify the repeatability presented by the CS. The control points shown in Figure 3.15 were used to verify the variability between scans. The chart containing the Range-values is presented in Figure 4.5, from which the standard deviation was calculated as $\hat{\sigma}_e = 5.44\ \mu m$.

Figure 4.5 - Part A: Intermediate evaluation (B) - clamping system VCM.

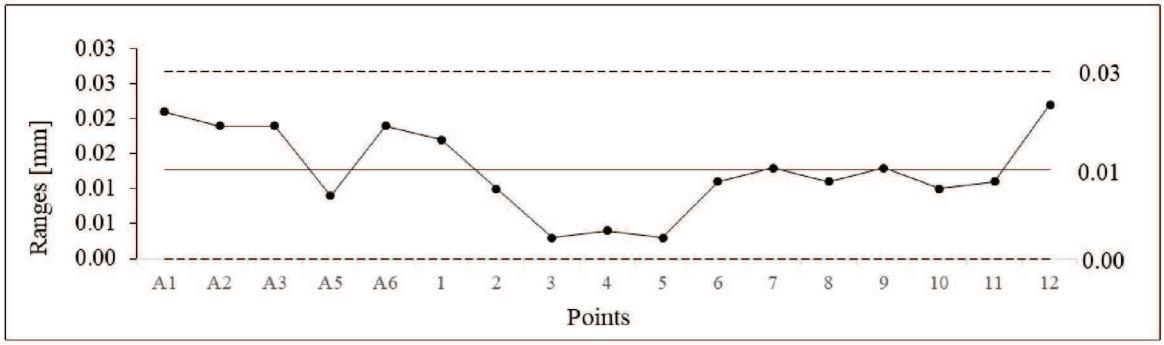

Source: the author.

Using the quality indicators proposed by Lartigue et al. [56] to characterize a point cloud/mesh (noisy, density, completeness) it was possible to qualitatively evaluate the mesh conformity with the expected result. The other quality indicator (accuracy) was evaluated by the comparison between the thickness measurements at specific points in the scanned part and measurements using an adapted micrometer to curved surfaces in the physical part. The results and comparison are shown in Table 4.3. A graphical analysis is allowed through Figure 4.6 and Figure 4.7.

Table 4.3 - Part A: Intermediate evaluation (C) - 3D data capture.

Point	Reference value* [mm]	$\bar{X}$ [mm]	Bias [mm]	Bias [%]	Evaluation
A2	2.09	2.09	0.004	0.21	✓
A1	1.96	1.95	-0.013	-0.66	✓
2	2.03	2.04	0.014	0.69	✓
4	1.99	1.98	-0.009	-0.45	✓
5	2.10	2.11	0.008	0.37	✓
A3	2.01	2.02	0.009	0.46	✓
7	2.03	2.02	-0.016	-0.79	✓
9	2.04	2.06	0.019	0.94	✓
10	2.15	2.14	-0.011	-0.51	✓
A5	2.06	2.08	0.014	0.66	✓
A6	2.19	2.20	0.017	0.80	✓
12	2.12	2.10	-0.011	-0.50	✓

Source: the author.

* Expanded measurement uncertainty: ± 0.023 mm (k = 2). To evaluate the measurement uncertainties the following sources were considered: type A (five replications) and type B (micrometer uncertainty, temperature variation, thermal expansion coefficient and thermometer uncertainty).

Figure 4.6 - Part A: Intermediate evaluation (C) - 3D data capture.

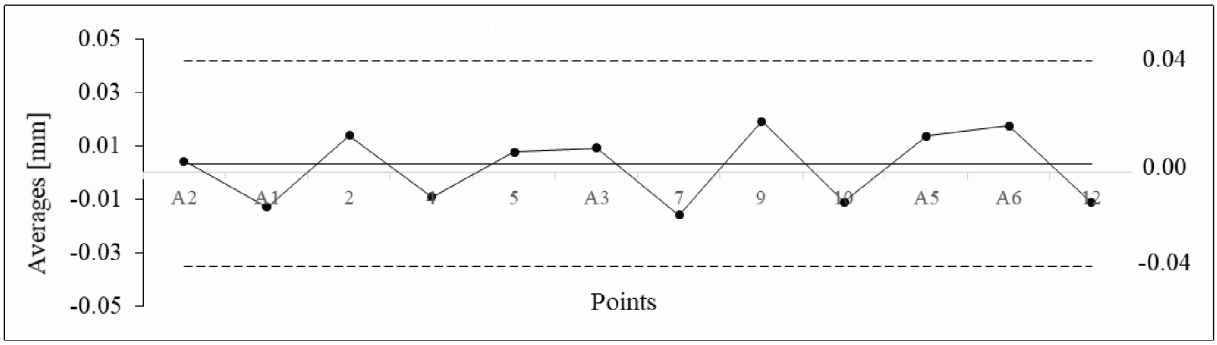

Source: the author.

Figure 4.7 - Part A: Intermediate evaluation (C) - 3D data capture.

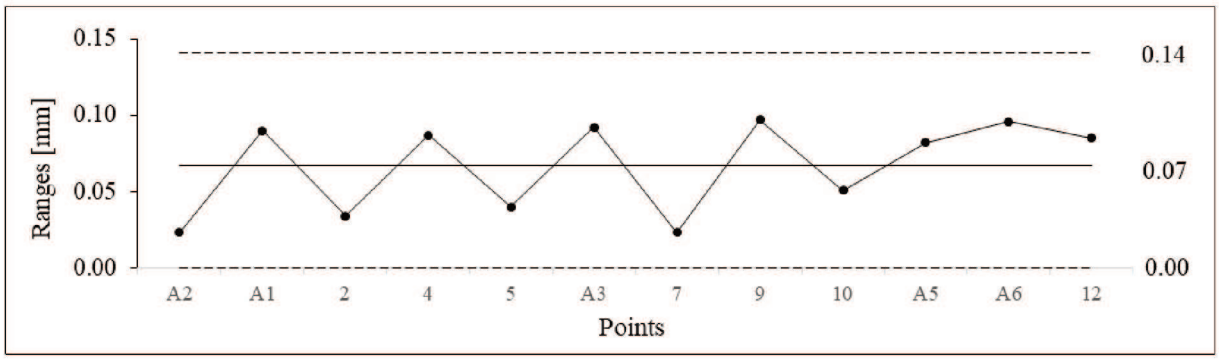

Source: the author.

This evaluation is important, since errors in the scanned part thickness interfere directly in the rigidity matrix, causing errors in the results. With the presented data, it was possible to conclude that the 3D data capture process has no significant influence on the part thickness, confirming the approval of the previously defined scanning method.

4.2.2 Modeling

The bibliographic review allowed to identify the best method for the CAD Reconstruction process. As shown in Figure 2.20, after capturing and analyzing the 3D data, a mesh classification and segmentation is required. Applying this method in part A, the mesh was segmented into three main parts to be modeled separately and later union: upper surface, lower surfaces and border as shown in Figure 4.8.

Figure 4.8 - Part A: Mesh segmentation for modeling process.

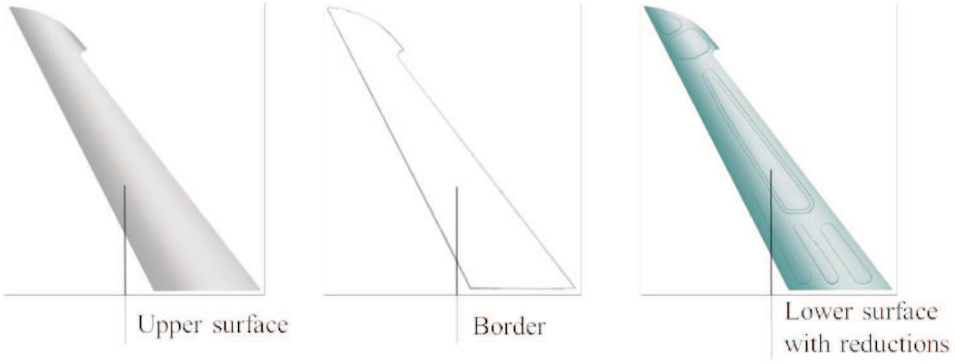

Source: the author.

In the Siemens NX® modeling environment, the surfaces were recreated through a curve mesh using a grid of splines built on the mesh, respecting the degrees of curvature and tangencies between the patches. For the evaluation of tangencies between the patches, a reflection analysis was performed, as the example shown in Figure 4.9.

Figure 4.9 - Part A: Modeling method using a grid of splines.

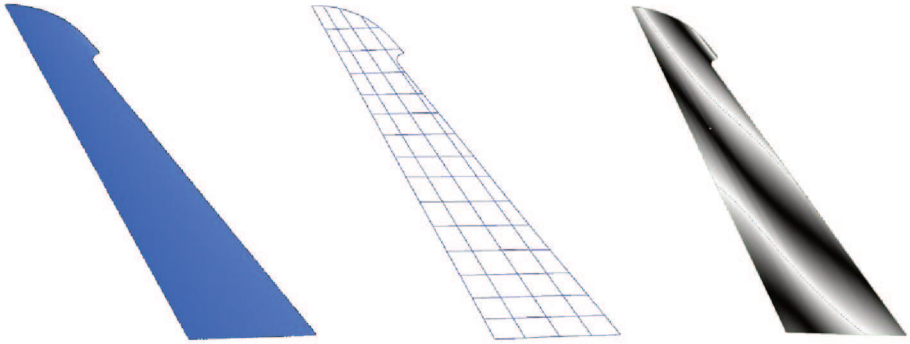

Source: the author.

For the modeling process evaluation (D acc. Figure 3.6), the reconstructed CAD was compared with its respective mesh, according to Figure 4.10. A numerical analysis was also performed by measuring the errors under the control points. These results are shown graphically in Figure 4.11. The modeling step presented good repeatability with a $\hat{\sigma}_e$ of 1.32 µm.

Figure 4.10 - Part A: Visual evaluation (D) - modeling.

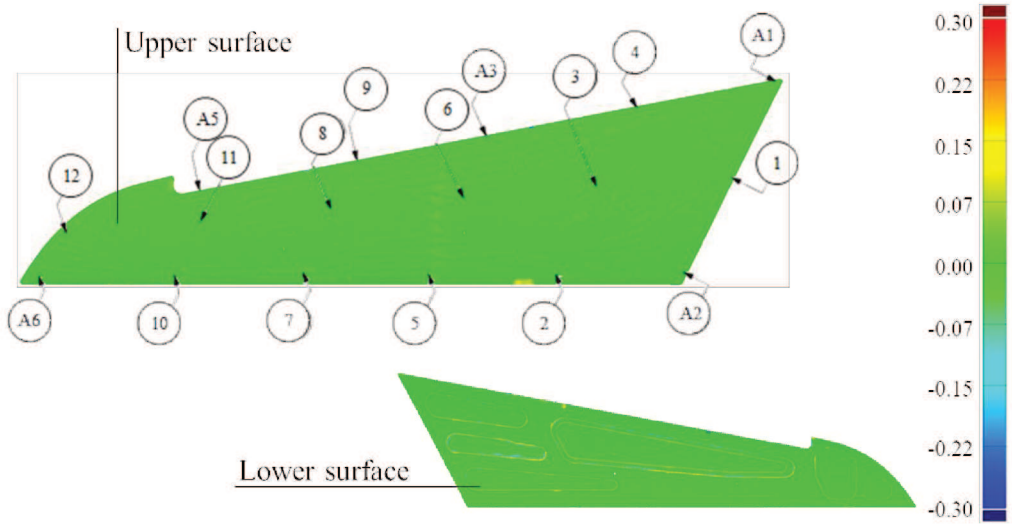

Source: the author.

Figure 4.11 - Part A: Intermediate evaluation (E) - modeling.

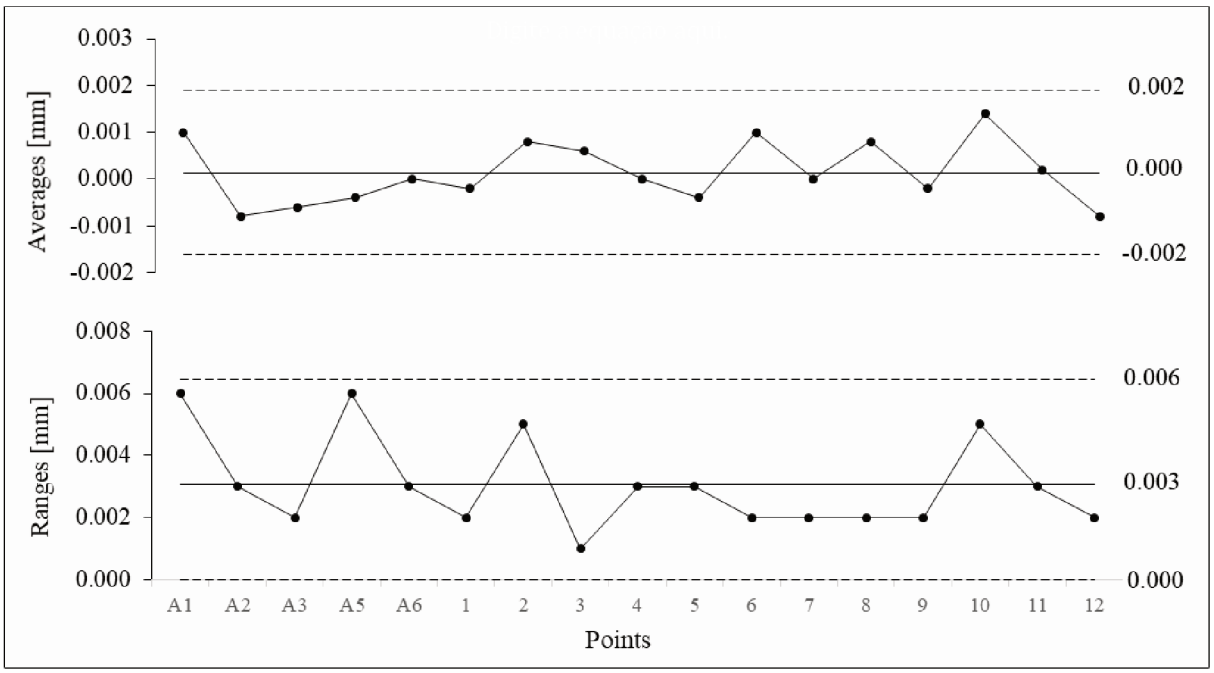

Source: the author.

4.2.3 FEM Simulation

The analysis was performed as 3D geometric linear simulation, because there is no plastic deformation during assembly, using parabolic tetrahedral elements with 10 nodes, according to Figure 2.23. The most important aspect in simulations, the boundary conditions specification, was performed by measuring the distance between the part and points representing the specified datum points.

Before the repetitions of the simulation process, it was necessary to define the best combination between the mesh size and the processing time. According to Section 3.2.2, this process evaluation step was done by controlling the maximum displacement of the part during the simulation. A representation of the mesh with the application of the boundary conditions (enforced displacement constrains applied to a node, and normal direction to the surface) is presented in the Figure 4.12.

Figure 4.12 - Part A: Representation of mesh and the boundary conditions.

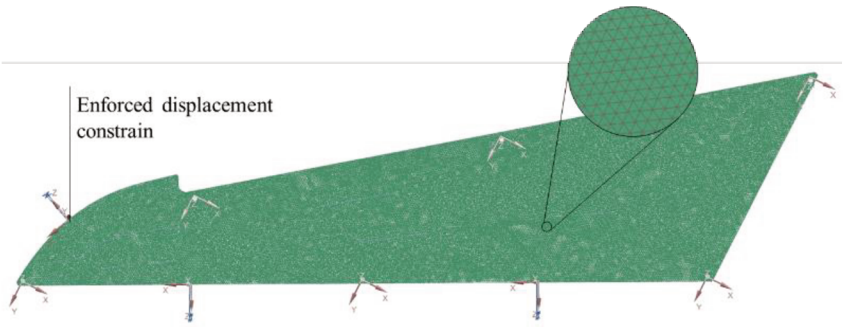

Source: the author.

When there are no significant gains from increasing mesh density, it is possible to combine the results with a linear fit. Allowing a maximum error of 1%, a line parallel to the previous one is also evaluated, allowing the definition of the best combination, as illustrated in Figure 4.13. The numerical results are shown in Table 4.4. Analyzing the data, it was possible to identify that the mesh size 3.00 mm is within the permitted error range, and presents a shorter processing time, so this was the configuration selected for the simulation's development.

Figure 4.13 - Part A: Process Evaluation (F) - meshing size analysis.

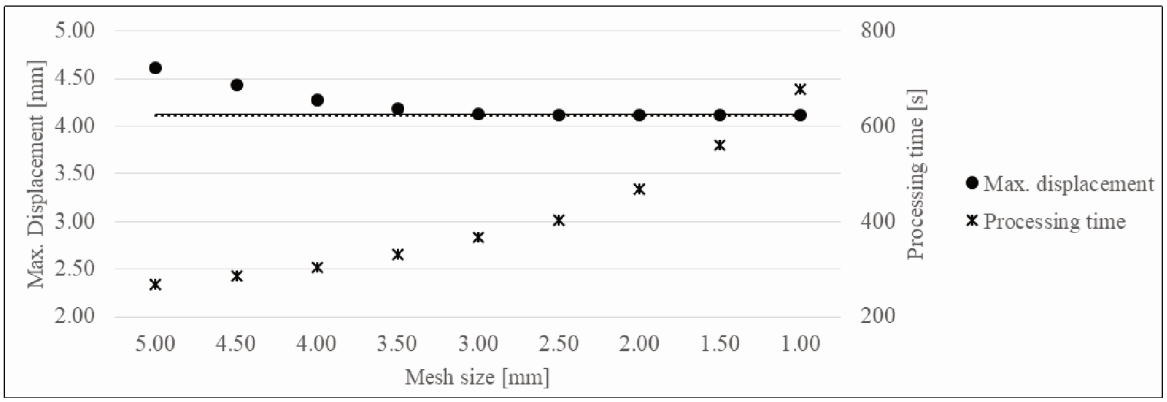

Source: the author.

Table 4.4 - Part A: Process evaluation (F) - meshing size analysis.

Continue

Mesh size [mm]	Max. displacement [mm]	Processing time [s]	Is this point within tolerance? (1%)
5.00	4.61	268	×
4.50	4.43	286	×
4.00	4.28	304	×
3.50	4.19	331	×

Mesh size [mm]	Max. displacement [mm]	Processing time [s]	Conclusion: Is this point within tolerance? (1%)
3.00	4.13	366	✓
2.50	4.11	403	✓
2.00	4.11	469	✓
1.50	4.12	561	✓
1.00	4.11	677	✓

Source: the author.

4.2.4 Evaluation

After the finite element simulation, and following the process, the deformed mesh geometry was exported, in a JT file and then converted to a STL file, applicable to the comparison in GOM Inspect software. The evaluation of these results occurred again through the control points and it was performed in two distinct forms: numerical and visual. The numerical results are presented in Figure 4.14 and shown a repeatability of $\hat{\sigma}_e$ = 8.39 µm for the datum points and of $\hat{\sigma}_e$ = 15.70 µm for the control points. The visual evaluation, using one of the repetitions, is allowed through the Figure 4.15. The chart shows that the point-to-point variation is much greater than the modeling process variation (difference between the same point in different measurement). This means that the process has good repeatability.

Figure 4.14 - Part A: Intermediate evaluation (G) - VCM

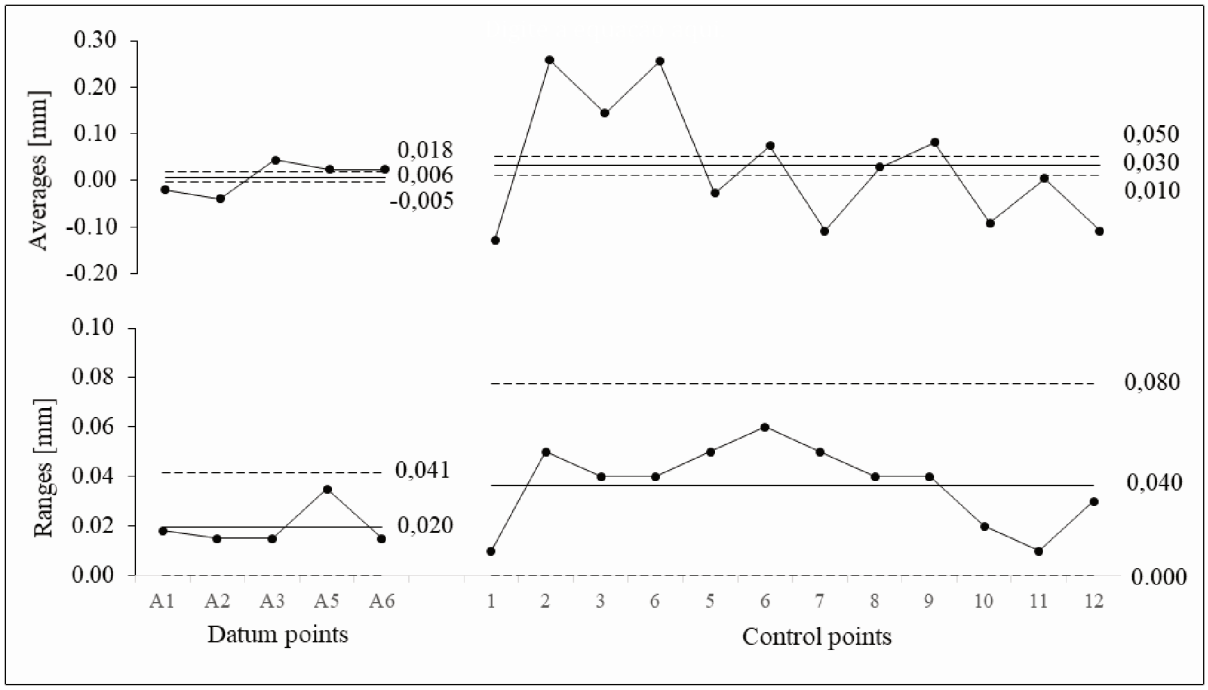

Source: the author.

Figure 4.15 - Part A: Visual evaluation (H) - VCM

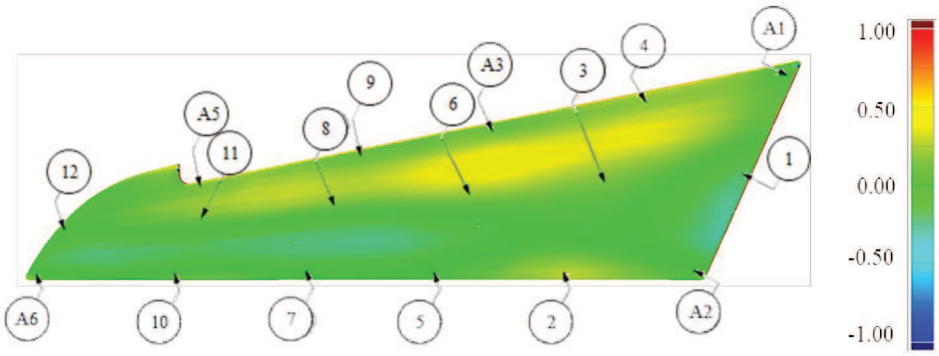

Source: the author.

4.2.5 Conventional Method

For the comparison with the proposed method, the part was also evaluated by the conventional method. For the development of this step, a physical clamping system was designed and assembled, as shown in Figure 4.16. After assembly, the physical CS was calibrated in a CMM. With the results, the CS was adjusted and recalibrated, the residual deviations after the calibration and adjustment are presented in Table 4.5.

Figure 4.16 - Part A: Physical clamping system.

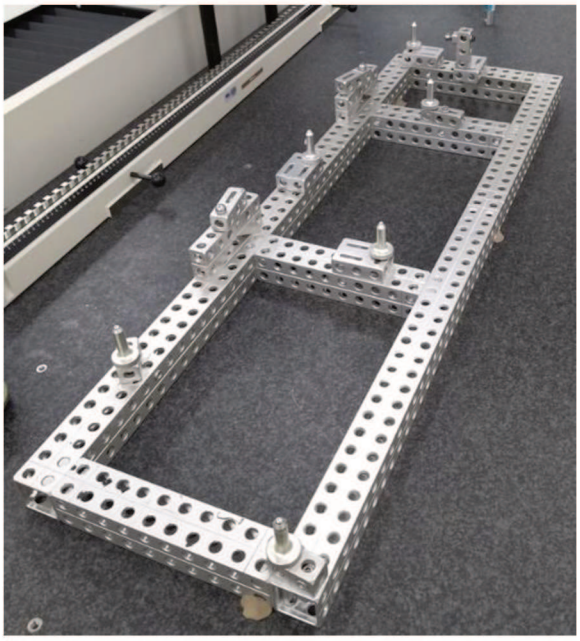

Source: the author.

Table 4.5 - Part A: Physical clamping system deviations.

Point	Deviation [mm]		
	X	Y	Z
A1	-0.017	-0,004	-0,105
A2	-0.007	0.035	-0.038
A3	0.163	0.058	0.101
A4	-0.080	0.115	-0.122
A5	-0.067	0.034	0.096
A6	-0.162	-0.120	-0.067
B1	-0.015	-0.004	-0.035
B2	0.110	-0.185	0.176
C1	0.075	0.072	-0.007

Source: the author.

The part was assembled and clamped to the calibrated in the physical CS calibrated. After this, the scans were performed. Again, to evaluate the repeatability of the CS, the scans were compared with an average mesh. The chart containing the Range-values is presented in Figure 4.17, from which the standard deviation was found as $\hat{\sigma}_e = 10.32\ \mu m$.

Figure 4.17 - Part A: Intermediate evaluation (I) - PCM.

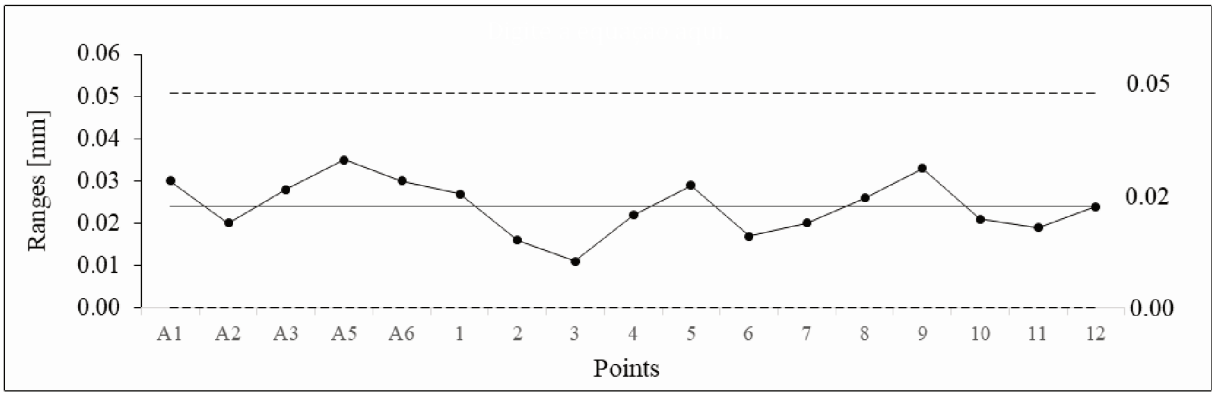

Source: the author.

The meshes resulting from the scanning process were evaluated by the same method as the virtually deformed meshes, also numerically and visually. However, by using the physical CS, it was impossible to capture the underside surface of the part. In this way, the alignment between the nominal CAD and the mesh was performed by the upper surface. The coordinates for the datum points were calculated by translating the points from the underside surface to the upper side surface in the normal surface direction.

After the alignment it was possible to carry out the vectorial comparison between the surfaces. Figure 4.18 shows the Average and Range-charts of the results for the measurements.

The repeatability resulting from the process was of $\hat{\sigma}_e$ = 8.60 µm for the datum points and of $\hat{\sigma}_e$ = 15.23 µm for the control points. Again, now for PCM, it is possible to identify the vectorial deviations of the surface in Figure 4.19. Positive deviations are represented by warm colors, while negatives by cold colors.

Figure 4.18 - Part A: Intermediate evaluation (J) - PCM.

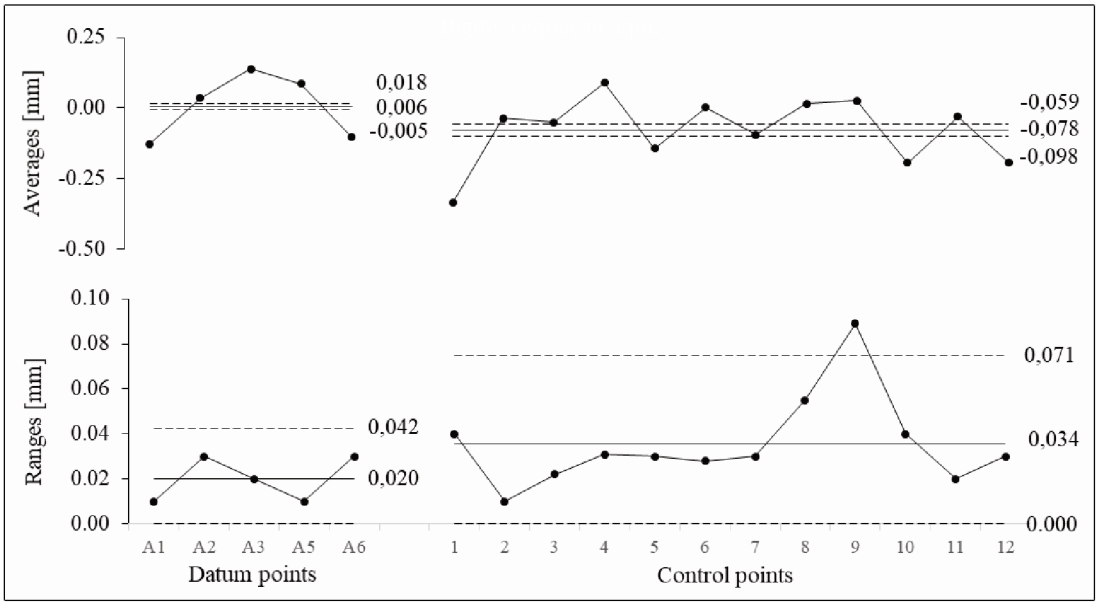

Source: the author.

Figure 4.19 - Part A: Visual evaluation (K) - PCM.

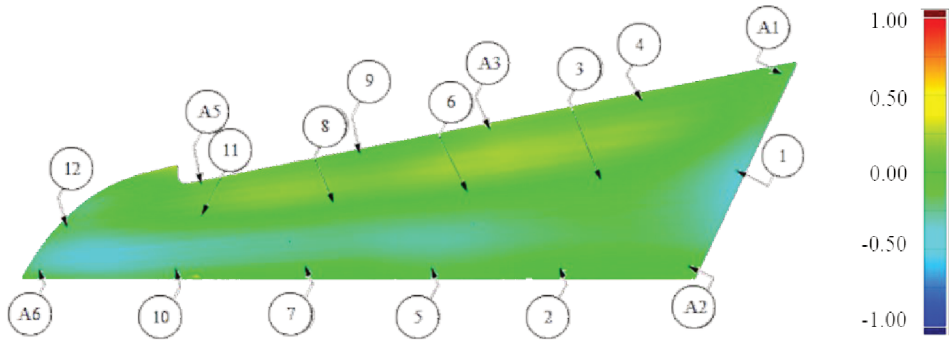

Source: the author.

4.2.6 Comparison of VCM and PCM

Now, with the evaluations through the both methods it is possible to compare them visually. Figure 4.20 shows the difference between the results presented by the virtual CS

method and the physical CS method. The maximum error presented, when comparing the two methods, was 0.134 mm, representing 3.2% of the displacement required for assembly. Evaluating the results statistically through a one-way analysis of variance, as defined in Section 3.2.3, it was possible to test the hypotheses set in introduction section.

Figure 4.20 - Part A: Comparison between VCM and PCM (L).

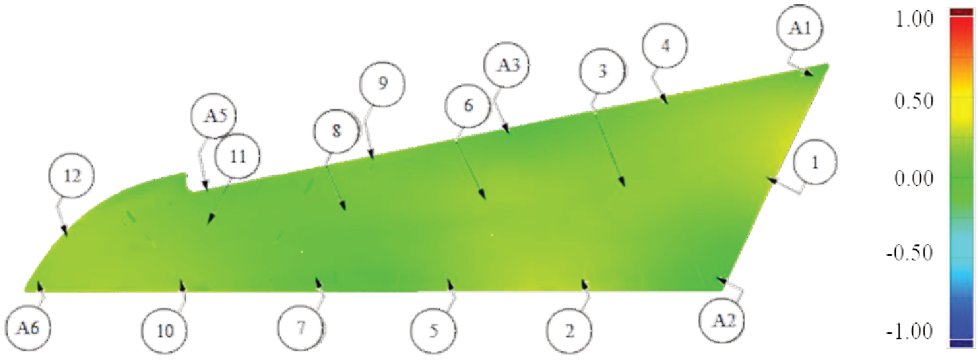

Source: the author.

The profile of the surface error presented in the five replicates through the evaluation by both methods are presented in Table 4.6, together with their average value, standard deviation (according to equation 3.7) and their variance (according to equation 3.8). Using the equations 3.10, 3.11 and 3.12, the value F_0 was calculated and resulted in 2.49. Comparing it with the value of $F_\alpha = 5.32$ to 0.05 of significance level and with degrees of freedom ν_1 and ν_2 of 1 and 8 respectively, it was possible to conclude that H0 is true and there are no significant differences between the methods. Figure 4.21 shows the average results of each method and its confidence interval (CI) ($\alpha = 0.05$).

Table 4.6 - Part A: Statistical evaluation - profile of the surface error.

	VCM [mm]	PCM [mm]
1	2.555	1.657
2	2.912	1.821
3	2.008	2.410
4	1.954	1.592
5	1.954	1.981
$\bar{X}$	2.278	1.892
$\hat{\sigma}_e$	411.87 µm	351.68 µm
$\widehat{\sigma^2}_e$	149.58 µm²	109.06 µm²

Source: the author.

Figure 4.21 - Part A: Statistical evaluation.

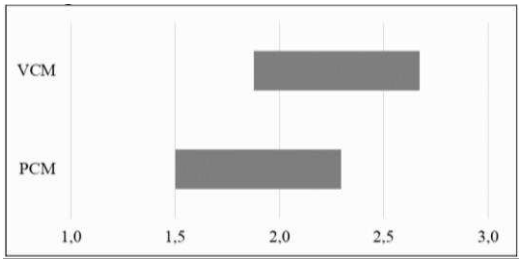

Source: the author.

4.3 CASE STUDY: PART B

4.3.1 Simplified clamping system and 3D data capture

Likewise, the process was repeated for Part B. This time, the level of complexity presented by the part required more attention in the process implementation. The simplified CS used to support the part during the scans is shown in Figure 4.22. The part is positioned on this device through the support on pins and fixed through a clamp-screw.

Figure 4.22 - Part B: Simplified clamping system.

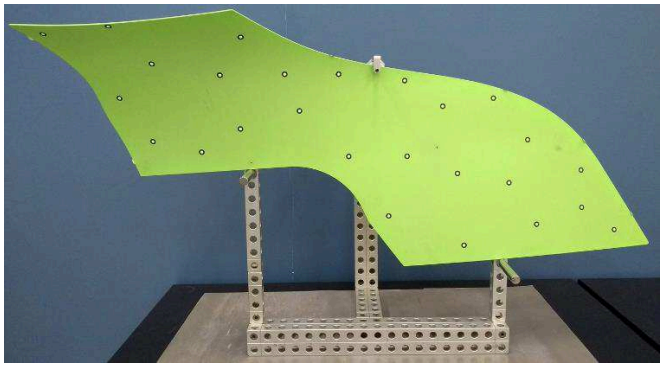

Source: the author.

Evaluating the repeatability of the clamping system, again combining the five meshes resulting from the scans in an average mesh, and then, comparing it with the scanned meshes through the control points (Figure 3.16), resulted in a repeatability of $\hat{\sigma}_e = 31.71\ \mu m$. The chart presenting the Range-values is shown in Figure 4.23.

Figure 4.23 - Part B: Intermediate evaluation (B) - clamping system VCM.

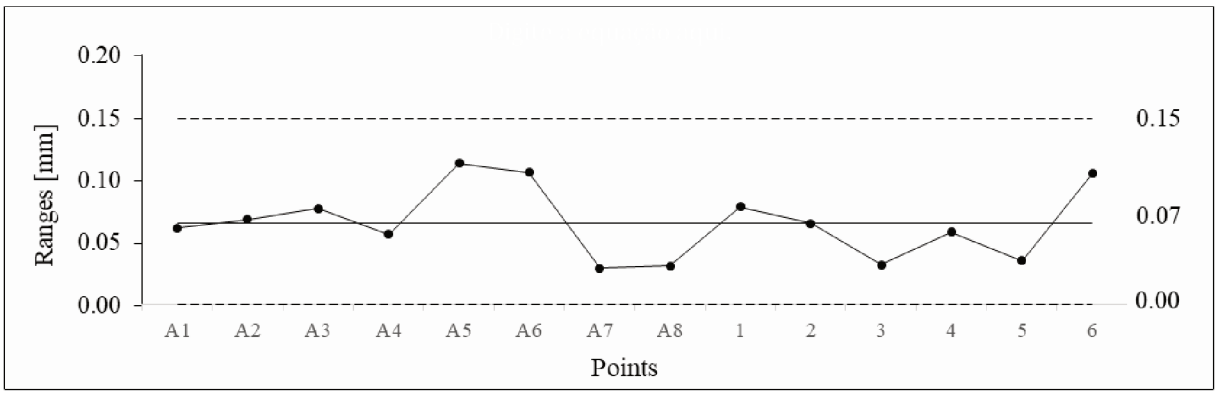

Source: the author.

Analyzing the quality indicator: accuracy, evaluated by the comparison between the thickness measurements at specific points in the scanned part and measurements using an adapted micrometer to curved surfaces in the physical part, the results attested the conformity of the mesh with the expected results (max. error of 3%). The numerical results are shown in Table 4.7 and the graphical analysis is depicted in Figure 4.24. Again, it was possible to conclude that the 3D data capture process has no significant influence on the part thickness, confirming the approval of the previously defined scanning method.

Table 4.7 - Part B: Intermediate evaluation (C) - 3D data capture.

Point	Reference value* [mm]	$\bar{X}$ [mm]	Bias [mm]	Bias [%]	Evaluation
A1	2.08	2.10	0.020	0.97	✓
A2	2.08	2.07	-0.013	-0.60	✓
A3	2.02	2.01	-0.007	-0.37	✓
A4	2.05	2.03	-0.019	-0.94	✓
A5	2.14	2.13	-0.013	-0.61	✓
A6	2.09	2.08	-0.012	-0.57	✓
A7	1.99	1.98	-0.020	-0.99	✓
A8	2.03	2.05	0.013	0.64	✓

Source: the author.
* Expanded uncertainty: ± 0.023 mm (k = 2). To calculate the measurement uncertainties the following sources were considered: type A (five replications) and type B (micrometer uncertainty, temperature variation, thermal expansion coefficient and thermometer uncertainty).

Figure 4.24 - Part B: Intermediate evaluation (C) - 3D data capture.

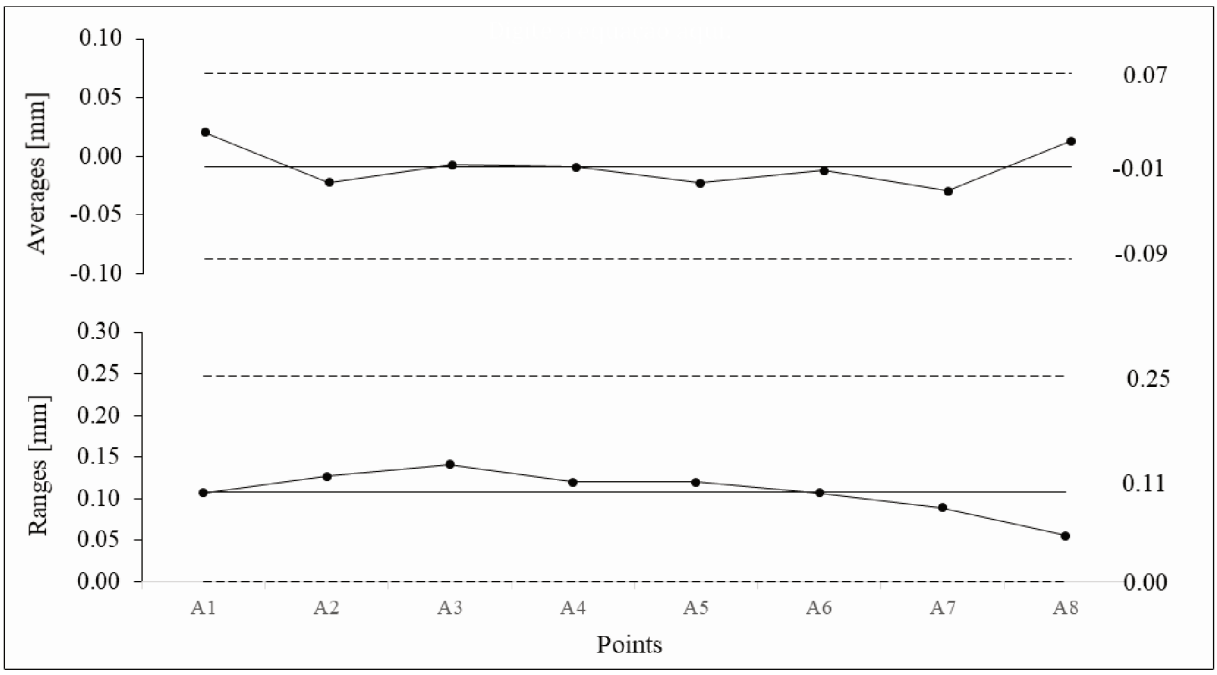

Source: the author.

4.3.2 Modeling

Adopting the same method used in part A, the mesh was segmented into three main parts to be modeled separately and later union: upper surface, lower surfaces and border as shown in Figure 4.25. Again, in the Siemens NX® modeling environment software, the surfaces were recreated through a curve mesh using a grid of splines built on the mesh, respecting the degrees of curvature and tangencies between the surfaces. For the evaluation of tangencies, a reflection analysis was performed, as the example shown in Figure 4.26.

Figure 4.25 - Part B: Mesh segmentation for modeling process.

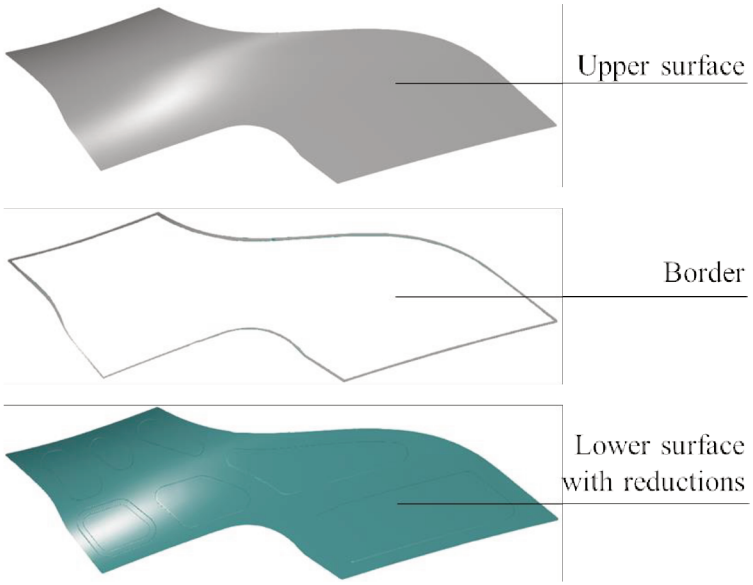

Source: the author.

Figure 4.26 - Part B: Modeling method using a grid of splines.

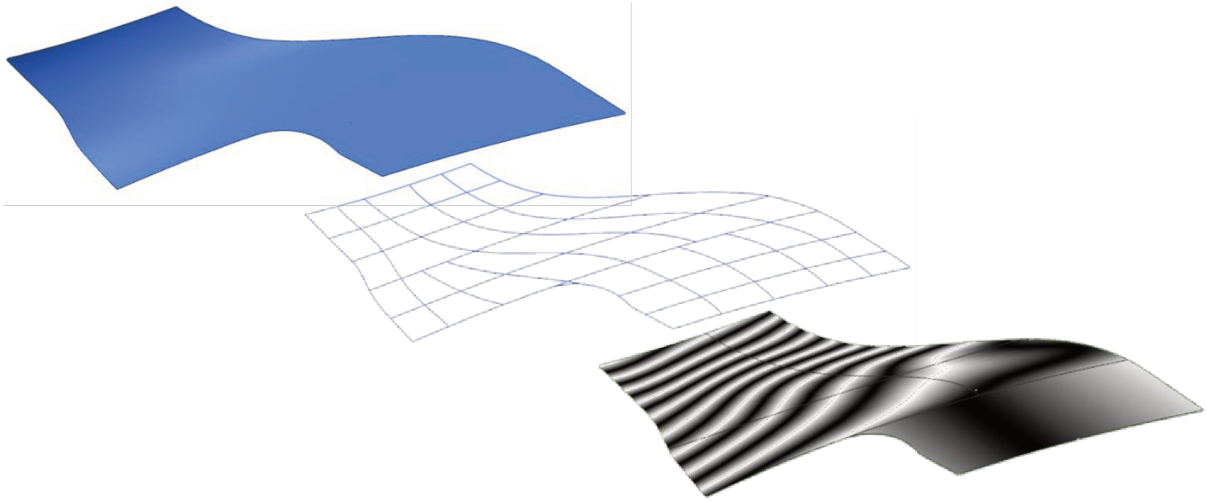

Source: the author.

For the modeling process evaluation, all reconstructed CADs were compared with their respective meshes, according to Figure 4.27. And the numerical analysis was also performed by measuring the errors under the control points. These results are shown graphically in Figure 4.28. The modeling step presented good repeatability with a $\hat{\sigma}_e$ of 1.42 µm.

Figure 4.27 - Part B: Visual evaluation (D) – modeling.

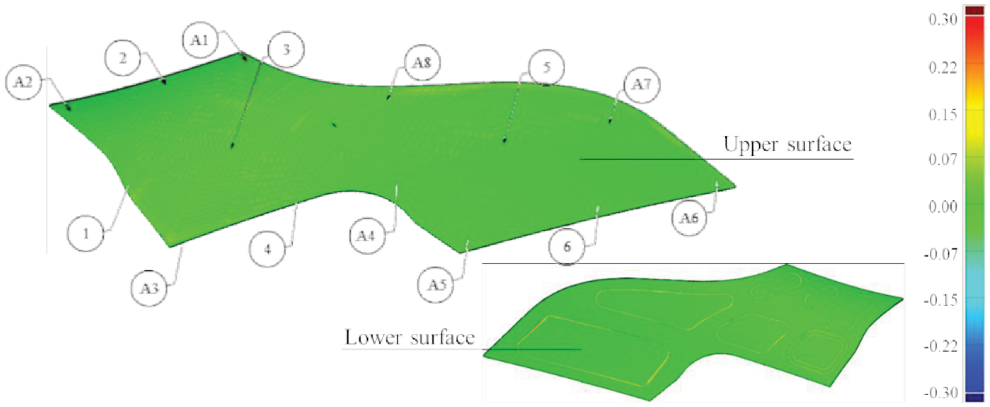

Source: the author.

Figure 4.28 - Part B: Intermediate evaluation (E) – modeling.

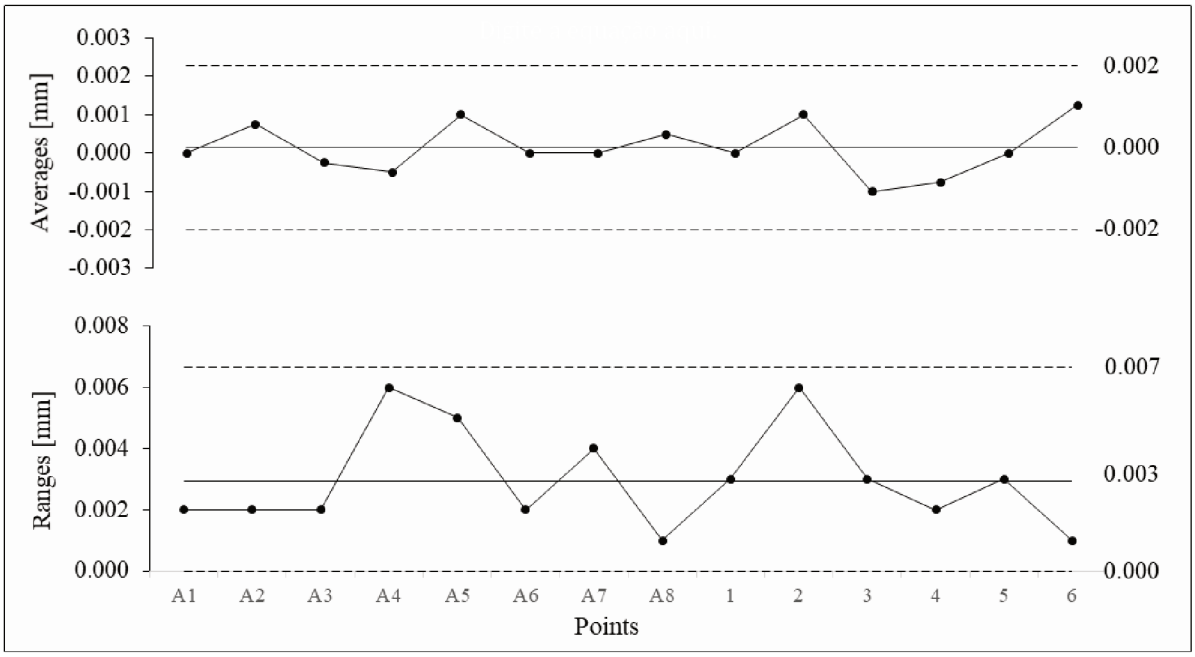

Source: the author.

4.3.3 Simulation

The simulation step was performed using the same elements of part A (using tetrahedral elements with 10 nodes) and following the same strategy for the boundary conditions specification (Figure 4.29). Again, before the repetitions of the simulation process, it was necessary to define the best combination between the mesh size and the processing time.

With the same method as part A, the found numerical results are shown in Table 4.8 and the results are plotted, as presented in Figure 4.30. In this case, the mesh size 5.00 mm is within the permitted error range and presents a shorter processing time, so this was the configuration selected for the simulations.

Figure 4.29 - Part B: Representation of mesh and the boundary conditions.

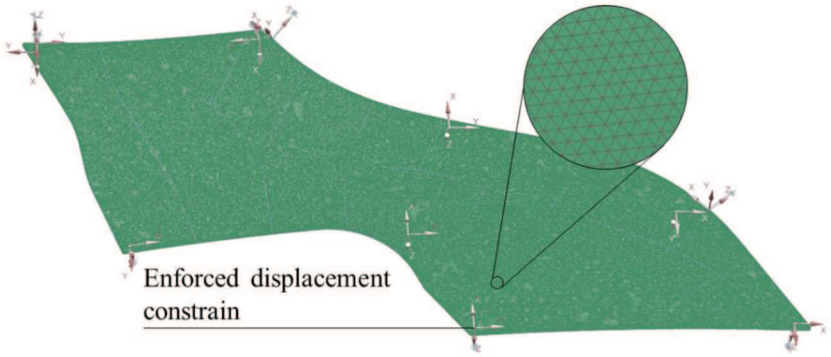

Source: the author.

Table 4.8 - Part B: Process evaluation (F) - meshing size analysis.

Mesh size [mm]	Max. displacement [mm]	Processing time [s]	Is this point within tolerance? (1%)
7.00	25.53	804	✗
6.50	23.98	858	✗
6.00	22.57	912	✗
5.50	21.66	993	✗
5.00	20.83	1098	✓
4.50	20.76	1209	✓
4.00	20.77	1407	✓
3.50	20.75	1683	✓
3.00	20.79	2031	✓

Source: the author.

Figure 4.30 - Part B: Process evaluation (F) - meshing size analysis.

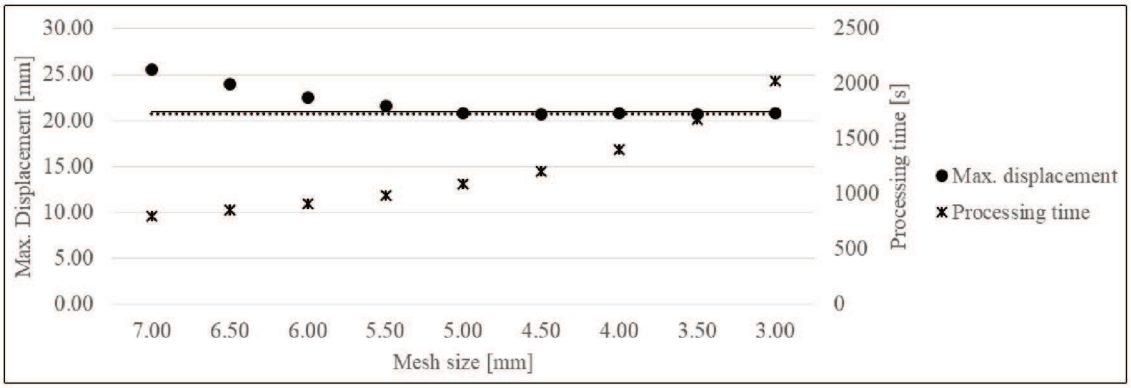

Source: the author.

4.3.4 Evaluation

The calculated deviations are presented graphically in Figure 4.31, showing a repeatability of $\hat{\sigma}_e$ = 7.22 µm in the datum points and of $\hat{\sigma}_e$ = 15.06 µm in the control points. The visual evaluation, with the vector deviations classified by colors, is presented in the Figure 4.32.

Figure 4.31 - Part B: Intermediate evaluation (G) - VCM.

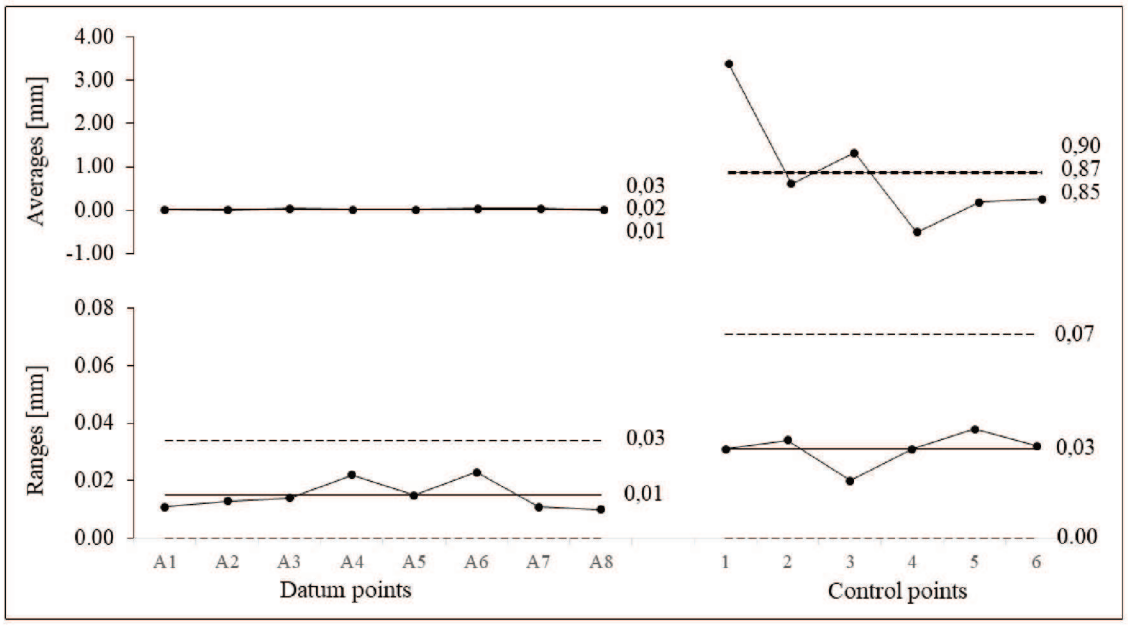

Source: the author.

Figure 4.32 - Part B: Visual evaluation (H) - VCM.

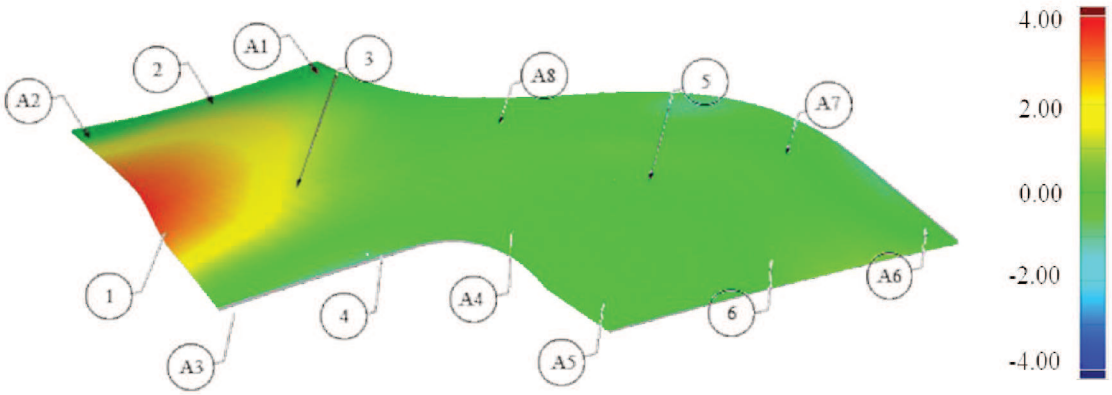

Source: the author.

4.3.5 Conventional Method

The physical clamping system developed for the evaluation of part B (Figure 4.33) and subsequent comparison with the results presented by the virtual clamping method followed the same process already presented for part A. The residual deviations found in the calibration are presented in Table 4.9.

Figure 4.33 - Part B: Physical clamping system.

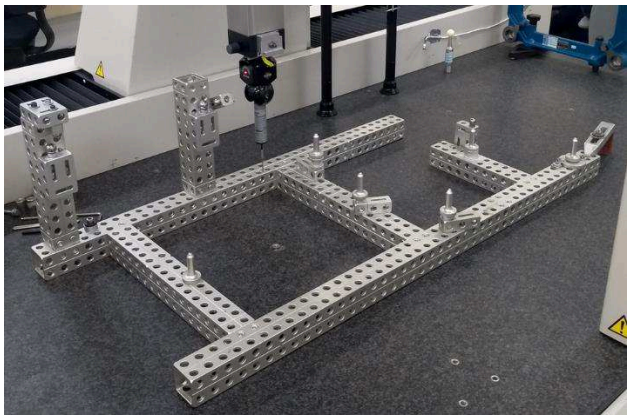

Source: the author.

Table 4.9 - Part B: Physical clamping system deviations.

Point	Deviation		
	X	Y	Z
A1	-0.061	-0.019	-0.012
A2	0.003	0.086	-0.080
A3	0.150	-0.156	0.031
A4	0.093	-0.106	0.039
A5	0.166	-0.075	0.101
A6	0.017	-0.004	0.086
A7	-0.150	0.032	-0.040
A8	-0.081	-0.029	0.073
B1	-0.170	0.001	-0.112
B2	0.101	0.150	0,099
C1	-0.068	0.120	-0.084

Source: the author.

In order to evaluate the repeatability of the physical CS, the scanned meshes of the part fixed in the CS were compared with an average mesh resulting from the combination of the five meshes. The chart containing the Range-values is presented in Figure 4.34. The results showed a $\hat{\sigma}_e = 8.40\,\mu\text{m}$.

Figure 4.34 - Part B: Intermediate evaluation (I) clamping system PCM.

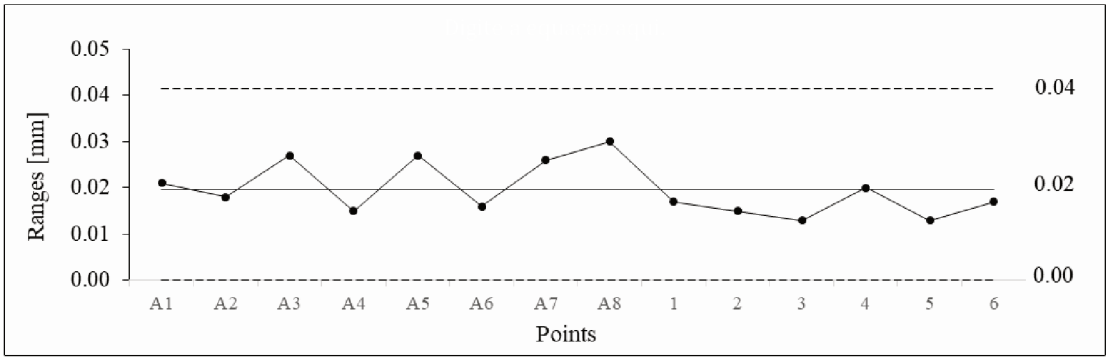

Source: the author.

The meshes were also evaluated by the same method as the virtually deformed meshes, also numerically and visually. For these scans, it was also possible to capture only the upper surface of the part. For this reason, again, the alignment was performed with the datum points translated from the lower to the upper surface.

The vectorial analysis, comparing the surfaces (real surface vs nominal CAD), are presented graphically in Figure 4.35 and visually in Figure 4.36. The repeatability resulting from the process was of $\hat{\sigma}_e$ = 12,95 µm in the datum points and $\hat{\sigma}_e$ = 32,96 µm in the control points.

Figure 4.35 - Part B: Intermediate evaluation (J) - PCM.

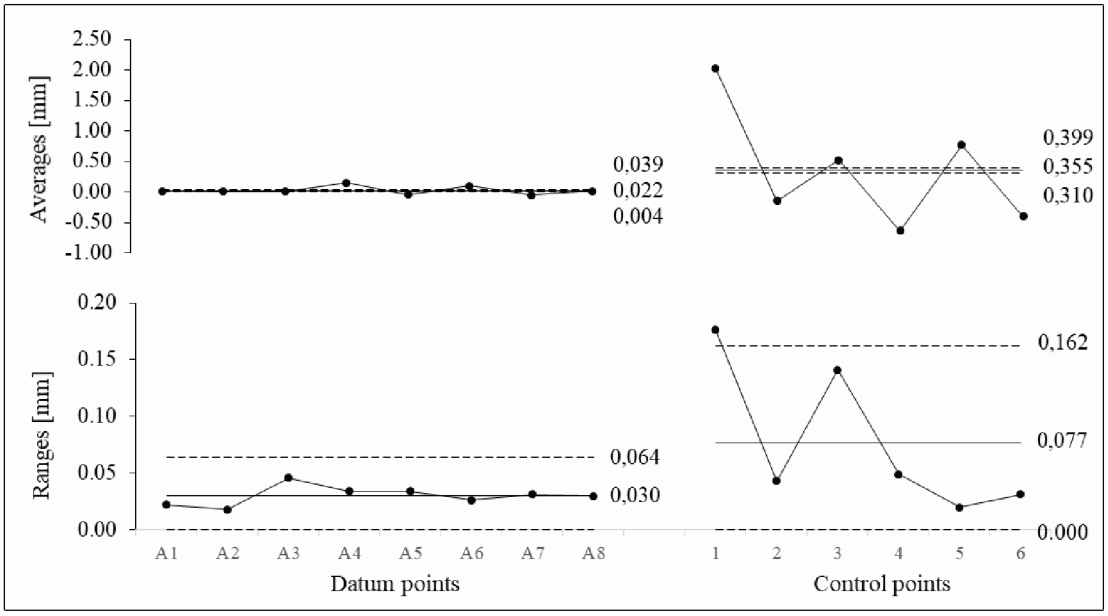

Source: the author.

Figure 4.36 - Part B: Visual evaluation (K) - PCM.

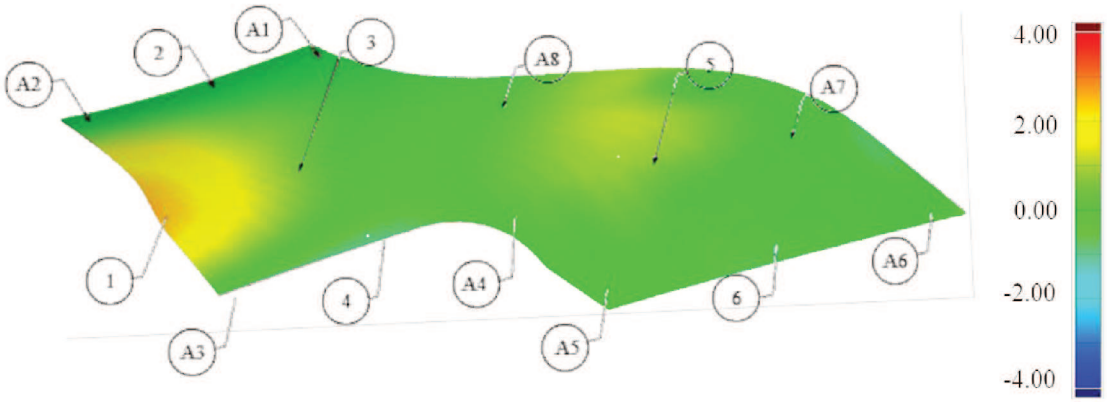

Source: the author.

4.3.6 Comparison of VCS and PCS

Comparing the methods visually, it was possible identify a bias near the control point 1, as shown in Figure 4.37. The reason identified by the presence of this difference was the position of datum point C1. As shown in Figure 4.38, for the bearing on the sphere representing this point datum, a force is required as indicated by the arrow. This force was not controlled and resulted, in addition to bias, in a significant decrease in the performance of the process repeatability, when compared to the virtualized method. However, the maximum error presented, when comparing the two methods, was 1.35 mm, representing 5.9% of the displacement required for assembly.

Figure 4.37 - Part B: Comparison between VCM and PCM (L)

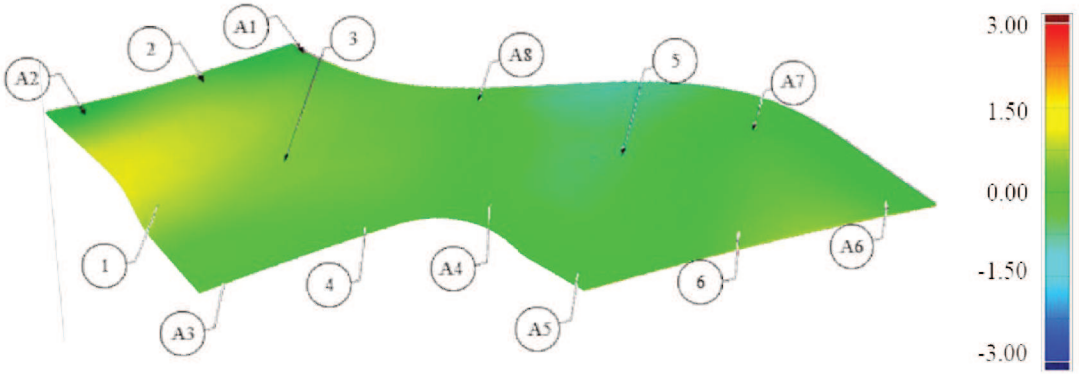

Source: the author.

Figure 4.38 - Part B: Representation of the force required for fixation.

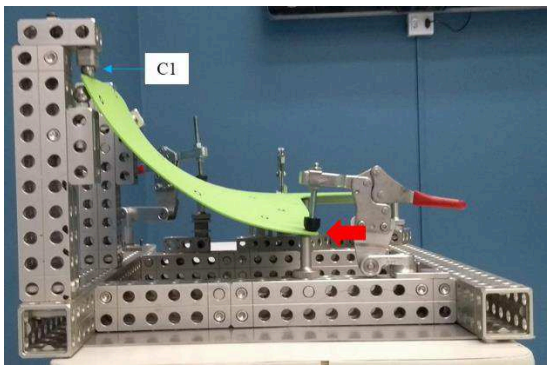

Source: the author.

Evaluating the results statistically, again through a one-way analysis of variance for Part B, it was possible to test the hypotheses, as defined in Section 3.2.3. The profile of the surface error presented in the five replicates through the evaluation by both methods are presented in Table 4.10.

Table 4.10 - Part B: Statistical evaluation - profile of the surface error.

	VCM [mm]	PCM [mm]
1	7.706	4.815
2	7.695	4.745
3	7.692	4.895
4	7.731	5.832
5	7.706	4.833
$\bar{X}$	7.706	5.024
$\hat{\sigma}_e$	16.77 µm	467.33 µm
$\widehat{\sigma^2}_e$	0.25 µm²	192.58 µm²

Source: the author.

Using equations 3.10, 3.11 and 3.12, the value F_0 was calculated and resulted in 173.65. Comparing it with the value of $F_\alpha = 5.32$ to 0.05 of significance level and with degrees of freedom ν_1 and ν_2 of 1 and 8 respectively, it was possible to conclude that H0 is false. In this case, there are significant differences between the methods. The main influence factor in this result was the HDR specification. The position of C1 datum point does not allowed a good inspection process repeatability, as could be observed in Section 4.3.5, resulting in a $\hat{\sigma}_e$ of 21.53

µm. Figure 4.39 shows the average results of each method and its confidence interval (CI) (α = 0.05).

Figure 4.39 - Part B: Statistical evaluation.

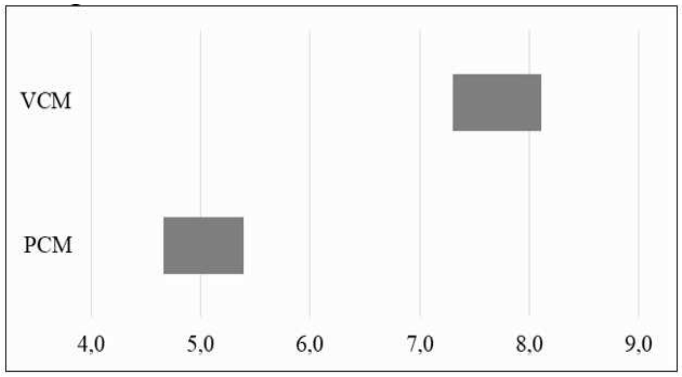

Source: the author.

4.4 GENERAL EVALUATION

As defined in Section 3.2.1, risk management consists of identifying, evaluating and prioritizing risks. In order to identify the difficulties presented in the process, a careful analysis of each developed step was necessary. Through the intermediary evaluations of the process performed through the two methods, it was possible to classify the steps that present greater possibilities of errors and to identify the main factors of this performance. This evaluation was performed through the standard deviations calculated at each evaluation step. These steps for the two methods are summarized in Table 4.11.

Table 4.11 - Performed evaluations.

Method	Evaluation	Symbol
VCM	Simplified Clamping System	SCS
	Modeling	MOD
	Simulation	SIM
PCM	Clamping System	PCS
	Conventional evaluation	COE

Source: the author.

Figure 4.40 graphically presents the performance results of each process step comparably for the two parts. In Figure 4.40 it is possible to identify that the part A showed a greater uniformity of the standard deviations in each step. Part B, however, resulted in a larger variation.

Figure 4.40 - Numerical comparison between VCM and PCM.

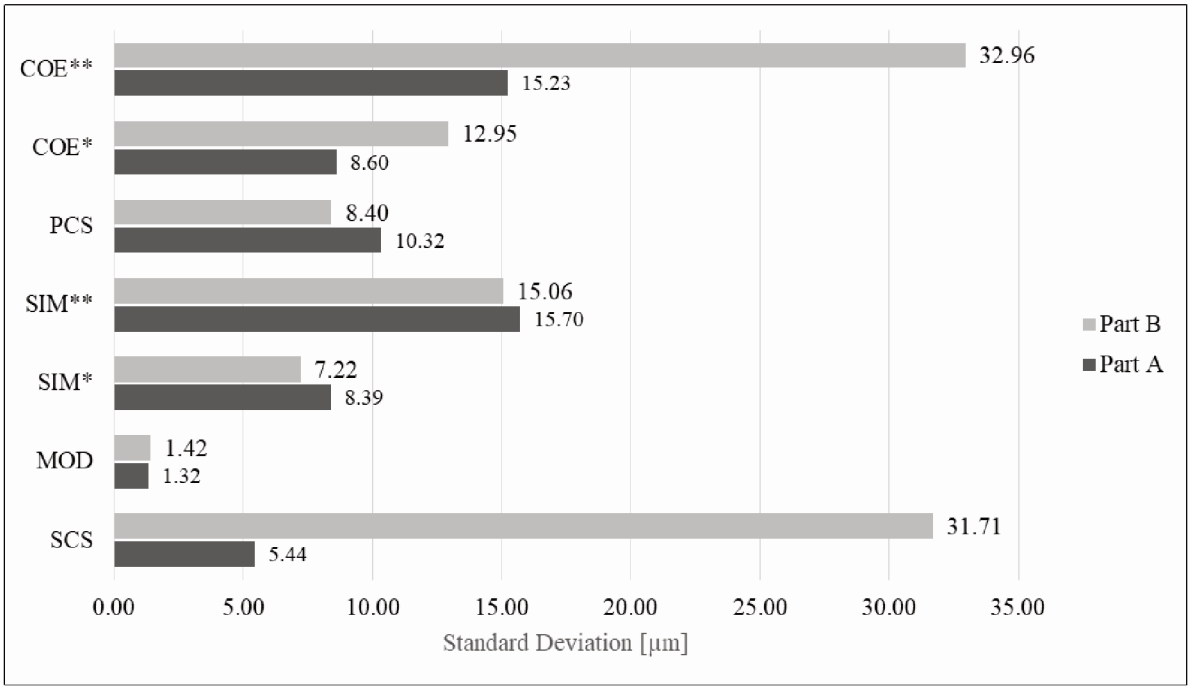

Source: the author.

* Datum points. ** Control points.

By evaluating the simplified clamping system (SCS), part B presented a very high $\hat{\sigma}_e$ and could be identified as the main source of possible errors. However, with the 3D data scanned and modeled, it is possible to indicate that in the simulation step there was a significant improvement of this performance. That is, the simulation process is capable of absorbing the variation shown in the simplified CS, as long as there are no large variations in the contact points between part and CS.

Following the worst performances, again in part B, evaluated by the conventional method. As previously mentioned, the bias presented by the inefficient specification of the datum points in the GPS step causes in the referencing process between mesh and CAD model, through best-fit due to HDF, this deterioration in the metrological performance of the PCM method. The modeling process was shown to be the most stable and presents the lowest variation. By examining the measurement process in detail, it was possible to identify possible sources of errors and to classify them into the following categories: environment, part

characteristics, method, scanning process, scanning hardware, processing software and simulation software. These sources of errors will be analyzed in the following sections.

Related to the environmental conditions, one of the most common factors is temperature, which affects not only the measurement system, but also the measured object. For the 3D scanner, as the light sources act as small heat sources, the software compensates the hardware temperature variation. Humidity and contamination can also be relevant factors, since they influence the light reflection from the part to the scanner. Furthermore, humidity can cause a dew condensation on camera and projector lenses, reducing their accuracy. In addition, Lemes further emphasizes that fringe projection scanners are very sensitive to light conditions [1].

Regarding the part, the main factor that can affect the results is the uncertainty associated with the material properties and the assumption of an isotropic material. The category of influences related to measurement method can include: the number and distribution of reference points markers, sampling, filtering, equipment handling, fixturing and of course the operator's influence (training, experience, care, and so forth).

One of the identified factors from the scanner hardware is related to the optical elements (lenses, prisms, mirrors, aperture) that can influence que image quality. As well the structural elements, the measurement volume, and the scanner calibration. About the processing software, the algorithms can introduce some errors in the results, associated with the software robustness, reliability and also the temperature correction process. The simulated process is influenced with more parameters than the real world, because it involves some assumptions and approximations. At the same time, the mathematical model, the boundary conditions and the discretization step can influence in the results.

To understand the impact of each factor and error source, there would be necessary to carefully prepare a series of experiments that would take into account only the specific impact of each individual factor, which were not addressed in this work.

5 CONCLUSION

The combination of optical scanning systems and virtual clamping method using simulated displacements to the geometric inspection process of non-rigid parts, trying to combine the two emerging technologies into a new, hybrid, can be a strong support to manufacturing process. However, this method showed that their usage requires a strong expertise and extremely careful choice of numerous adjustable parameters.

The experiments showed that, when the VCM is compared with the conventional method (PCM), both of them present similar and consistent metrological performances, when the appropriate boundary conditions are accurately described. However, the VCM results in a better repeatability, since it eliminates the interactions between part and clamping system.

The results also allowed an analysis of the process with a greater chance to interfere in the results and the main factors that led to this performance. It is shown that the major contribution to measurement errors/uncertainty comes from the scanning process. However, if the simplify clamping system is well described in the process of gravity neutralization, such errors can be absorbed.

The Virtual Clamping Method also follows the current trend of transferring the complexity from de physical world to the cyber world. The VCM method has the potential of:

- removing limitations to the physical realization of GD&T constraints;
- providing easy access to all relevant part surfaces;
- reducing the measurement setup and image acquisition times;
- reducing the CAPEX (Capital Expenditure) with expensive and complex clamping systems;
- reducing the OPEX (Operations Expenditure) with storage, maintenance and dimensional verification of fixtures.

Additionally, it was possible to identify some limitations of using this method, which are expressed below:

- simple physical fixtures are still needed to hold the part during scanning and make possible the accurate correction of gravity effects;
- the modelling process (RE) and FEM simulation processes should be streamlined to promote the industrial acceptance of the method;

- the (practical) metrological confirmation of measurement processes that make intensive use of computer simulation is still a pending issue.

To summarize, the VCM method proved to be highly relevant for the tasks of measuring non-rigid parts for the production chain, however, some studies are still necessary, for example:

- evaluate the use of other 3D scanning technologies to capture de 3D surfaces;
- perform an analysis of the VCM method applicability across the range of non-rigid parts, as shown in Figure 2.1;
- study the influence of finite element types;
- development of an optimized algorithm to measure virtually the distance between the reference points and the mesh, and the direction for using these data as constrains in finite element simulation;
- understand the impact of each source of error / uncertainty raised in the former section through a series of experiments, isolating one variable at a time, until its behavior is known.

REFERENCES

[1] S. Lemes, **Validation of numericals simulations by digital scanning of 3d sheet metal objects**, University of Ljubljana, Ljubljana, 2010.

[2] V. Sabri, S. A. Tahan, X. T. Pham, D. Moreau and S. Galibois, "Fixtureless profile inspection of non-rigid parts using the numerical inspection fixture with improved definiton of displacement boundary conditions", **International Journal of Advanced Manufacturing**, vol. 82, nº 5, pp. 1343-1352, feb 2016.

[3] R. Ascione and W. Polini, "Measurement of nonrigid freeform surfaces by coordinate measuring machine", **The International Journal of Advanced Manufacturing Technology**, vol. 51, pp. 1055-1067, may 2010.

[4] International Organization for Standardization, **ISO 10579: Geometrical product specifications (GPS) - Dimensioning and tolerancing - Non-rigid parts**, Geneva, 2010.

[5] A. Aidibe and A. Tahan, "The inspection of deformable bodies using curvature estimation and Thompson-Biweight test", **The International Journal of Advanced Manufacturing Technology**, vol. 71, pp. 1733-1747, 22 jan 2014.

[6] G. N. Abenhaim, A. Desrochers and A. Tahan, "An Investigation of the Repeatability of Nonrigid Parts Measurements: A Case Study of an Aluminum Panel", **12th CIRP Conference on Computer Aided Tolerancing**, 2012.

[7] Intenational Organization for Standardization, **ISO TR 14638: Geometrical Product Specification - Masterplan**, Swizerland , 1995.

[8] The American Society of Mechanical Engineers, **ASME Y14.5: Dimensioning and Tolerancing,** New York, 2018.

[9] J. Hill, **FICTIV/WHG: An Introduction to Geometric Dimensioning and Tolerancing,** 14 feb 2017. [Online]. Available: https://is.gd/gAUGgr. [Acessed on 04 may 2019].

[10] Y. Wu and Q. Gu, "The Composition Principle of the Datum Reference Frame", **Procedia CIRP Conference on Computer Aided Tolerancing (CAT)** , Gothenburg, 2016.

[11] D. Whitney, M. Anderson, C. Cadet, C. Fine, D. Gossard, A. Thornton, M. Groover, R. Nagel, T. Ozsoy and H. Stenger, **Agile pathfinders in the aircraft and automobile industries: a progress report**, US Air Force Wright Patterson AFB, 1995.

[12] J. D. Meadows, **Measurement of Geometric Tolerances in Manufacturing**, Boca Raton: CRC Press, 1998.

[13] M. Petitcuenot , L. Pierre and B. Anselmetti, “ISO specifications of complex surfaces: Application on aerodynamic profiles”, **12th CIRP Conference on Computer Aided Tolerancing**, Huddersfield, 2014.

[14] Intenational Organization for Standardization, **ISO 1101: Geometrical product specifications (GPS) - Geometrical tolerancing - Tolerances of form, orientation, location and run-out**, [-], Switzerland, 2017.

[15] S. Zirmi, H. Paris and I. Belaidi, “Analyse de la conception d’un montage d’usinage `a l’aide d’´el´ements modulaires”, **Mécanique & Industries**, vol. 8, pp. 1-6, 7 mar 2007.

[16] W. Cai, S. J. Hu and J. X. Yuan, “Deformable Sheet Metal Fixturing: Principles, Algorithms, and Simulations”, **Journal of Manufacturing Science and Engineering**, vol. 118, pp. 318-323, aug 1996.

[17] J. A. Camelio, S. J. Hu and D. Ceglarek, “Impact of fixture design on sheet metal assembly variation”, **Journal of manufacturing Systems**, vol. 23, nº 3, pp. 182-193, 2004.

[18] G. Moroni, W. Polini and M. Rasella, “Non-rigid free form surface inspection : an aeronautical composite component case study”, **Proceedings of 10th CIRP Conference on Computer Aided Tolerancing**, 2007.

[19] K. Arámbula, H. Siller, L. De Chiffre, C. Rodríguez and A. Cantatore, “Evaluation of metrology technologies for free form surfaces”, **International Journal of Metrology and Quality Engineering**, vol. 3, nº 1, pp. 55-62, 26 sep 2012.

[20] V. Kupriyanov, **Comparison of optical and tactile Coordinate Measuring Machines in a production environment**, HAMK Häme University of Applied Sciences, Riihimäki, 2018.

[21] Y. Li and P. Gu, “Free-form surface inspection techniques state of the art review”, **Computer-Aided Design**, vol. 36, nº 13, pp. 1395-1417, 28 feb 2004.

[22] R. Schafmeister and K. Reißner, **Principles of the Surface deviation**, Brawnschweig, 2010.

[23] K. Blaedel, D. Swift, A. Claudet, E. Kasper and S. Patterson, **Metrology of Non-Rigid Objects**, Lawrence, 2002.

[24] C. Lartigue, F. Thiebaut, P. Bourdet and N. Anwer, “Dimensional metrology of flexible parts: Identification of geometrical deviations from optical measurements”, **Advanced Mathematical and Computational**, vol. 7, pp. 196-203, 2006.

[25] K. Hirata, T. Yajima and Y. Sonda, **Shape Inspection Method and Apparatus**, US 7589844B2, 2009.

[26] A. Weckenmann and A. Gabia, "Testing formed sheet metal parts using fringe projection and evaluation by virtual distortion compensation", **Fringe 2005**, 2006.

[27] A. Weckenmann and J. Weickmann, "Optical inspection of formed sheet metal parts applying fringe projection systems and virtual fixation", **Metrology and Measurement Systems**, vol. 4, pp. 321-334, jan 2006.

[28] A. Jaramillo, P. Boulanger and F. Prieto, "On-line 3-D Inspection of Deformable Parts Using FEM Trained Radial Basis Functions", **12th International Conference on Computer Vision**, 2009.

[29] A. Jaramillo, F. Prieto and P. Boulanger, "Fixtureless inspection of deformable parts using partial captures", **International Journal of Precision Engineering and Manufacturing**, pp. 77-83, jan 2013.

[30] H. Radvar-Esfahlan and S.-A. Tahan, "Nonrigid geometric metrology using generalized numerical inspection fixtures", **Precision Engineering**, vol. 36, nº 1, pp. 1-9, jan 2012.

[31] I. Gentilini and K. Shimada, "Predicting and evaluating the post-assembly shape of thin-walled components via 3D laser digitization and FEA simulation of the assembly process", **Computer-Aided Design**, vol. 43, nº 3, pp. 316-328, 2011.

[32] G. N. Abenhaim, A. S. Tahan , A. Desrochers and J.-F. Lalonde, "Aerospace panels fixtureless inspection methods with restraining force requirements: a technology review", **SAE Technical Paper Collection**, pp. 1-12, 24 sep 2013.

[33] G. N. Abenheim, **Nouvelle méthode d'inspection des pièces flexibles sans gabarit de conformité**, Montréal, 2009.

[34] S. S. Karganroudi, J.-C. Cuillière, V. François and S.-A. Tahan, ""What-if" scenarios towards virtual assembly-state mounting for non-rigid parts inspection using permissible loads", **The International Journal of Advanced Manufacturing Technology**, vol. 97, nº 1-4, pp. 353-373, jul 2018.

[35] A. Aidibe, A. S. Tahan and G. N. Abenhaim, "Distinguishing profile deviations from a part's deformation", **WSEAS Transactions on Applied and Theoretical Mechanics**, vol. 7, nº 1, pp. 18-28, jan 2012.

[36] G. N. Abenheim, A. S. Tahan, A. Desrochers and R. Maranzana, “A novel approach for the inspection of flexible parts without the use of special fixtures”, **Journal of Manufacturing Science and Engineering**, vol. 133, pp. 1-11, feb 2011.

[37] A. Aidibe, **Inspection des pièces flexibles sans gabarit de conformation**, Montréal, 2014.

[38] A. Aidibe and A. Tahan, “The Coherent Point Drift Algorithm Adapted for Fixtureless Metrology of Non-rigid Parts”, **13th CIRP Conference on Computer Aided Tolerancing**, vol. 27, pp. 84-89, 01 may 2015.

[39] R. Wang, F. Zhai, B. Wu and Y. Ji, “The research of springback compensation design method based on reverse modeling”, **AIP Conference Proceedings 1864**, pp. 01-06, 03 aug 2017.

[40] E. Savio, L. De Chifre and R. Schmitt, “Metrology of freeform shaped parts”, **CIRP Annals Manufacturing Technology**, pp. 810-835, 22 nov 2007.

[41] S. Martínez, E. Cuesta, J. Barreiro and B. Álvarez, “Analysis of laser scanning and strategies for dimensional and geometrical control”, **The International Journal of Advanced Manufacturing Technology**, vol. 46, pp. 621-629, jan 2010.

[42] J. Vagovský, I. Buranský and A. Görög, “Evaluation of Measuing Capabiliy of the Optical 3D Scanner”, **25th DAAAM International Symposium on Intelligent Manufacturing and Automation**, Vienna, 2015.

[43] F. Li, D. Stoddart and I. Zwierzak, “A performance test for a fringe projection scanner in various ambient light conditions”, **10th CIRP Conference on Intelligent Computation in Manufacturing Engineering**, Rotherdam, 2017.

[44] N. Van Gestel, S. Cuypers, P. Bleys and J.-P. Kruth, “A performance evaluation test for laser line scanners on CMMs”, **Optics and Lasers in Engineering**, vol. 47, pp. 336-342, apr 2009.

[45] A. Satyanarayana, M. Krishna, A. Chandrakanth and R. Pradyumna, “Influence of LASER CMM Process Parameters on Dimensional Inspection of Standard Spheres”, **Materials Today**, vol. 5, nº 2, pp. 3965-3970, 24 mar 2018.

[46] C. R. G. d. Lima, **Um estudo comparativo de sistema de medição aplicáveis ao controle dimensional de superfícies livres em peças de médio e grande porte**, Florianópolis, 2006.

[47] P. J. Besl and N. D. McKay, “A method for registration of 3D shapes”, **IEEE Transactions on Pattern Analysis and Machine Intelligence**, vol. 14, pp. 239-256, feb 1992.

[48] J. L. Bentley, “Multidimensional binary search trees used for associative searching”, **Communications of the Association for Computing Machinery**, vol. 18, pp. 509-517, 1975.

[49] J. H. Friedman, J. L. Bentley and R. A. Finkel, “An algorithm for finding best matches in logarithmic expected time”, **ACM Transactions on Mathematical Software**, pp. 209-226, 1977.

[50] E. M. Bispo e R. B. Fischer, “Free-form surface matching for surface inspection”, **Proceedings of the 6th IMA Conference on the Mathematics of Surfaces**, pp. 119-136, 1996.

[51] X. Huang, P. Gu and R. F. Zernicke, “Localization and comparison of two free-form surfaces”, **Computer-Aided Design**, vol. 28, nº 12, pp. 1017-1022, dez 1996.

[52] P. Gu and X. Huang, “CAD-model based inspection of sculptured surfaces with datums”, **International Journal of Production Research**, vol. 36, nº 5, pp. 1351-1367, 15 nov 2010.

[53] H. J. Pahk and W. J. Ahn, “Precision inspection system for aircraft parts having very thin features based on CAD/CAI integration”, **The International Journal of Advanced Manufacturing Technology**, vol. 12, nº 6, pp. 442-449, nov 1996.

[54] Y. Li and P. Gu, “Feature-Based Alignment and Comparison between Portion and Whole of Free-Form Surfaces”, **CIRP Annals - Manufacturing Technology**, vol. 54, nº 1, pp. 135-138, 2005.

[55] Y. Li and P. Gu, “Inspection of free-form shaped parts”, **Robotics and Computer-Integrated Manufacturing**, vol. 21, nº 4-5, pp. 421-430, oct 2005.

[56] C. Lartigue, A. Contri and P. Bourdet, “Digitised point quality in relation with point exploitation”, **Measurement**, vol. 32, nº 3, pp. 193-203, oct 2002.

[57] M. Mahmud, D. Joannic, M. Roy, A. Isheil and J.-F. Fontaine, “3D part inspection path planning of a laser scanner with control on the uncertainty”, **Computer-Aided Design**, pp. 345-355, apr 2011.

[58] F. Buonamici, M. Carfagni, R. Furferi, L. Governi, A. Lapini and Y. Volpe, “Reverse engineering modeling methods and tools: a survey”, **Computer-Aided Design & Applications**, vol. 15, nº 3, pp. 443-464, 04 may 2018.

[59] W. B. Thompson, J. C. Owen, J. De St. Germain, S. R. Stark Jr. and T. C. Henderson, “Feature-Based Reverse Engineering of Mechanical Parts”, **IEEE Transations on Robotics and Automation**, vol. 15, nº 1, pp. 57-66, feb 1999.

[60] J. Wang, D. Gu, Z. Yo, C. Tan and L. Zhou, “A framework for 3D model reconstruction in reverse engineering”, **Computers & Industrial Engineering**, vol. 63, nº 4, pp. 1189-1200, dez 2012.

[61] S. Alai, “A Review of 3D Design Parameterization Using Reverse Engineering”, **International Journal of Emerging Technology and Advanced Engineering**, vol. 3, nº 10, pp. 171-179, 2013.

[62] Y. Li, X. Wu, Y. Chrysathou, A. Sharf, D. Cohen-Or and N. J. Mitra, “GlobFit: Consistently Fitting Primitives by Discovering Global Relations”, **ACM Transactions on Graphics**, vol. 30, nº 4, pp. 1-12, 2011.

[63] T. Várady, M. A. Facello and Z. Terék, “Automatic extraction of surface structures in digital shape reconstruction”, **Computer-Aided Design**, vol. 39, nº 5, pp. 379-388, may 2007.

[64] N. Werghi, R. Fisher, A. Ashbrook and C. Robertson, “Shape Reconstruction Incorporating Multiple Nonlinear Geometric Constraints”, **Constraints**, vol. 7, nº 2, pp. 117-149, apr 2002.

[65] W. E. Lorensen and H. E. Cline, “Marching Cubes: A High Resolution 3D Surface Construction Algorithm”, **Computer Graphics**, vol. 21, nº 4, pp. 163-169, jul 1987.

[66] H. Edelsbruner, D. G. Kirkpatrick and R. Seidel , “On the Shape of A Set of Points In The Plane”, **IEEE Transactins on Information Theory**, vol. 29, nº 4, pp. 551-559, jul 1983.

[67] F. Bernardini, J. Mitleman, H. Rushmeier, C. Silva and G. Taubin, “The Ball-Pivoting Algorithm for Surface Reconstruction”, **IEEE Transactions on Visualizatin ad Computer Graphics**, vol. 5, nº 4, pp. 349-359, oct 1999.

[68] M. Kazhdan, M. Bolitho and H. Hoppe, “Poisson Surface Reconstruction”, **Eurographics Symposium on Geometry Processing**, Cagliari, Sardinia, Italy, 2006.

[69] G. Cuccuru, E. Gobbetti, F. Marton, R. Pajarola and R. Pintus, “Fast Low-Memory Streaming MLS Reconstruction of Point-Sampled Surfaces”, **Proceedings of the Graphics Interface 2009 Conference**, Kelowna, 2009.

[70] A. Agathos, I. Pratikakis, S. Perantonis, N. Sapidis and P. Azariadis, “3D Mesh Segmentation Methodologies for CAD applications”, **Computer-Aided Design & Applications**, vol. 4, nº 6, pp. 827-841, 2007.

[71] P. Theologou, I. Pratikakis and T. Theoharis, “A comprehensive overview of methodologies and performance evaluation frameworks in 3D mesh segmentation”, **Computer Vision and Image Understanding**, vol. 135, pp. 49-82, jun 2015.

[72] M. Berger, A. Tagliasacchi, L. Seversky, P. Alliez, J. Levine, A. Sharf and C. Silva, “State of the Art in Surface Reconstruction from Point Clouds”, **Eurographics SATAR (Proc of EG'14)**, 2014.

[73] T. Wilvert, **Numerical assessment of the minimum distance between holes in 3d components and evaluation of the use of twist drills in the Hole-Drilling Method**, Florianópolis, 2018.

[74] C. R. Maliska, **Transferência de calor e mecânica dos fluidos computacional**, 2 ed. ed., Rio de Janeiro: LCT, 2004.

[75] R. Andujar Moreno, **What does sha function mean in finite element formulation?**, 17 jul 2011. [Online]. Available: https://is.gd/8bqYuL. [Acessed on 19 apr 2019].

[76] F. Klocke, **Manufacturing Processes 1: Cutting**, Aachen: RWTH, 2011.

[77] D. R. Simioni, **Fluidodinâmica da liberação de óleo submerso em água: estdo experimental e de simulação**, Florianópolis, 2014.

[78] V. Y. Belozyorov, “New solution method of linear static output feedback design problem for linear control systems”, **Linear Algebra and its Applications**, vol. 504, pp. 204-227, 1 sep 2016.

[79] Witte Barskamp KG, “Modular Fixturing Systems ALUFIX,” Witte Barskamp KG, [Online]. Available: https://www.witte-barskamp.com/modular-fixturing-systems/alufix-classic-alufix-eco/. [Acessed on 27 05 2019].

[80] GOM GmbH, **ATOS Compact Scan**, Braunschweig, 2012.

[81] A. Alves Filho, **Elementos Finitos: A base da tecnologia CAE**, 6. ed., São Paulo: Érica, 2013.

[82] International Organization for Standization, **ISO 3001: Risk management – Guidelines**, Swizerland, 2018.

[83] D. J. Wheeler and R. W. Lyday, **Evaluating the measurement process**, Knoxville: SPC Press, 1989.

[84] D. J. Wheeler, **Advanced Topics in Statistical Process Control**, Knoxville: SPC Press, Inc., 1995.

[85] V. D. I. &. V. D. E. E. Informationstechnik, **VDI/VDE 2634-2: Optical 3-D measuring systems - Optical systems based on area scanning**, Berlin, 2002.

[86] Chrysler Group LLC, Ford Motor Company, General Motors Corp., **Measurement System Analysis: Referece Manual 4th edition**., 2010.

[87] G. Box, "Non-Normality and Tests on Variances", **Biometrika**, vol. 40, nº 3-4, pp. 318-335, 1953.

[88] C. A. Markowski and E. P. Markowski, "Conditions for the Effectiveness of a Preliminary Test of Variance", **The American Statistician**, vol. 44, nº 4, pp. 322-326, nov 1990.

[89] A. Gelman, "Analysis of variance - why it is more important than ever", **The Annals of Statistics**, vol. 33, nº 1, pp. 1-53, 2005.

[90] D. Montgomery and G. Runger, **Estatística Aplicada e Probabilidade para Engenheiros**, 5th ed., LTC, 2012.

[91] O. Podkovyrov, Artist, **Blue winglet modern passenger aircraft**. [Art].

[92] The Aluminum Association, Inc., **International Alloy Designations and Chemical Composition Limits for Wrought Aluminum and Wrought Aluminum Alloys**, Arlington, 2015.